Evaluation of Calcium Phosphate Nanoparticles Mineralized with Proteins and Peptides for Use as Adjuvants in Protein and Nucleic Acid Vaccines

David Y. Chiu

A dissertation

submitted in partial fulfillment of the

requirements for the degree of

Doctor of Philosophy

University of Washington

2013

Reading Committee:

James D. Bryers, Chair

Francois Baneyx

James Carothers

Program Authorized to Offer Degree:

Chemical Engineering

University of Washington

Abstract

Evaluation of Calcium Phosphate Nanoparticles Mineralized with Proteins and Peptides for Use as Adjuvants in Protein and Nucleic Acid Vaccines

David Y. Chiu

Chair of the Supervisory Committee:
Professor James D. Bryers
Department of Bioengineering

Subunit and inactivated vaccines are a safer but less immunogenic alternative to live attenuated vaccines. Adjuvants are often added to subunit and inactivated vaccine formulations to boost immune responses. Aluminum mineral adjuvants are the most commonly used adjuvants in human vaccines and are strong stimulators of antibody-mediated immune response. However, aluminum adjuvants elicit weak or absent cell-mediated T_H1 and cytotoxic CD8 T-cell responses.

As an alternative adjuvant, calcium phosphate (CaP) is an ideal material due to its biocompatibility and biodegradability. Additionally, CaP has been used as an adjuvant in approved human vaccines in several European countries. When CaP is precipitated in the absence of a capping agent, large polydisperse and polymorphous micron-sized particles are formed. Particle size has been shown to be an important parameter for vaccine antigen carriers and adjuvants, and particles in the nanometer size range are of particular interest due to their unique cellular uptake and biodistribution properties.

CaP binding dodecapeptides selected by cell surface display biopanning were used in *E. coli* thioredoxin A derivatives (TrxA::CaP) and thioredoxin A derivative-ovalbumin fusion proteins (TrxA::CaP-OVA) to mineralize sub-100nm CaP nanoparticles (NPs). Addition of CaP

NP adjuvant to TrxA::CaP-OVA vaccine formulations significantly increased the population of antigen specific splenic effector-memory CD8+ T-cells in immunized mice after challenge with WSN-OVA_I, an OVA expressing influenza A strain.

Due to autoimmunity concerns, the thioredoxin A derivative CaP mineralization agents were replaced with a disulfide-constrained cyclic peptide containing an identified CaP binding motif (cPN38). Addition of cyclic peptide mineralized CaP NPs to OVA vaccine formulations, increased sensitization of antigen-specific IFN-γ (T_H1 cytokine) secreting splenocytes in immunized mice.

As compared to protein antigen vaccines, nucleic acid vaccines containing pDNA or mRNA encoding genes are advantageous due to their ease of production, inherently immunogenicity, and ability to target the endogenous MHC-I loading pathway. When added to OVA pDNA vaccines, CaP NPs increased antigen-specific humoral and splenocyte IFN-γ responses. Conversely, CaP NPs had no adjuvant effect in OVA mRNA vaccines.

Increased cell-mediated (T_H1) and cytotoxic (CD8) T-cell responses were observed when CaP NP adjuvant was added to OVA protein and pDNA vaccine formulations. As an alternative adjuvant to aluminum compounds, CaP NP adjuvants may be effective in vaccines against intracellular pathogens in which an antibody-mediated immune response alone is insufficient for protective immunity.

Table of Contents

Acknowledgements

The author would like to thank his co-advisors Dr. Francois Baneyx and Dr. James Bryers for mentoring him and allowing him the opportunity to conduct research in their labs. He would also like to thank the former and current members of his supervisory committee, Dr. Beth Traxler, Dr. Daniel Schwartz, Dr. Suzie Pun, Dr. James Carothers, Dr. Richard Darveau, and Dr. David Beck for their valuable and constructive guidance.

He would also like to thank members of the Baneyx and Bryers groups for their support and contributions to his research. In particular, he would like to thank Dr. Weibin Zhou for assisting in all phases of the research conducted in the Baneyx lab. Additionally, he would like to thank Dr. Sathana Kitayaporn for his assistance with SEM images, Dr. Connie Cheng for training him in tissue culture techniques, and Dr. Lin Yan for training him with animal models. The author would also like to thank members of Dr. Terrance Kavanagh's group and Dr. Murali-Krishna Kaja's group, in particular Albanus Moguche, for their collaboration with the vaccination studies.

Finally, the author would like to thank his friends and family, Shean, Loretta, James and Stephanie Chiu, for their support. He would like to dedicate this work to his wonderful wife Thao Thanh "Jenny" To for carrying him through graduate school.

The research presented in this dissertation was supported by a Grand Challenge Exploration grant from the Bill and Melinda Gates Foundation, a National Science Foundation-Nanotechnology and Inter- disciplinary Research Team award on Protein-Aided Nano-manufacturing (CMMI-0709131), the National Science Foundation (NSF) Genetically Engineered Materials Science and Engineering Center (DMR-0520657), and National Institutes of Health Grants P30ES007033, U19ES019545, and R01AI074661.

Chapter 1: Introduction and Background

The development of vaccines has led to the reduction or eradication of various infectious diseases (smallpox, rabies, polio, diphtheria, tetanus, etc.) that have afflicted humans for much of recorded history. However, effective vaccines have yet to be developed for many diseases including malaria and HIV/AIDS, both of which have respective annual mortality rates of ~780,000 (2009)[171] and ~2,000,000 (2010).[100] Thus, the development of new vaccines is of utmost importance for global health.

Vaccines protect hosts through the creation of pathogen-specific memory B and T-cells. Proliferation and differentiation of naïve T-cells into effector cells is initiated by activated antigen-presenting dendritic cells in the lymph nodes. T-cells are classified into two categories based on the expression of the cell surface markers CD4 and CD8. CD4 T-cells recognize cells presenting exogenous peptide fragments bound to major histocompatibility complex II (MHC-II). Degradation of endocytosed proteins by proteases and peptide loading onto MHC-II occurs within endosomes. CD4 T-cells serve many functions including: activation of macrophages to kill endocytosed intracellular pathogens (cell-mediated T_H1 response), activation of B-cells to produce antibodies (T_H1 and T_H2 response), activation of fibroblasts and epithelial cells to produce chemokines that recruit neutrophils to sites of infection (T_H17 response), and regulation of other immune cells to prevent autoimmunity and suppression of T-cell response after an infection has subsided (regulatory T-cell response). CD8 T-cells (AKA cytotoxic T-cells) recognize cells presenting endogenously produced peptides bound to MHC-I. MHC-I loading of peptides occurs in the cytosol and loaded peptides are derived from endogenously produced proteins degraded by the proteasome. Extracellular peptides can also be loaded onto MHC-I through a less frequent and poorly understood phenomenon known as “cross-presentation.” The

primary function of CD8 T-cells is to induce apoptosis in infected cells. B-cells produce antigen-specific antibodies that serve three main functions: neutralization of a pathogen through surface binding, facilitation of opsonization by phagocytic cells, and the initiation of the classical pathway of complement. Once a B-cell has bound an antigen, it migrates to the spleen where it then proliferates after stimulation by helper T-cells. T_H1 and CD8 T-cell responses are important for fighting intracellular pathogen infections and T_H2 response is important for extracellular pathogens. Neutralizing antibodies can also play an important role in preventing infections with certain intracellular pathogens. After an infection has cleared, a small percentage of effector cells are retained and become long-lived memory cells. Memory B and T-cells are able to differentiate and proliferate more quickly than naïve cells upon antigen restimulation. An effective vaccine must induce pathogen-specific memory B and T-cells that can act quickly to clear a pathogen at the early onset of infection.

Early evidence of vaccination dates back to mid-17th century China when smallpox immunizations were carried out by inoculating children with pulverized smallpox scabs.[22] Widespread vaccination was not practiced until the late 18th century with the advent of Edward Jenner's cowpox vaccine against smallpox.[12] Early vaccination was carried out with *attenuated vaccines* containing live pathogens with decreased virulency. Administration of attenuated vaccines typically causes a mild infection thereby conferring future immunity against a specific pathogen. While eliciting strong immune responses, attenuated vaccines have the potential to revert to a more virulent form and are not suitable for immunocompromised individuals. Despite these limitations, attenuated vaccines have been proven to be safe and effective for some pathogens. In the US, attenuated vaccines have been approved for vaccination against

tuberculosis, influenza, measles, mumps, and rubella (MMR), rotavirus, smallpox, typhoid, and varicella.

In contrast to attenuated vaccines, *inactivated vaccines* contain pathogens killed by heat or chemical treatment. Since there are no live cells, inactivated vaccines lack the inherent risks associated with attenuated vaccines but still contain antigens and immunostimulatory molecules. Inactivated vaccines are approved in the US for: hepatitis A, Japanese encephalitis, polio, seasonal influenza, rabies, diphtheria, and tetanus.

Subunit vaccines contain antigens that are either purified from a pathogen or produced recombinantly. Subunit vaccines have decreased formulation variability and heterogeneity as compared to inactivated vaccines, plus subunit vaccines lack any toxic compounds derived from killed pathogens that may cause local adverse reactions.[110] For example, the DTP vaccine against diphtheria, tetanus, and pertussis contains killed whole cells of *B. pertussis* and due to safety concerns the DTP vaccine has been replaced in the US with the DTaP vaccine that contains acellular purified *B. pertussis* antigens.[80] Subunit vaccines are a safer alternative for vaccines against pathogens which cause chronic infections. Subunit vaccines recently approved in the US include the hepatitis B and human papillomavirus vaccines.

While generally safer than attenuated vaccines, inactivated vaccines and subunit vaccines, to a greater extent, are often less immunogenic and *adjuvants* are commonly added to potentiate the immune response.[125, 156] Any vaccine additive that increases immunogenicity is considered an adjuvant. Compounds as varied as agar, tapioca, lecithin, starch oil, saponin, and breadcrumbs have been shown to act as adjuvants in diphtheria and tetanus toxoid vaccines.[70] However, adjuvants must balance a fine line between immunostimulation and toxicity. While a

wide range of materials have been used as adjuvants, the most commonly used adjuvants are typically pathogen-associated molecular patterns, oil-in-water emulsions, and mineral compounds.

The immune system detects the presence of pathogenic bacteria, viruses, and parasites with pattern recognition receptors that recognize ubiquitous repetitive structures, known as pathogen-associated molecular patterns. Toll-like receptors (TLRs) are a type of pathogen recognition receptor that strongly stimulates innate and adaptive immunity through the expression of cytokines, chemokines, and co-stimulatory molecules when activated by ligand binding. TLR ligands are very potent adjuvants but safety concerns exist because they elicit such a strong immune response when delivered systemically. Many research groups are currently exploring the TLR-9 ligand CpG as an adjuvant. CpG motifs are unmethylated cytosine guanine repeats found in bacterial and viral DNA. In vertebrates, CpG motifs are relatively infrequent and are typically methylated on the cytosine residues.[180] Certain CpG oligonucleotides have been found to be more immunostimulatory (GACGTT in mice and rabbits and GTCGTT in humans).[103] CpG motifs are effective at inducing a T_H1 response and have been delivered with poly(lactic-*co*-glycolic) acid (PLGA) particles, aluminum hydroxide, liposomes, MF59®, and calcium phosphate.[121, 177] Lipopolysaccharide (LPS) is the major component of the outer membrane of gram-negative bacteria and LPS has been established as a potent adjuvant.[91] LPS stimulates both humoral and cell-mediated immunity but most forms of LPS are too toxic for human use.[67] Research progress has been made towards low biologically reactive LPS forms and monophosphoryl lipid A has been explored as an adjuvant due to its lowered toxicity as compared to di- and triphosphoryl forms of LPS.[36] Currently, the only non-aluminum adjuvant approved in vaccine formulations by the FDA is monophosphoryl lipid A (3-*O*-desacyl-4'-

monophosphoryl lipid A) in combination with aluminum hydroxide in the HPV vaccine Cervarix® (GlaxoSmithKline Biologicals).

Freund's complete adjuvant is a very potent adjuvant and is composed of a mineral oil-and-water emulsion containing killed mycobacteria (usually *M. tuberculosis*). Freund's complete adjuvant is too toxic for human use, and use in animals is limited due to abscess formation, inflammation, and granuloma and cyst formation at the site of injection.[67] Interestingly, Freund's incomplete adjuvant, which is an oil-and-water emulsion without mycobacteria, still retains an adjuvant effect despite the absence of immunostimulatory molecules from killed mycobacteria. Like Freund's complete adjuvant, Freund's incomplete adjuvant is not approved for use in humans due to adverse reactions at the site of injection.[70] An emulsion adjuvant recently approved in Europe is MF59® (Novartis). MF59® is a proprietary squalene-based oil-and-water emulsion adjuvant used in Novartis' seasonal influenza vaccine Fluad®. The mechanism of action for emulsion adjuvants is poorly understood and is believed to be due to the "depot effect" where antigen is slowly released from the adjuvant at the site of injection. However, similar biodistribution of antigen has been observed in vaccines with and without MF59®, indicating that a repository effect is not a likely explanation for emulsion adjuvancy.[45]

Aluminum compounds [hydrated potassium aluminum sulfate ($KAl(SO_4)_2 \cdot 12H_2O$), aluminum hydroxide ($Al(OH)_3$, aluminum phosphate ($AlPO_4$), and proprietary amorphous aluminum hydroxyphosphate sulfate (Merck)] are the most commonly used adjuvants in approved human vaccine formulations in the US. Although aluminum adjuvants as a whole are commonly referred to as "alum," alum specifically refers to hydrated potassium aluminum sulfate. The adjuvant effect of potassium aluminum sulfate was first reported in 1926, with increased immune responses observed in guinea pigs after vaccinations with diphtheria toxoid

precipitated with potassium aluminum sulfate as compared to vaccinations with soluble toxoid.[57] Potassium aluminum sulfate precipitated vaccines can be highly heterogeneous and vaccines containing antigen adsorbed to preformed aluminum hydroxide and aluminum phosphate have largely replaced potassium aluminum sulfate precipitated vaccines.[112] However, potassium aluminum sulfate is still used to precipitate antigens in approved US vaccines [*e.g.* DTaP (Tipedia®, Sanofi Pasteur) and hepatitis B (Recombivax HB®, Merck) vaccines].

Despite widespread use in human vaccines, the mechanism of action for aluminum adjuvants is not well understood. The "depot effect" is a commonly suggested mechanism for adjuvancy. Adsorptive capacity and strength of adsorption between antigen and aluminum adjuvants has been shown to correlate with adjuvancy[31, 73] but a repository effect alone is insufficient to explain aluminum compound adjuvancy. The depot effect has been challenged in experiments showing rapid desorption of antigen from aluminum hydroxide and phosphate after injection.[66, 196] Also, serum proteins have been shown to displace adsorbed proteins from aluminum hydroxide and aluminum phosphate *in vitro*.[79] An alternative mechanism for aluminum adjuvancy is the stimulation of monocytes, eosinophils, and cytokine production at the site of injection. Monocytes are precursors of macrophage and dendritic cells. Human peripheral blood monocytes pulsed with tetanus toxoid adsorbed to aluminum hydroxide secreted higher levels of the inflammatory cytokine IL-1 and stimulated increased T-cell proliferation after *in vitro* co-culture as compared to monocytes pulsed with soluble toxoid.[123] Treatment of human peripheral blood monocytes with aluminum hydroxide *in vitro* stimulated the production of the T_H2 cytokine IL-4 but not the T_H1 cytokine IFN-γ.[186] Eosinophils are pro-inflammatory white blood cells that have anti-parasitic and bactericidal activity and are also important mediators of allergic response. *In vivo* injection of aluminum hydroxide has been shown to attract eosinophils

to the site of injection.[164] After intraperitoneal injection of aluminum hydroxide without antigen in mice, increased splenic IL-4 expressing eosinophils were detected and shown to prime B-cells.[191] Localized necrosis of muscle fibers after intramuscular injection of aluminum hydroxide may also play a role in adjuvancy by releasing danger signals from necrotic cells.[190] One such danger signal, uric acid, has been shown to influence the immune response to aluminum adjuvanted vaccines. After intraperitoneal injection of aluminum hydroxide and ovalbumin antigen, increased ovalbumin positive monocytes were detected in mediastinal lymph nodes as compared to ovalbumin only injections. Increased uric acid levels were observed at the site of injection and treatment of uricase reduced antigen positive monocyte populations suggesting that aluminum hydroxide attracts monocytes to the site of injection by stimulating uric acid production.[101]

Aluminum adjuvants have a long safety record and have been shown to elicit increased antibody responses in some vaccines. However, aluminum adjuvants tend to elevate allergy-associated IgE response[72, 96] possibly by attracting and stimulating eosinophils at the site of infection. The major limitation of aluminum adjuvants is their inability to induce cell-mediated T_H1 and cytotoxic T-cell responses[113, 15, 16, 30] precluding their use in some vaccines against intracellular pathogens in which a T_H2 antibody mediated response alone is insufficient for protective immunity.[184] Aluminum adjuvants have also been shown to have a weak or absent adjuvant effect in vaccines against influenza,[37] typhoid,[34] malaria,[107, 171] and herpes simplex virus (HSV).[53, 76]

Despite widespread use, the previously stated limitations of aluminum adjuvants necessitate the development and evaluation of alternative adjuvants in new vaccines. Entire vaccine formulations, not the adjuvant alone, are evaluated by the FDA and new adjuvants may

be used in vaccine formulations as long as the formulation itself passes the rigorous safety standards put forth by the FDA. Therefore, the addition of new adjuvants to vaccine formulations may help improve efficacy in vaccines currently limited by available adjuvants.

Calcium phosphate (CaP) is another mineral adjuvant has been used and approved as a vaccine adjuvant in several European countries.[65, 1, 90] CaP is an ideal biomaterial because it is a natural constituent of the human body and is generally regarded to be safe, biocompatible and biodegradable[60]. As an alternative adjuvant to aluminum compounds, CaP may be an effective substitute in vaccines that require cell-mediated or cytotoxic T-cell response and in vaccines in which aluminum adjuvants have failed to show any adjuvant effect.

Unlike aluminum adjuvants, CaP does not elicit elevated IgE responses.[69, 76, 157] As an adjuvant in HSV-2 vaccines, CaP elevated IgG and IgG2a responses and decreased IgE response in mice as compared to aluminum adjuvants.[76] When CaP was combined with CpG and used as an adjuvant for influenza vaccines, elevated IFN-γ response was observed in murine splenic CD4 and CD8 T-cells.[99] CaP has also been shown to increase macrophage induced memory T-cell proliferation.[159] In vaccines containing diphtheria and tetanus toxoids, aluminum adjuvants typically elicit higher IgG response as compared to CaP.[69, 175] Adjuvancy is often measured by antibody response but evaluating antibody response alone ignores potential stimulation of cell-mediated and cytotoxic T-cells.

The size of particles used for vaccine delivery has been shown to influence immunogenicity. Particles less than 500nm in size have increased uptake by dendritic cells *in vitro* as compared to larger particles.[33, 51] Recent advances in vaccine delivery have focused on the use of sub-100nm nanoparticles and studies have found that sub-100nm particles stimulate

elevated B and T-cell responses as compared to larger particles.[50, 141, 146, 155] Increased trafficking to draining lymph nodes through passive diffusion into the lymphatic network has been observed after intradermal delivery of 20nm particles as compared to 100nm particles.[155] 100nm has been found to be a critical size cutoff because the diameter of the aqueous channels draining from the interstitium into the lymphatic network is approximately 100nm.[75, 131]

When precipitated in the absence of a capping agent, calcium phosphate tends to form large micron sized polydisperse and polymorphous particles.[49] Reproducible CaP precipitation remains challenging due to variability in stoichiometry, crystallinity, morphology, and size with slight changes in pH, temperature, Ca/PO_4 ratio, and precipitation technique.[5, 160] Also, controlling CaP particle size in the nanometer range is difficult due to Oswald ripening and the tendency for smaller particles to form large aggregates.[23, 90, 95] CaP particle size is often controlled with microemulsions[18, 43, 138] or by using a variety of capping agents such as: citrate,[76, 116, 128, 203] surfactants,[23] phosphate-functionalized porphyrin,[52] oligonucleotides,[144, 176, 198] and ovalbumin.[207]

CaP is the main mineral constituent of vertebrate teeth and bones and is present in a form similar to monoclinic hydroxyapaptite $[Ca_5(PO_4)_3(OH)]$.[129] Biological apatite is very accommodating to chemical substitutions and ionic substitutions can change the mineral's crystallite size and dissolution rate. The body alters the solubility properties of different apatite minerals (bone apatite, enamel apatite, dentin apatite) via ionic substitutions. Substitutions in the biological apatite crystal lattice include carbonate, fluorine, and chlorine ions.[200] Vertebrate bones are composites of plate shaped CaP nanocrystals (30-50nm long, 20-25nm wide, and 1.5-4nm thick) imbedded in a matrix of collagen and non-collagenous proteins.[54, 147] One non-collagenous protein osteocalcin, has been shown to be critical to the nucleation and size control

of apatite crystals through binding of γ-carboxylated glutamic acid residues to calcium ions in the hydroxyapatite crystal lattice face.[44, 82]

Solid binding peptides selected through biopanning using phage or cell surface display libraries have been shown to nucleate and cap a wide range of inorganic materials including Cu_2O,[35] Ag,[63] and ZnS.[208, 209] A biomimetic approach using CaP binding proteins identified through phage or cell surface display may be useful for mineralizing CaP particles in the sub-100nm size range.

Adjuvants are frequently used in vaccines but are mostly limited to aluminum adjuvants. Exploration of alternative adjuvants is needed to address the limitations of aluminum adjuvants. As an alternative adjuvant, CaP has an established safety profile in human vaccines. CaP particles in the sub-100nm size range may be able to exploit some of the unique biological properties of nanoparticles.

Proteins and peptides containing CaP binding motifs selected through biopanning are shown herein to mineralize and control the size of CaP particles in the sub-100nm size range. The resulting CaP NPs were evaluated *in vivo* for adjuvancy in protein and nucleic acid vaccines. Adjuvancy was evaluated by analyzing antibody, CD8 T-cell, and splenocyte IFN-γ response after vaccination. Increases in CD8 T-cell and splenocyte IFN-γ response observed after addition of CaP NP adjuvant to vaccine formulations suggests that CaP NPs may be useful as an adjuvant in intracellular vaccines.

Chapter 2: Calcium Phosphate Binders and Thioredoxin Vaccines

Bioconjugate Chemistry

Article

pubs.acs.org/bc

Biomineralization and Size Control of Stable Calcium Phosphate Core–Protein Shell Nanoparticles: Potential for Vaccine Applications

David Chiu,[†] Weibin Zhou,[†] Sathana Kitayaporn,[†] Daniel T. Schwartz,[†] Kaja Murali-Krishna,[‡,∥] Terrance J. Kavanagh,[§] and François Baneyx*,[†]

[†]Department of Chemical Engineering, [‡]Department of Immunology, and [§]Department of Environmental and Occupational Health Sciences, University of Washington, Seattle, Washington 98195, United States

ABSTRACT: Calcium phosphate (CaP) polymorphs are nontoxic, biocompatible and hold promise in applications ranging from hard tissue regeneration to drug delivery and vaccine design. Yet, simple and robust routes for the synthesis of protein-coated CaP nanoparticles in the sub-100 nm size range remain elusive. Here, we used cell surface display to identify disulfide-constrained CaP binding peptides that, when inserted within the active site loop of *Escherichia coli* thioredoxin 1 (TrxA), readily and reproducibly drive the production of nanoparticles that are 50–70 nm in hydrodynamic diameter and consist of an approximately 25 nm amorphous calcium phosphate (ACP) core stabilized by the protein shell. Like bone and enamel proteins implicated in biological apatite formation, peptides supporting nanoparticle production were acidic. They also required presentation in a loop for high-affinity ACP binding as elimination of the disulfide bridge caused a nearly 3-fold increase in hydrodynamic diameters. When compared to a commercial aluminum phosphate adjuvant, the small core–shell assemblies led to a 3-fold increase in mice anti-TrxA titers 3 weeks postinjection, suggesting that they might be useful vehicles for adjuvanted antigen delivery to dendritic cells.

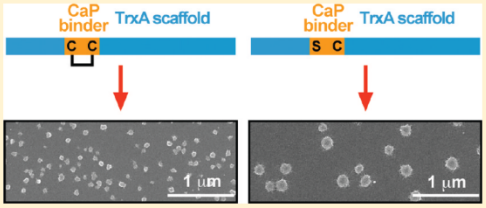

■ INTRODUCTION

Because they are highly biocompatible and nontoxic, calcium phosphate (CaP) nanoparticles have been explored in applications ranging from hard tissue regeneration to the delivery of small molecules, oligonucleotides, and proteins.[1,2] CaP also holds promise as a vaccine adjuvant[3−5] where nanoscale formulations have been shown to be more effective than micrometer-sized particles at targeting lymph node dendritic cells (DCs) for enhancing immunity.[6,7] Unfortunately, unstabilized CaP colloids have a strong tendency to aggregate, and their controlled synthesis is challenging because even small variations in pH, temperature, calcium:phosphate ratio, or precipitation technique can significantly affect particle stoichiometry, crystallinity, morphology, and size.[8−10] A wide variety of CaP synthesis schemes have been developed, ranging from microemulsion technologies[11−13] to the use of citrate,[14] surfactants,[15] porphyrin,[16] and oligonucleotides[17] as capping agents. However, reproducible production of stable CaP colloids in the sub-100 nm range remains difficult, and their controlled conjugation with peptides or proteins by any mechanism other than adsorption requires multiple chemical derivatization and purification steps.

In vertebrate bones, CaP is present in the form of hydroxyapatite [HA; $Ca_{10}(PO_4)_6(OH)_2$] nanocrystals that are 30–50 nm long, 20–25 nm wide, and 1.5–4 nm thick.[18] These nanoplates are embedded in a composite of collagen fibrils and noncollagenous proteins that exhibit Ca^{2+} and hydroxyapatite binding properties by virtue of being phosphorylated and rich in negatively charged (acidic) residues.[19] Several noncollagenous phosphoproteins have been shown to promote HA nucleation and to control the kinetics of crystal growth,[19,20] suggesting that they may be good candidates for the biomimetic mineralization of CaP nanoparticles. However, the same proteins can also inhibit mineralization, and the mechanisms that are at play for either process remain unclear and controversial.[19,20]

Solid binding peptides (SBPs) isolated by phage or cell surface display[21] present an alternative to naturally occurring proteins for the biomineralization of technologically valuable materials.[22] In this molecular biomimetic approach to material synthesis, SBPs are used either in isolation or as part of a larger protein or organism to nucleate, organize, and assemble inorganic structures with nanoscale control of composition and architecture.[23,24] The approach is powerful. For example, we have shown that "designer proteins" incorporating SBPs can be used to nucleate and cap Cu_2O nanoparticles under thermodynamically unfavorable conditions,[25] organize these nanoparticles onto DNA guides,[25] control the size and shape of silver crystals,[26] and mineralize multicolored ZnS quantum dots whose protein shell is active for antibody binding.[27,28]

Here, we describe disulfide-constrained CaP binding peptides that, when inserted within the active site loop of *Escherichia coli*

Received: December 2, 2011
Revised: January 19, 2012
Published: January 22, 2012

Table 1. Physicochemical Characteristics of CaP Binding Peptides Isolated by Cell Surface Display and Tested for Mineralization Ability (top) and Comparison to Hydroxyapatite Binding Peptides Identified by Phage Display (bottom)

Name	Sequence[a]	M_r (Da)	pI	Hydropathy[b]	Reference
PN21	*CGP*LGMRSESAIGKE*GPC*	1277.4	6.14	-0.483	This work
PN38	*CGP*EDIDAVSVGEVQ*GPC*	1260.3	3.43	0.017	This work
PN52	*CGP*PAQAHPWPHRYG*GPC*	1416.5	9.18	-1.517	This work
PA01[c]	*CGP*VRRLMGGSWKRV*GPC*	1444.7	12.3	-0.483	This work
PA44	*CGP*KDVVVGVPGGQD*GPC*	1169.3	4.21	-0.033	This work
PA93	*CGP*GHLSPRFRGGR*GPC*	1296.4	12.3	-1.175	This work
HABP1	*C*MLPHHGA*C*	761.9	6.69	-0.129	45
CLP12	NPYHPTIPQSVH	1389.5	6.92	-1.025	46
HA-1	SVSVGMKPSPRP	1214.4	11.0	-0.475	51
S	STLPIPHEFSRE	1412.5	5.38	-0.758	52
V	VTKHLNQISQSY	1417.5	8.57	-0.725	52

[a]Amino acids are color-coded as follows: hydrophobic, gray; acidic, red; basic, cyan; hydroxyl side chain, olive; amide side chain, teal. Invariant tripeptides flanking the dodecamers are italicized. [b]Positive hydropathy scores denote hydrophobic sequences, while negative scores denote hydrophilic ones. The higher and lower the score, the more hydrophobic and hydrophilic, respectively, the sequence is. [c]The PA01 sequence was isolated more than 50 times on both annealed and nonannealed samples.

thioredoxin 1 (TrxA), reproducibly mineralize nanoparticles that are 50−70 nm in hydrodynamic diameter and consist of an ≈25 nm amorphous calcium phosphate (ACP) core stabilized by a protein shell. We further show that disruption of the disulfide bond causes an increase of ∼3-fold in the diameter of mineralized particles, indicating that the conformation of an SBP can have a profound influence on the mineralization process. Finally, we provide preliminary evidence that the small CaP core−protein shell nanoparticles might be effective vehicles for delivery of adjuvanted antigen to DCs.

EXPERIMENTAL PROCEDURES

Electrodeposition of Calcium Phosphate on Titanium. CaP chips were synthesized using a modification of published protocols.[29,30] Briefly, calcium phosphate was electrodeposited with a constant current of −2.5 mA/cm^2 for 20 min at 60 °C on a 0.127 mm thick titanium foil [>99.9% (Sigma-Aldrich)] from an electrolyte consisting of 100 mM $Ca(NO_3)_2$ and 50 mM $NH_4H_2PO_4$. All experiments were conducted in a quiescent 150 mL cell using a platinum wire for a counter-electrode. Half of the samples were annealed by being heated for 8 h at 450 °C in an oven while the rest were dried with N_2.

Selection of CaP Binding Peptides. The FliTrx cell surface display system (Invitrogen) was used to select disulfide-constrained CaP binding dodecapeptides through five rounds of biopanning as previously described.[28,31] Independent selections were conducted on ∼1 cm^2 annealed and non-annealed substrates. Randomly selected colonies (78 for annealed samples and 66 for nonannealed samples) were sequenced using the Big Dye Terminator sequencing kit (Applied Biosystems) using either 5′-ATTCACCTGACTGAC-GAC-3′ as a forward primer or 5′-CCCTGATATTCGT-CAGCG-3′ as a reverse primer. Six clones lacking internal cysteine residues and exhibiting a broad range of hydrophobicities and isoelectric points (Table 1) were selected for further studies.

Construction, Expression, and Purification of CaP Binding Proteins. Derivatives of *E. coli* thioredoxin 1 (TrxA) displaying disulfide-constrained CaP binding peptides in place of the Cys-Gly-Pro-Cys active site sequence of native TrxA were constructed as previously described.[28] Briefly, pFliTrx derivatives encoding the target dodecapeptides were digested with *Apa*LI and *Rsr*II, and the purified 220 bp fragment was ligated with the backbone of pT-Trx[32] that had been digested with the same enzymes. The resulting plasmids were named pTrxA-PA*x* or pTrxA-PN*x*, where PA and PN refer to sequences selected on annealed (PA) and nonannealed (PN) CaP chips, respectively, and *x* denotes the numerical identifier of the CaP binding peptide. The Cys^{32} residue of TrxA::PA44 and TrxA::PN21 was converted to a serine by site-directed mutagenesis of the corresponding plasmids using the QuikChange (Stratagene) kit and primers 5′-CTGGGCA-GAGTGGTCCGGTCCGAAAGATG-3′ and 5′-CATCTTTCGGACCGGACCACTCTGCCCAG-3′. The integrity of all constructs was verified by DNA sequencing.

BL21(DE3) cells harboring the plasmids described above were grown to midexponential phase (A_{600} ≈ 0.5) in 500 mL of LB medium supplemented with 34 μg/mL chloramphenicol. Protein synthesis was initiated by addition of 0.4 mM isopropyl thiogalactopyranoside (IPTG), and cultures were immediately transferred to a water bath held at 25 °C. After being incubated at this temperature for 4 h, cells were sedimented by centrifugation at 3000*g* for 15 min, resuspended in 20 mM Tris-HCl (pH 7.5), 2.5 mM EDTA, and 1 mM PMSF to a concentration of 100 A_{600} units/mL, and disrupted by three cycles of homogenization on a French pressure cell operated at 10000 psi. Insoluble material was removed by centrifugation at 14000*g* for 15 min. Aliquots of clarified extracts (≈15 mL) were transferred to 30 mL Corex tubes and held in an 80 °C water bath for 10 min to precipitate the majority of host proteins. Aggregated fractions were removed by centrifugation at 14000*g* for 10 min. Supernatants were diluted with 60 mL of buffer A [20 mM Tris-HCl (pH 7.5)] and loaded onto a DE52 (Whatman) anion exchange column (7.0 cm length and 1.0 cm diameter) equilibrated in buffer A. The column was developed in the same buffer at a rate of 1 mL/min for 60 min to wash out contaminants, and purified designer proteins were recovered in the 25−100 mM NaCl fractions of a 60 min gradient elution (0 to 500 mM NaCl in buffer A). Proteins were dialyzed against ddH_2O overnight and stored at −80 °C. Purity was determined on overloaded gels using a modified sodium dodecyl sulfate−polyacrylamide gel electrophoresis protocol.[33]

Biomineralization of CaP Nanoparticles. For biomineralization experiments, a 1.8 mL solution containing 5 μM

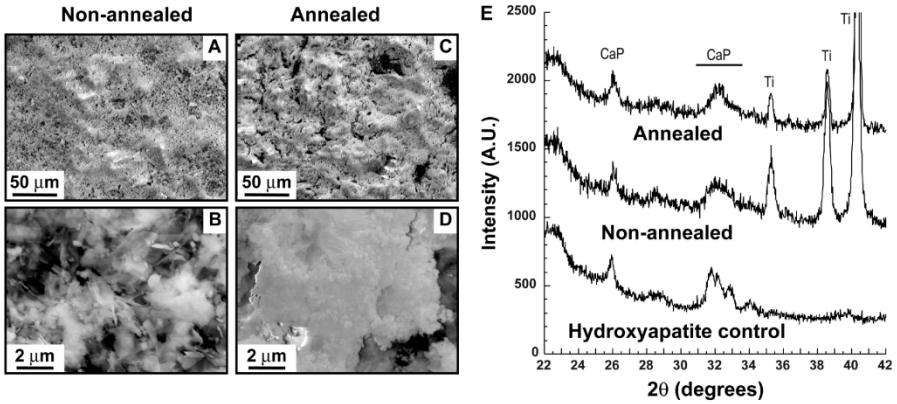

Figure 1. Characterization of CaP chips. Nonannelaed (A and B) and annealed (C and D) samples were imaged by SEM at two different magnifications. Panel E shows XRD spectra for both samples. Hydroxyapatite powder was used as a control. Reflections corresponding to CaP phases and the underlying Ti substrate are labeled.

protein in a 1 mM $(NH_4)_2HPO_4/NH_4H_2PO_4$ mixture (pH 7.5) was placed in a 15 mL, round-bottom, disposable borosilicate tube (VWR) that had been cleaned with ddH_2O, acetic acid, acetone, and ultrapure ddH_2O, in sequence, and fitted with a 1 cm diameter stir bar. The mixture was held at 4 °C for 30 min at a stirring rate of 6 (Corning PC-310), after which 200 μL of a 16.7 mM solution of $Ca(NO_3)_2$ was fed in 8 μL increments ~5 s apart using a 25G delivery needle or Pipetman (Eppendorf P20). The mixture was allowed to age for 2 h at 4 °C and held at room temperature for 12−24 h before being characterized.

Analytical Techniques. Hydrodynamic diameters were measured by dynamic light scattering (DLS) on a Nano-ZS Zetasizer (Malvern). For transmission electron microscopy (TEM) imaging, 5 μL of the solution was deposited on a carbon-coated copper TEM grid and allowed to air-dry. Low- and high-resolution TEM images and selected area electron diffraction (SAED) patterns with an aperture size of 40 μm were collected on a FEI Tecnai G2 F20 S/TEM instrument operated at an accelerating voltage of 200 kV. For scanning electron microscopy (SEM) imaging, samples (≈100 μL) were allowed to contact clean, ≈1 cm^2 silicon wafers for 30 min, and excess fluid was removed by wicking with a laboratory tissue. The substrate was rinsed with ddH_2O to remove salts, air-dried, and coated with a 7−10 nm Au/Pd film. Micrographs were taken with a FEI Sirion scanning electron microscope at an acceleration voltage of 10 keV. Energy dispersive X-ray spectroscopy (EDS) was used to find the average ratio of calcium, phosphorus, and oxygen in the substrate. X-ray diffraction (XRD) measurements were taken on a Bruker D8 Focus instrument using Cu Kα radiation. Data were collected for 2θ values ranging from 22° to 42° with 0.02° steps.

Animal Studies. The adjuvancy effect of biofabricated CaP nanoparticles was compared to that of AdjuPhos (Brenntag Biosector), a commercial aluminum phosphate adjuvant consisting of 0.49% (w/w) aluminum and 1.52% phosphate. CaP nanoparticles were synthesized using TrxA::PA44 as described in Biomineralization of CaP Nanoparticles except that all solutions were made in endotoxin-free water (MD Bio) and all glassware was passivated by being rinsed in tap water, acetic acid, ddH_2O, acetone, and ultrapure ddH_2O before being autoclaved at 120 °C for 30 min. Pyrogens were inactivated by baking the glassware at 250 °C for 30 min. After being aged at 4 °C for 2 h, samples were filtered through a 0.22 μm cellulose acetate filter and split into two halves, one of which was used for DLS characterization and protein assays and the other for immunization in mice. The final protein concentration was found to be 3.2 μM by a Bradford assay because of losses incurred during filtration. However, the size of the particles remained in the 70 nm range. As a control, a preparation of 3.2 μM TrxA::PA44 in a 1 mM $(NH_4)_2HPO_4/NH_4H_2PO_4$ mixture (pH 7.5) was filtered through a 0.22 μm membrane and supplemented with 1.65 mM AdjuPhos (an aluminum concentration identical to that of the calcium in the nanoparticles). Groups of five C57BL/6 mice (6−10 weeks old and weighing 20−30 g) were injected subcutaneously with 4 × 50 μL of the preparations described above into the four foot pads for a total antigen load of 8 μg. No inflammation was observed at injection sites, and animals were bled at 9 and 21 days. Anti-TrxA IgG titers were measured in serum with an enzyme-linked immunosorbent assay (ELISA) essentially as described previously[34] using plates coated with wild-type TrxA and validated for linearity with mouse anti-TrxA rabbit monoclonal antibodies (Invitrogen, clone C63C6).

RESULTS

Selection of Calcium Phosphate Binding Peptides. Among the various inorganic compounds that hold promise for DC maturation, we selected calcium phosphate (CaP) because it is cheap, biocompatible, biodegradable, and likely to be safe. CaP adjuvants are typically synthesized by uncontrolled precipitation schemes, yielding a broad distribution of agglomerates that range in size from 300 nm to 4 μm and have calcium:phosphate (Ca:P) molar ratios ranging from 1.35 to 1.83.[35] In one of the most detailed analyses to date, Jiang and co-workers[36] reported that a commercial adjuvant manufactured by the former Reheis Inc. consisted of calcium-deficient hydroxyapatite with a Ca:P ratio of 1.39 and contained needlelike particles and irregularly shaped plates. However, others[37] have found commercial adjuvants to have a Ca:P ratio

of 1.5, a molecular composition closer to that of tricalcium phosphate [$Ca_3(PO_4)_2$].

Our first task was to generate CaP "chips" that were chemically and morphologically representative of commercial CaP adjuvants and compatible with the FliTrx cell surface display system that we have previously used to identify SBPs.[28,31] To this end, we electrodeposited ≈10 μm thick calcium phosphate films on titanium foil from a $Ca(NO_3)_2$/$NH_4H_2PO_4$ electrolyte (Electrodeposition of Calcium Phosphate on Titanium). Because high temperatures drive off coordinated water from inorganic materials, half of the samples were annealed by heating at 450 °C for 8 h, while the rest were dried under a nitrogen stream and characterized as deposited.

SEM imaging revealed that the annealed samples (Figure 1C,D) consisted primarily of spherical nodules, while nonannealed chips also contained crystalline platelets and needles (Figure 1A,B). The Ca:P ratio was found to be 1.44 for annealed samples and 1.32 for nonannealed samples by energy dispersive X-ray spectroscopy (EDS) analysis in the scanning electron microscope. In addition, reflections characteristic of calcium phosphate-containing phases were identified in the 26° and 31−34° 2θ regions of both samples by X-ray diffraction [XRD (Figure 1E)]. Thus, our electrodeposited CaP chips are compositionally and morphologically similar to typical calcium phosphate adjuvants.[35−37]

In the *E. coli* FliTrx cell surface display system,[38] random dodecapeptides are displayed as disulfide-constrained loops within the active site of *E. coli* thioredoxin 1 (TrxA), which is itself inserted within the major flagellar protein FliC. We used FliTrx biopanning to isolate CaP binding peptides on both annealed and nonannealed substrates. Because there are multiple solutions to the problem of inorganic binding,[21] sequences obtained after biopanning did not converge toward a consensus. We arbitrarily chose a subset of six peptides exhibiting a broad range of pIs and hydrophilicities for further work with the expectation that some would function as efficient CaP mineralizers. Three of these (PN series) were isolated using nonannealed chips, while the others (PA series) were selected on annealed substrates (Table 1).

Protein-Aided Mineralization of CaP Nanoparticles. An accurate comparison of the mineralizing ability of these CaP binding peptides would ideally require that they exhibit the same solubility (which is generally not true of short hydrophobic peptides such as those listed in Table 1) and that they be displayed within the same structural context. To address this issue, we constructed a series of *E. coli* TrxA derivatives in which the authentic cysteine-glycine-proline-cysteine (CGPC) active site sequence was replaced with one of the CaP binding dodecamers in Table 1 flanked by invariant Cys-Gly-Pro (CGP) and Gly-Pro-Cys (GPC) tripeptides. The resulting proteins, which are monomeric and range in molecular mass from 12.87 to 13.14 kDa, were expressed at ∼35% of the level of the total cellular protein and in a mostly soluble form using T7-driven transcription (Figure 2, lanes 1−3). Because TrxA exhibits high thermostability,[39] it was possible to achieve 80% purification by heating crude cell extracts at 80 °C for 10 min and removing aggregated host proteins by centrifugation (Figure 2, lanes 4 and 5). High-purity material (≈99%) could then be recovered in a single ion exchange chromatography step (Figure 2, lane 6).

Because calcium phosphate does not exhibit useful optical absorption or emission properties, we screened CaP binding TrxA derivatives for their ability to mediate nanoparticle

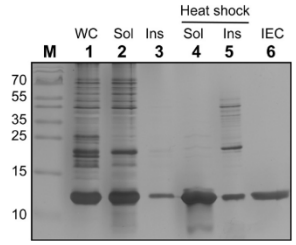

Figure 2. Purification of TrxA::PA44 by heat shock and ion exchange chromatography (IEC): lane M, markers; lane WC, whole cells; lanes Sol and Ins, soluble and insoluble fractions, respectively, before and after incubation at 80 °C for 10 min; lane IEC, ion exchange chromatography purification of heat-shocked soluble fractions. The positions of the molecular mass markers (lane M) are indicated in kilodaltons on the left of the gel, which was stained with silver to reveal purified protein and contaminants.

formation using dynamic light scattering (DLS), a technique that provides information about the hydrodynamic diameter of colloids in suspension. We dedicated significant effort to optimizing the synthesis step and tested different calcium and phosphate salts, pH values, protein concentrations, mixing regimes, temperatures, and aging times, eventually settling on the protocol described in Biomineralization of CaP Nanoparticles. Experiments conducted in the absence of protein or with wild-type TrxA gave rise to the precipitation of large polydisperse species (Figure 4A,B). However, among the six proteins tested, three (TrxA::PN21, TrxA::PN38, and TrxA::PA44) proved suitable for the reproducible production of sub-100 nm CaP particles. Of note, TrxA::PA01 was ineffective in mediating nanoparticle formation in spite of the fact that the PA01 sequence was isolated multiple times on both annealed and nonannealed chips. Thus, there is no correlation between promiscuous binding and nanoparticle synthesis ability.

Hydrodynamic diameters determined by DLS were 70 ± 20 nm in the case of TrxA::PN21 and TrxA::PN38 and 60 ± 20 nm in the case of TrxA::PA44. The colloids were clear and stable for at least 3 weeks when stored at 4 °C, indicating the presence of a capping protein shell. TEM imaging of TrxA::PA44-mineralized samples (Figure 3A,B) confirmed the presence of roughly spherical species that had an average diameter of 25 ± 5 nm (n = 110). The discrepancy with diameters obtained by DLS is likely due to the difficulty in obtaining good contrast when imaging CaP by TEM and to the fact that hydrated particles are bounded by a protein shell that adds to their size. Based on the lack of observable particle faceting and the fact that selected area electron diffraction (SAED) patterns were diffuse and lacked rings or spots (Figure 3C), it is likely that the templated material is amorphous calcium phosphate [ACP; $Ca_9(PO_4)_6$], a noncrystalline phase of calcium phosphate that is the initial solid precipitating from supersaturated solutions.[40]

Controlling Particle Size: Influence of the Disulfide Bond. CaP binding sequences are displayed within a disulfide-bonded loop both during the initial FliTrx screen and following transfer to the soluble TrxA scaffold. This conformational context has been shown to influence the adhesion of certain solid binding peptides to their cognate inorganics,[41−44] but how it impacts materialization remains unclear. To explore this issue,

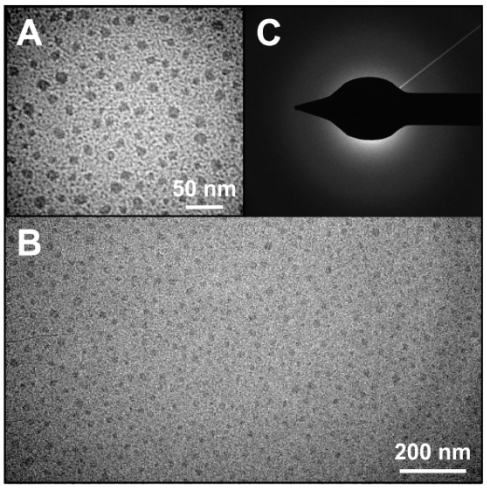

Figure 3. TEM analysis of nanoparticles produced in the presence of TrxA::PA44. High-resolution (A) and low-resolution (B) TEM images show the characteristic size and polydispersity of CaP nanoparticles obtained under our experimental conditions. (C) Selected area electron diffraction (SAED) patterns were diffuse with no distinguishable spots or rings, suggesting that the mineral is amorphous calcium phosphate (ACP).

we use site-directed mutagenesis to convert the first cysteine residue of TrxA::PA44 to serine and conducted side by side mineralization experiments with no protein, wild-type TrxA, TrxA::PA44, and the TrxA::PA44-C32S mutant. Samples were transferred to silicon oxide substrates, coated with a 7−10 nm layer of gold−palladium, and imaged by SEM.

In agreement with DLS data and consistent with the low-solubility product of calcium phosphate, precipitation in the absence of additive gave rise to heterogeneous populations enriched in micrometer size particles (Figure 4A) while mineralization in the presence of wild-type TrxA led to the formation of aggregates consisting of interconnected nodules extending over large dimensions (Figure 4B). As expected from TEM imaging (Figure 3), and in sharp contrast with the results described above, samples prepared in the presence of TrxA::PA44 were populated by discrete and mostly spherical particles whose mean size (70 ± 15 nm; $n = 44$) was within the expected range when taking into account the thickness of the Au/Pd coating. Remarkably, altering the conformation of the PA44 peptide by elimination of the disulfide bond led to a net reduction in the number of particles and a concomitant 3-fold increase in average diameter as determined by analysis of SEM images (170 ± 30 nm; $n = 55$) and confirmed by DLS measurements (210 ± 50 nm). Similar results were obtained when the same cysteine to serine substitution was introduced into TrxA::PN21. We conclude that the conformational context plays an important role in determining the affinity and/or capping ability of several of our binders, a feature that can be exploited for manufacturing core−shell particles of different sizes.

Immunogenicity. Conjugates between nanoparticles and antigenic molecules hold potential for effective vaccination because of the fact that particles with diameters inferior to 100 nm drain to the lymph nodes where the probability of encountering immature DCs increases.[6,7] We therefore used TrxA::PA44 to synthesize CaP nanoparticles as described above, except that depyrogenated glassware and endotoxin-free water were used in all steps and that the solution was filtered through a sterile 0.2 μm membrane to eliminate large particulate contaminants. Groups of five C57BL/6 mice were vaccinated subcutaneously with the nanoparticle formulation (8 μg of total protein load) or with the same amount of soluble TrxA::PA44 supplemented with enough of the commercial adjuvant AdjuPhos so that the Al^{3+} concentration would equal that of Ca^{2+} in the nanoparticulate formulation. After 9 days, anti-TrxA titers were slightly higher in the serum of nanoparticle-treated animals than in control mice (Figure 5). However, whereas antibody levels remained constant over time in the control group, they were more than 3 times higher in mice vaccinated with the nanoparticle formulation 21 days postchallenge.

■ DISCUSSION

We have isolated disulfide-constrained dodecapeptides suitable for the synthesis of stable sub-100 nm nanoparticles consisting of an ACP core capped by a protein shell. The three sequences supporting nanoparticle formation [PA44, PN21, and PN38 (Table 1)] contained at least two and up to four negatively charged aspartates (D) and/or glutamates (E). Overrepresentation of these acidic amino acids was not unexpected because they have high affinity for Ca^{2+} ions and are found in high proportions and local densities in proteins involved in biological apatite formation.[18,19] In contrast, the three CaP binders that failed to yield stable nanoparticles (PN52, PA01, and PA93) all contained three or more basic residues and carried a net positive charge under our synthesis conditions (pH 7.5). Remarkably, hydroxyapatite binders identified by others through bacteriophage display (Table 1) were also enriched with histidines (H), arginines (R), and lysines (K). Two of these peptides were previously tested for CaP mineralization, albeit under different conditions than used in the present study. In a synthetic form, peptide HABP1 caused the formation of octacalcium phosphate [OCP; $Ca_8H_2(PO_4)_6{\cdot}5H_2O$] crystals that projected from a central core and were 400−800 nm in width and several micrometers in length.[45] On the other hand, synthetic CLP12 promoted the mineralization of micrometer-sized hydroxyapatite plates consisting of randomly oriented ≈20 nm nanocrystals.[46] It is therefore clear that acidic amino acids are not absolutely required for a peptide to either bind CaP or template the mineralization of thermodynamically stable calcium phosphate polymorphs (e.g., HA and OCP). However, our results suggest that aspartic acid and glutamic acid are important for capping and stabilizing nanoscale clusters of ACP, which should be the first CaP phase to precipitate out of solution.[40] Considering that ACP can convert to more energetically favorable phases such as OCP and biological apatites,[47] it is tempting to hypothesize that transient sequestration of ACP nanoparticles could be one of the mechanisms by which acidic bone and enamel-associated proteins regulate biomineralization. This process would be a useful complement to face-specific adsorption mechanisms[20] in preventing runaway crystal growth.

The phage and cell surface display libraries that are typically used to pan for solid binding peptides (SBPs) can yield linear or disulfide-bonded sequences.[21] In traditional applications (e.g., epitope mapping and identification of protein interaction

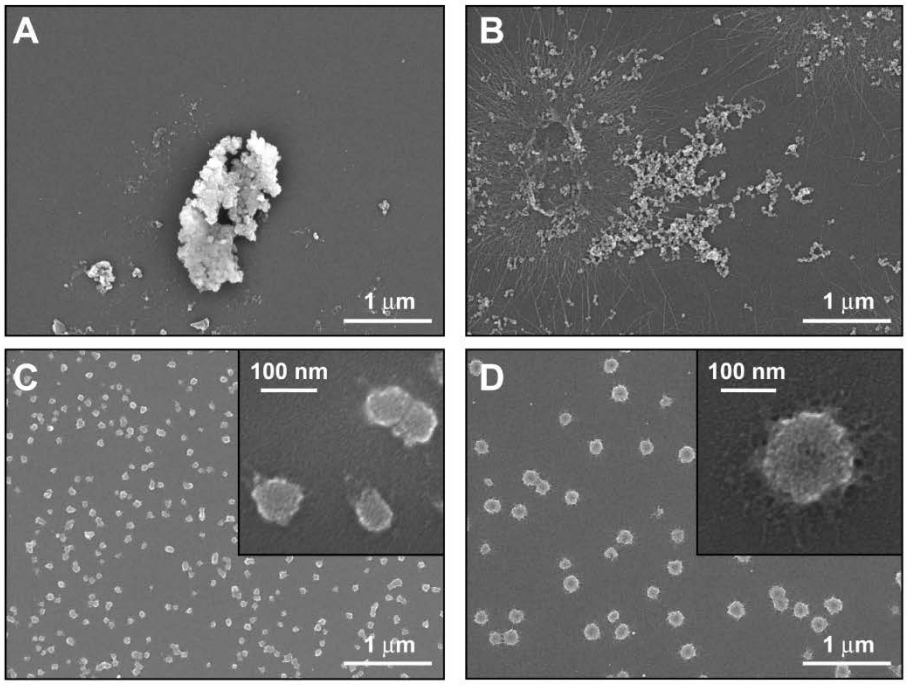

Figure 4. SEM imaging of CaP structures mineralized in the absence of protein (A) or in the presence of wild-type TrxA (B), TrxA::PA44 (C), and TrxA::PA44-C32S (D). The insets of panels C and D show higher-resolution images.

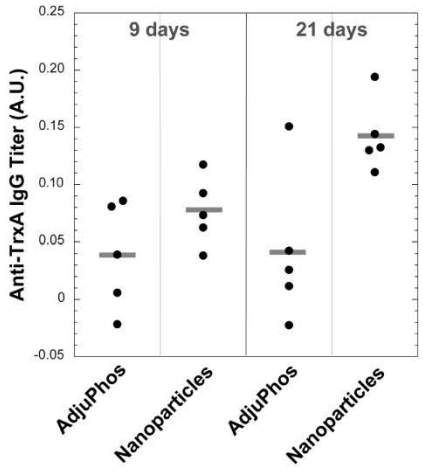

Figure 5. Anti-TrxA IgG titers in the serum of C57BL/6 mice measured by an ELISA 9 and 21 days postchallenge with TrxA::PA44 and alum or TrxA::PA44-stabilized nanoparticles. Titers for individual animals and cohort means (horizontal bars) are shown. Data are corrected for preimmune backgrounds. Confidence levels are 84.6% for 9 day data and 98.5% for 21 day data.

domains), disulfide-bonded peptides are generally more efficient binders because they exhibit a low degree of conformational freedom and make stable contacts with protein targets. In solid binding, however, the impact of conformational flexibility is less clear. For instance, we previously reported that presentation in a disulfide-constrained loop is critical for a cuprous oxide binding peptide to adhere to this material.[42] Similarly, a disulfide-bonded conformation increased the affinity of both a platinum- and gold-binding peptide for Pt and Au surfaces, respectively, relative to the corresponding linear conformations.[43,44] By contrast, presentation in a loop had no effect on the adsorption behavior of a different gold binder[43] and decreased the affinity of a TiO_2/SiO_2 binding peptide for these oxides.[41] PA44 and PN21 likely belong to the former category of solid binders because a lower affinity of TrxA::PA44-C32S (and TrxA::PN21-C32S) for CaP, paired with the rapid kinetics of ACP formation,[47] would manifest itself by the growth of larger particles before protein capping occurs. From a practical standpoint, the ability to manipulate particle size via a single mutation in the CaP binding sequence should prove useful for tethering different loads of protein/antigen on the nanoparticle surface.

The observation that nanoparticles <100 nm in diameter preferentially accumulate in the lymph nodes where they encounter a high concentration of immature DCs has been exploited in the design of synthetic nanovaccines that are more efficient at triggering adaptive immunity.[6,48−50] The TrxA::PA44-mineralized particles described herein are in the proper

size range for effective diffusion into the lymphatic system and comprise a CaP core that may serve as a "danger signal" to activate DC maturation. As a preliminary test of our design, we vaccinated mice with TrxA::PA44 that was in a nanoparticle-bound formulation or supplemented with the commercial adjuvant AdjuPhos. We found that although anti-TrxA levels were comparable in the two cohorts 9 days postinjection, there was 3 times more anti-TrxA in the serum of animals vaccinated with nanoparticles than in the control group ($p < 0.05$) after 3 weeks. We are aware that absolute antibody titers were low, which is likely due to the fact that *E. coli* TrxA is 30% identical to mouse TrxA and a poor immunogen. Nevertheless, our results suggest that direct mineralization of antigen shell−CaP core nanoparticles might be a simple and cost-effective route for nanovaccine manufacturing. We are currently exploring this concept further using TrxA::PA44−ovalbumin fusion proteins.

■ CONCLUSIONS

We have identified CaP binding dodecapeptides that are acidic and suitable for the synthesis of calcium phosphate core−protein shell nanoparticles. The hydrodynamic diameter of these hybrid structures can be varied from ∼60 to ∼200 nm by eliminating the disulfide bond holding the CaP binding sequence in a constrained loop. Considering that the nanoparticle formulation enhances TrxA immunogenicity and because TrxA fusions are easy to construct and purify, such inorganic core−protein shell architectures might prove useful for delivering adjuvanted antigens to DCs.

■ AUTHOR INFORMATION

Corresponding Author

*Telephone: (206) 685-7659. Fax: (206) 685-3451. E-mail: baneyx@uw.edu.

Present Address

[‖]Department of Pediatrics, Emory University School of Medicine, Atlanta, GA 30322.

Author Contributions

D.C. and W.Z. contributed equally to this work.

Notes

The authors declare no competing financial interest.

■ ACKNOWLEDGMENTS

We are grateful to Zahra Afsharinejad for performing the ELISAs and to Shobana Vaidyanathan for help with animal studies. This work was supported by a Grand Challenge Exploration grant from the Bill and Melinda Gates Foundation, a National Science Foundation-Nanotechnology and Interdisciplinary Research Team award on Protein-Aided Nanomanufacturing (CMMI-0709131), the National Science Foundation (NSF) Genetically Engineered Materials Science and Engineering Center (DMR-0520657), and National Institutes of Health Grants P30ES007033 and U19ES019545. Part of the work was conducted at the University of Washington Nanotech User Facility, a member of the NSF National Nanotechnology Infrastructure Network.

■ ABBREVIATIONS

ACP, amorphous carbon phosphate; CaP, calcium phosphate; TrxA, *E. coli* thioredoxin 1; ACP, amorphous calcium phosphate; DC, dendritic cell; HA, hydroxyapatite; SBP, solid binding peptides; OCP, octacalcium phosphate.

■ REFERENCES

(1) Bose, S., and Tarafder, S. (2011) Calcium phosphate ceramic systems in growth factor and drug delivery for bone tissue engineering: A review. *Acta Biomater.*, DOI: DOI: 10.1016/j.actbio.2011.11.017.

(2) Uskoković, V., and Uskoković, D. P. (2011) Nanosized hydroxyapatite and other calcium phosphates: Chemistry of formation and application as drug and gene delivery agents. *J. Biomed. Mater. Res., Part B 96*, 152−191.

(3) Aggerbeck, H., Fenger, C., and Heron, I. (1995) Booster vaccination against diphtheria and tetanus in man: Comparison of calcium-phosphate and aluminum hydroxide as adjuvants. *Vaccine 13*, 1366−1374.

(4) He, Q., Mitchell, A., Morcol, T., and Bell, S. J. D. (2002) Calcium phosphate nanoparticles induce mucosal immunity and protection against herpes simplex virus type 2. *Clin. Diagn. Lab. Immunol. 9*, 1021−1024.

(5) He, Q., Mitchell, A. R., Johnson, S. L., Wagner-Bartak, C., Morcol, T., and Bell, S. J. D. (2000) Calcium phosphate nanoparticle adjuvant. *Clin. Diagn. Lab. Immunol. 7*, 899−903.

(6) Manalova, V., Flace, A., Bauer, M., Schwarz, K., Saudan, P., and Bachman, M. F. (2008) Nanoparticles target distinct dendritic cell populations according to their size. *Eur. J. Immunol. 38*, 1404−1413.

(7) Reddy, S. T., Rehor, A., Schmoekel, H. G., Hubbell, J. A., and Swartz, M. A. (2006) In vivo targeting of dendritic cells in lymph nodes with poly(propylene sulfide) nanoparticles. *J. Controlled Release 112*, 26−34.

(8) Al-Qasas, N. S., and Rohani, S. (2005) Synthesis of pure hydroxyapatite and the effect of synthesis conditions on its yield, crystallinity, morphology and mean particle size. *Sep. Sci. Technol. 40*, 3187−3224.

(9) Ferraz, M. P., Monteiro, F. J., and Manuel, C. M. (2004) Hydroxyapatite nanoparticles: A review of preparation methodologies. *J. Appl. Biomater. Biomech. 2*, 74−80.

(10) Rodriguez-Lorenzo, L. M., and Vallet-Regi, M. (2000) Controlled crystallization of calcium phosphate apatites. *Chem. Mater. 12*, 2460−2465.

(11) Bose, S., and Saha, S. K. (2003) Synthesis and characterization of hydroxyapatite nanopowders by emulsion technique. *Chem. Mater. 15*, 4464−4469.

(12) Morgan, T. T., Muddana, H. S., Altinoglu, E. I., Rouse, S. M., Tabaković, A., Tabouillot, T., Russin, T. J., Shanmugavelandy, S. S., Butler, P. J., Eklund, P. C., Yun, J. K., Kester, M., and Adair, J. H. (2008) Encapsulation of organic molecules in calcium phosphate nanocomposite particles for intracellular imaging and drug delivery. *Nano Lett. 8*, 4108−4115.

(13) Roy, I., Mitra, S., Maitra, A., and Mozumdar, S. (2003) Calcium phosphate nanoparticles as novel non-viral vectors for targeted gene delivery. *Int. J. Pharm. 250*, 25−33.

(14) Martins, M. A., Santos, C., Almeida, M. M., and Costa, M. E. (2008) Hydroxyapatite micro- and nanoparticles: Nucleation and growth mechanisms in the presence of citrate species. *J. Colloid Interface Sci. 318*, 210−216.

(15) Cai, Y. R., Liu, Y. K., Yan, W. Q., Hu, Q. H., Tao, J. H., Zhang, M., Shi, Z. L., and Tang, R. K. (2007) Role of hydroxyapatite nanoparticle size in bone cell proliferation. *J. Mater. Chem. 17*, 3780−3787.

(16) Ganesan, K., Kovtun, A., Neumann, S., Heumann, R., and Epple, M. (2008) Calcium phosphate nanoparticles: Colloidally stabilized and made fluorescent by a phosphate-functionalized porphyrin. *J. Mater. Chem. 18*, 3655−3661.

(17) Welzel, T., Meyer-Zaika, W., and Epple, M. (2004) Continuous preparation of functionalised calcium phosphate nanoparticles with adjustable crystallinity. *Chem. Commun. 21*, 1204−1205.

(18) Palmer, L. C., Newcomb, C. J., Kaltz, S. R., Spoerke, E. D., and Stupp, S. I. (2008) Biomimetic systems for hydroxyapatite mineralization inspired by bone and enamel. *Chem. Rev. 108*, 4754−4783.

(19) George, A., and Veis, A. (2008) Phosphorylated proteins and control over apatite nucleation, crystal growth and inhibition. *Chem. Rev. 108*, 4670−4693.
(20) Hunter, G. K., O'Young, J., Grohe, B., Karttunen, M., and Golberg, H. A. (2010) The flexible polyelectrolyte hypothesis of protein-biomineral interaction. *Langmuir 26*, 18639−18646.
(21) Baneyx, F., and Schwartz, D. T. (2007) Selection and analysis of solid-binding peptides. *Curr. Opin. Biotechnol. 18*, 312−317.
(22) Dickerson, M. B., Sandhage, K. H., and Naik, R. R. (2008) Protein- and peptide directed synthesis of inorganic materials. *Chem. Rev. 108*, 4935−4978.
(23) Sarikaya, M., Tamerler, C., Jen, A. K., Schulten, K., and Baneyx, F. (2003) Molecular biomimetics: Nanotechnology through biology. *Nat. Mater. 2*, 577−585.
(24) Sarikaya, M., Tamerler, C., Schwartz, D. T., and Baneyx, F. (2004) Materials assembly and formation using engineered polypeptides. *Annu. Rev. Mater. Res. 34*, 373−408.
(25) Dai, H., Choe, W. S., Thai, C. K., Sarikaya, M., Traxler, B. A., Baneyx, F., and Schwartz, D. T. (2005) Nonequilibrium synthesis and assembly of hybrid inorganic-protein nanostructures using an engineered DNA binding protein. *J. Am. Chem. Soc. 127*, 15637−15643.
(26) Grosh, C., Schwartz, D. T., and Baneyx, F. (2009) Protein-based control of silver growth habit using electrochemical deposition. *Cryst. Growth. Des. 9*, 4401−4406.
(27) Zhou, W., and Baneyx, F. (2011) Aqueous, protein-driven synthesis of transition metal-doped ZnS immuno-quantum dots. *ACS Nano 5*, 8013−8018.
(28) Zhou, W., Schwartz, D. T., and Baneyx, F. (2010) Single pot biofabrication of zinc sulfide immuno-quantum dots. *J. Am. Chem. Soc. 132*, 4731−4738.
(29) Balamurugan, A., Benhayoune, H., Dumelie, N., Laquerriere, P., and Ferreira, J. M. F. (2008) Electrodeposition of fluorine-doped calcium phosphate coatings onto Ti6Al4V alloy: Chemical and structural characterization. *J. Am. Ceram. Soc. 91*, 2797−2801.
(30) Dumelie, N., Benhayoune, H., Richard, D., Laurent-Maquin, D., and Balossier, G. (2008) In vitro precipitation of electrodeposited calcium-deficient hydroxyapatite coatings on Ti6Al4V substrate. *Mater. Charact. 59*, 129−133.
(31) Thai, C. K., Dai, H., Sastry, M. S., Sarikaya, M., Schwartz, D. T., and Baneyx, F. (2004) Identification and characterization of Cu_2O- and ZnO-binding polypeptides by *Escherichia coli* cell surface display: Toward an understanding of metal oxide binding. *Biotechnol. Bioeng. 87*, 129−137.
(32) Yasukawa, T., Kanei-Ishii, C., Maekawa, T., Fujimoto, J., Yamamoto, T., and Ishii, S. (1995) Increase of solubility of foreign proteins in *Escherichia coli* by coproduction of the bacterial thioredoxin. *J. Biol. Chem. 270*, 25328−25331.
(33) Okajima, T., Tanabe, T., and Yasuda, T. (1993) Nonurea sodium dodecyl sulfate-polyacrylamide gel electrophoresis with high-molarity buffers for the separation of proteins and peptides. *Anal. Biochem. 211*, 293−300.
(34) Zhang, W., Zhang, W., Tang, Y., Zhang, J., and Liu, J. N. (2006) Characterization of an anti-thioredoxin monoclonal antibody. *Biotechnol. Lett. 28*, 183−188.
(35) Gupta, R. K., Rost, B. E., Relyved, E., and Siber, G. R. (1995) Vaccine design. In *Vaccine design* (Powell, M. F., and Newman, M. J., Eds.) pp 239−241, Plenum Press, New York.
(36) Jiang, D., Premachandra, G. S., Johnston, C., and Hem, S. L. (2004) Structure and adsorption properties of commercial calcium phosphate adjuvant. *Vaccine 23*, 693−698.
(37) Relyved, E. H. (1986) Preparation and use of calcium phosphate adsorbed vaccines. *Dev. Biol. Stand. 65*, 131−136.
(38) Lu, Z., Murray, K. S., Van Cleave, V., LaVallie, E. R., Stahl, M. L., and McCoy, J. M. (1995) Expression of thioredoxin random peptide libraries on the *Escherichia coli* cell surface as functional fusions to flagellin: A system designed for exploring protein-protein interactions. *Nat. Biotechnol. 13*, 366−372.
(39) LaVallie, E. R., DiBlasio, E. A., Kovacic, S., Grant, K. L., Schendel, P. F., and McCoy, J. M. (1993) A thioredoxin gene fusion expression system that circumvents inclusion body formation in the *E. coli* cytoplasm. *Nat. Biotechnol. 11*, 187−193.
(40) Zhao, J., Liu, Y. J., Sun, W.-B., and Zhang, H. (2011) Amorphous calcium phosphate and its applications in dentistry. *Chem. Cent. J. 5*, 40.
(41) Chen, H. B., Su, X. D., Neoh, K.-G., and Choe, W. S. (2009) Context-dependent adsorption behavior of cyclic and linear peptides on metal oxide. *Langmuir 25*, 1588−1593.
(42) Choe, W. S., Sastry, M. S. R., Thai, C. K., Dai, H., Schwartz, D. T., and Baneyx, F. (2007) Conformational control of inorganic adhesion in a designer protein engineered for cuprous oxide binding. *Langmuir 23*, 11347−11350.
(43) Hnilova, M., Oren, E. E., Seker, U. O. S., Wilson, B. R., Collino, S., Evans, J. S., Tamerler, C., and Sarikaya, M. (2008) Effect of molecular conformations on the adsorption behavior of gold-binding peptides. *Langmuir 24*, 12440−12445.
(44) Seker, U. O. S., Wilson, B., Dincer, S., Kim, I. W., Oren, E. E., Evans, J. S., Tamerler, C., and Sarikaya, M. (2007) Adsorption behavior of linear and cyclic genetically engineered platinum binding peptides. *Langmuir 23*, 7895−7900.
(45) Gungormus, M., Fong, H., Kim, I. L., Evans, J. S., Tamerler, C., and Sarikaya, M. (2008) Regulation of in vitro calcium phosphate mineralization by combinatorially selected hydroxyapatite-binding peptides. *Biomacromolecules 9*, 966−973.
(46) Chung, W. J., Kwon, K. Y., Song, J., and Lee, S. W. (2011) Evolutionary screening of collagen-like peptides that nucleate hydroxyapatite crystals. *Langmuir 27*, 7620−7628.
(47) Rabadjeva, D., Gergulova, R., Titorenkova, R., Tepavitcharova, S., Dyulgerova, E., Balarew, C., and Petrov, O. (2010) Biomimetic transformations of amorphous calcium phosphate: Kinetic and thermodynamic studies. *J. Mater. Sci.: Mater. Med. 21*, 2501−2509.
(48) Fifis, T., Gamvrellis, A., Crimeen-Irwin, B., Pietersz, G. A., Li, J., Mottram, P. L., McKenzie, I. F. C., and Plebanski, M. (2004) Size-dependent immunogenicity: Therapeutic and protective properties of nano-vaccines against tumors. *J. Immunol. 173*, 3148−3154.
(49) Reddy, S. T., Swartz, M. A., and Hubbell, J. A. (2006) Targeting dendritic cells with biomaterials: Developing the next generation of vaccines. *Trends Immunol. 27*, 573−579.
(50) Reddy, S. T., van der Vlies, A. J., Simeoni, E., Angeli, V., Randolph, G. J., O'Neil, C. P., Lee, K. L., Swartz, M. A., and Hubbell, J. A. (2007) Exploiting lymphatic transport and complement activation in nanoparticle vaccines. *Nat. Biotechnol. 25*, 1159−1164.
(51) Weiger, M. C., Park, J. J., Roy, M. D., Stafford, C. M., Karim, A., and Becker, M. L. (2010) Quantification of the binding affinity of a specific hydroxyapatite binding peptide. *Biomaterials 31*, 2955−2963.
(52) Segvich, S. J., Smith, H. C., and Kohn, D. H. (2009) The adsorption of preferential binding peptides to apatite-based materials. *Biomaterials 30*, 1287−1298.

Chapter 3: Thioredoxin-Ovalbumin Vaccines

The work detailed in this chapter was a collaborative effort between the groups of Dr. Francois Baneyx and Dr. Murali Krishna-Kaja. Dr. Weibin Zhou constructed the plasmid encoding the fusion protein (pTrxA::PA44-OVA), David Chiu purified the fusion protein (TrxA::PA44-OVA) and prepared vaccine formulations, and Albanus Moguche carried out the *in vivo* immunization and challenge experiments.

3.1: Introduction

The mineralization of calcium phosphate (CaP) nanoparticles (NPs) with an *E. coli* thioredoxin CaP binding derivative (TrxA::PA44) was previously detailed in Chapter 2. CaP NPs were evaluated as adjuvants in TrxA::PA44 vaccines, and anti-TrxA antibodies were elevated in mice immunized with vaccines containing CaP NP adjuvant as compared to commercial aluminum phosphate adjuvant. Applications of a thioredoxin vaccine are limited and studies using thioredoxin as an antigen mainly focus on the purification of anti-thioredoxin antibodies used for analysis or purification of thioredoxin and thioredoxin fusion proteins.[38, 85, 181, 205]

As a model antigen, ovalbumin (OVA) is well characterized and many OVA-specific immunologic reagents and systems are available. The phosphoglycoprotein OVA is the major protein in hen egg whites[179] and is a non-inhibitory member of the serpin family.[87] OVA has been identified as an allergen in egg whites and is used as a model antigen due to its mild immunogenicity.[133, 201]

Increased solubility of recombinant proteins expressed in *E. coli* has been observed when *E. coli* thioredoxin A (trxA) was used as a gene fusion partner.[105] A fusion protein between TrxA::PA44 and OVA retains the CaP binding ability of the trxA derivative (TrxA::PA44) while also presenting the OVA antigen. The TrxA::PA44-OVA fusion protein was constructed,

expressed, and purified. When evaluated for CaP mineralization ability, purified TrxA::PA44-OVA mineralized sub-100nm CaP NPs using a CaP formulation similar to that previously described.[27]

To evaluate adjuvancy, mice were immunized with TrxA::PA44-OVA vaccines with and without CaP NPs. Following vaccination, mice were challenged with influenza A strain (WSN)-OVA_I^{185} that expresses an ovalbumin T-cell epitope on the phage surface. Adjuvancy was assessed by serum antibody response after immunization and by splenocyte CD8 T-cell response after challenge.

3.2: Materials and Methods

See "Zhou, W., Moguche, A., Chiu, D., Murali-Krishna, K, Baneyx, F. (in press), Just-in-time vaccines: Biomineralized calcium phosphate core-immunogen shell nanoparticles induce long-lasting CD8+ T cell responses in mice. *Nanomedicine: Nanotechnology, Biology, and Medicine*." in Appendix A for additional details.

3.2.1: Expression and purification of TrxA::PA44-OVA

BL21(DE3) *E. coli* cells harboring pTrxA::PA44-OVA were grown to *A*600 ≈ 0.5 at 37°C in 500 mL of LB medium supplemented with 34 μg/mL chloramphenicol. Flasks (2L) were transferred to a water bath and held at 25°C for 10 min. Protein synthesis was induced by addition of 1 mM isopropyl β-D-1-thiogalactopyranoside (IPTG). After 4 hrs, cells were harvested by centrifugation at 3,000 *g* for 15 min, and resuspended in 20 mM Tris-HCl, pH 7.5 supplemented with 2.5 mM EDTA and 1 mM PMSF to an *A*600 of 50. Cells were disrupted by three cycles of homogenization in a French pressure cell operated at 10,000 psi and the lysate was separated into soluble and insoluble fractions by centrifugation at 14,000 *g* for 15 min. Pellets containing the inclusion body material were resuspended by vortexing into 5 mL of Buffer A (20 mM Tris-HCl, pH 7.5, 2.5 mM EDTA, 1 mM PMSF) supplemented with 1% (v/v) Triton X-100. Following centrifugation at 14,000 *g* for 10 min, the supernatant was discarded and the wash step was repeated once as above and twice more using Buffer A alone. Washed inclusion bodies were resuspended in 15 mL of Buffer A supplemented with 6 M of guanidine hydrochloride and incubated at room temperature for 1h with gentle shaking. After removing any remaining insoluble material by centrifugation at 14,000 *g* for 10 min, unfolded protein aliquots (5 mL) were refolded by dropwise addition into 95 mL of Buffer A with gentle stirring. The remaining guanidine hydrochloride was removed by 16 hr dialysis against 2L of Buffer A, with

buffer changes at 1 and 4 hrs. The refolded protein was filtered through a 0.45 μm cartridge and loaded on a 1 cm column packed with 5 g of DE52 Cellulose (Whatman) pre-equilibrated in Buffer A. The column was developed at 1 mL/min in Buffer A and TrxA::PA44-OVA was eluted with 200 mM NaCl in Buffer A after a 50 mM NaCl in Buffer A step to remove contaminants.

3.2.2: Nanoparticle mineralization and characterization

Calcium phosphate (CaP) nanoparticles were produced as described elsewhere[27] with the exception of TrxA::PA44-OVA as the mineralization agent instead of TrxA::PA44. Briefly, 200 μL of a 16.7 mM $Ca(NO_3)_2$ solution was added dropwise to 1.8 mL of a well-stirred mixture of 1.11 mM $(NH_4)_2HPO_4/NH_4H_2PO_4$, pH 7.5 supplemented with 4.44 μM TrxA::PA44-OVA that had been previously incubated at 4°C for 30 min. After addition of the calcium precursor solution, the mixture was allowed to age at 4°C for 2 h with high-speed stirring with a small magnetic stir bar. Endotoxin-free water and disposable glassware cleaned with acetic acid, acetone and water was used in all steps.

Particle size was determined by DLS using a Malvern Nano ZS zetasizer. Refractive index (RI) of CaP particles was assumed to be equal to tricalcium phosphate (RI=1.628). Absorbance was 0.01 according to the manufacturer's instructions and dispersant was set to water at 25°C. Data collection was set to 10 runs per reading and particle size was presented as the mean of the maximum peak height from three readings.

For SEM imaging, samples (≈ 100 μL) were allowed to contact clean, ≈ 1 cm^2 silicon wafers for 30 min and excess fluid was removed by wicking with a laboratory tissue. The wafer was rinsed with ddH_2O to remove salts, air dried and sputter coated with a 7-10 nm Au/Pd film. Micrographs were taken with a FEI Sirion SEM at 10 keV acceleration voltage.

3.3: Results

3.3.1: Construction, expression, and purification of TrxA::PA44-OVA

A plasmid encoding the fusion protein combining the thioredoxin CaP binding variant TrxA::PA44 with ovalbumin (termed pTrxA::PA44-OVA), was constructed by Dr. Weibin Zhou and verified by DNA sequencing (see App. A for details). TrxA::PA44-OVA was expressed in *E. coli* BL21(DE3) cells upon induction with IPTG. Cells were then disrupted with a French press and cellular fractions were analyzed by SDS-PAGE gel. The fusion protein was mostly expressed in insoluble inclusion bodies. Inclusion bodies were denatured with guanidine hydrochloride and refolded. Dialyzed refolded protein was then purified on a DE52 anion exchange column. SDS-PAGE analysis of AEC fractions (Fig. 3.1 and 3.2) revealed that the fusion protein was eluted in a pure (>95%) form with the expected molecular weight (55kDa).

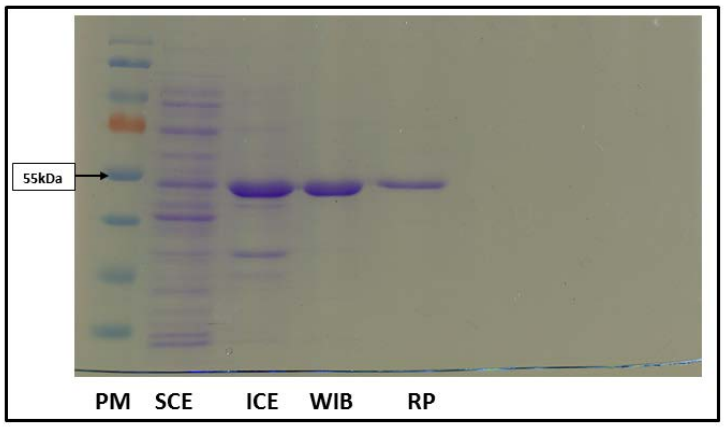

Fig. 3.1: SDS-PAGE gel of Trx::PA44-OVA fusion protein in cellular fractions, Lanes, (PM): Protein Marker, Fermentas SM0671, (SCE): Soluble crude cell extract, (ICE): Insoluble crude cell extract, (WIB): Washed inclusion bodies, (RP): Refolded TrxA::PA44-OVA

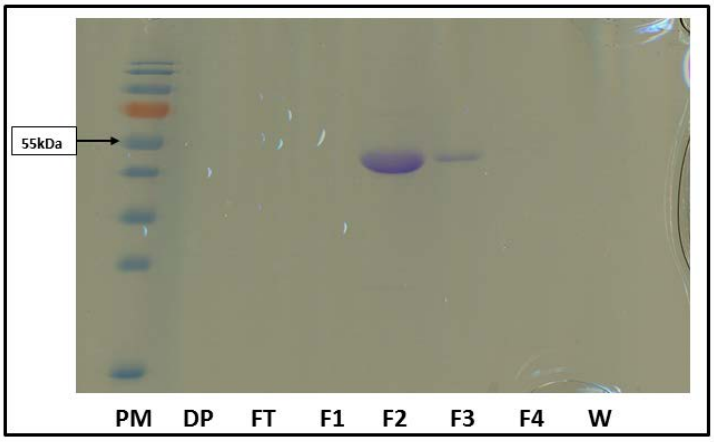

Fig. 3.2: SDS-PAGE gel of Trx::PA44-OVA anion exchange chromatography fraction, Lanes, (PM): Protein Marker, Fermentas SM0671, (DP): Dilute refolded TrxA::PA44-OVA, (FT): Flow through, (F1): 50mM NaCl fraction, (F2): 200mM NaCl fraction 1, (F3): 200mM NaCl fraction 2, (F4): 300mM NaCl fraction, (W): 500mM NaCl wash

3.3.2: Characterization of calcium phosphate nanoparticles mineralized with TrxA::PA44-OVA

CaP NPs were prepared using a modification of the formulation used for CaP and TrxA::PA44 immunizations previously described.[27] Precursor solutions and the mixing technique remained the same but the TrxA::PA44-OVA fusion protein was used instead of TrxA::PA44. CaP particles mineralized with the fusion protein were found to be 44 ± 3 nm as determined by DLS. Analysis of SEM images taken by Dr. Sathana Kitayaporn revealed that particles were 75 ± 12 nm (n=50), which includes a 7-10nm Au/Pd coating used for SEM visualization (Fig. 3.3). Particle size measurements were consistent between DLS and SEM analysis after the Au/Pd coating is taken into account.

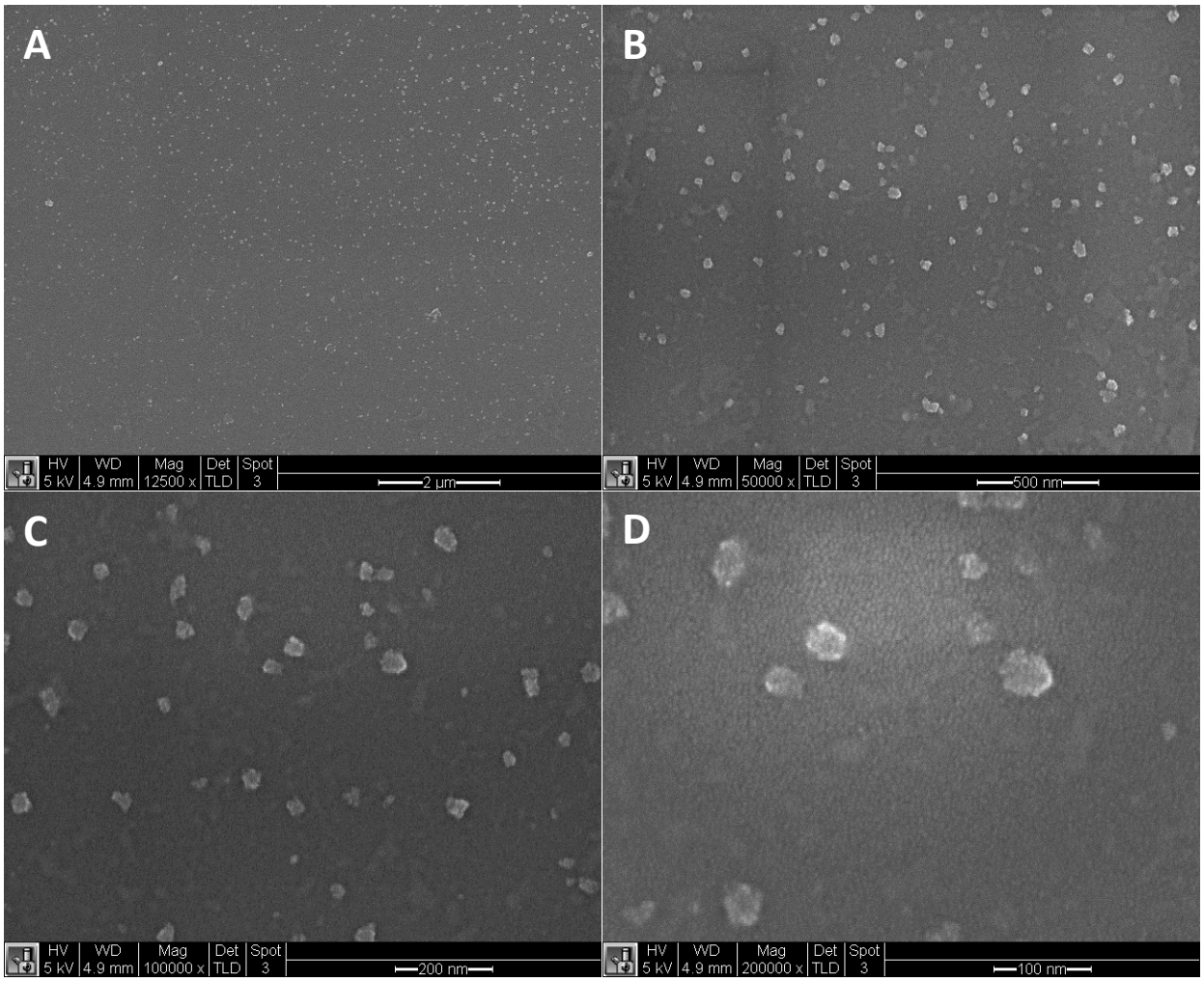

Fig. 3.3: SEM images of CaP and Trx::PA44-OVA particles at (A) 12,500x, (B) 50,000x, (C) 100,000x, and (D) 200,000x magnifications.

3.3.3: Evaluation of calcium phosphate adjuvants *in vivo*

CaP NP adjuvancy was tested *in vivo* by Albanus Moguche (see App. A for additional details). Groups of C57Bl/6 mice received vaccine formulations containing TrxA::PA44-OVA (18µg per mouse) with and without CaP NPs (32.4µg/mouse). Anti-OVA IgM, total IgG, and IgG1 sera levels were comparable in mice immunized with protein only vaccines and protein and

CaP NP vaccines indicating that the CaP nanoparticles were ineffective at increasing T_H2 responses in these formulations.

Mice from each vaccination group were challenged with (WSN)-OVA_I, a recombinant influenza A/WSN/33 (H1N1) virus displaying the $ovalbumin_{257-264}$ epitope (SIINFEKL) on the phage surface-exposed neuraminidase stalk.[185] One mouse from each vaccination group was challenged 4-months post-vaccination, and lung cell surface marker and cytokine expression were analyzed after stimulation with the OVA epitope SIINFEKL. The mouse vaccinated with the protein and CaP NP formulation had twice as many CD44+ (marker for effector-memory T-cells), IFN-γ+ lung cells after peptide stimulation as compared to the mouse vaccinated with the protein only formulation.

Mice (n=6) from each vaccination group were also challenged 8-months post-vaccination. Seven days post-challenge, mice (n=3) from each group were sacrificed and splenocytes were analyzed for SIINFEKL specific effector and memory CD8+ T-cells. Total effector-memory T-cell response after WSN-OVA challenge was similar between all groups, indicating similar levels of infection. Mice from the group immunized with TrxA::PA44-OVA and CaP NPs had significantly higher ($P<0.05$) levels of antigen specific splenic CD8+ T-cells than mice immunized with protein only vaccines. The remaining mice (n=3) from the challenge group were monitored for weight loss. Mice previously immunized with protein and CaP NP formulations had significantly less weight loss 8-days post challenge as compared to the naïve and protein-only vaccine groups. Two mice from the naïve and protein only vaccine groups had to be sacrificed 9-days post-challenge due to a weight loss over 20% but mice vaccinated with protein and CaP NP formulations retained 85-90% of their weight 10-days post-challenge.

3.4: Summary

When overexpressed in *E. coli*, heterologous proteins often form insoluble aggregates known as inclusion bodies.[135, 167] Increased solubility of overexpressed proteins has been observed when trxA was used as a gene fusion partner.[105] trxA is a thermostable and highly soluble protein,[84] and trxA, as a N-terminal fusion partner, may increase fusion protein solubility during translation by stabilizing unfolded protein intermediates. Coexpression of trxA has also been shown to increase solubility of overexpressed heterologous proteins in *E. coli*.[202] trxA has a highly conserved active site loop involved in the reduction and oxidation of disulfide bonds[194] and may increase the solubility of coexpressed proteins by preventing incorrect disulfide bond formation by altering the redox environment of the cytoplasm in *E. coli*.

When TrxA::PA44-OVA was expressed in *E. coli*, the majority of the fusion protein was in an insoluble form. The trxA CaP binding derivative, TrxA::PA44, has a CaP binding dodecapeptide inserted within the trxA active site loop and alteration of the trxA active site loop may abrogate potential benefits to expressed protein solubility.

OVA has a single N-linked glycosylation site at Asn-392[74] and glycosylation of eukaryotic proteins can improve protein stability and solubility.[167] Since *E. coli* lacks the ability to glycosylate expressed proteins, the lack of OVA glycosylation may also contribute to fusion protein instability and inclusion body formation.

After inclusion bodies were washed, denatured, and refolded, TrxA::PA44-OVA was purified by anion exchange chromatography. The purified fusion protein still maintained the ability to mineralize CaP particles in the sub-100nm size range, demonstrating that construction

of fusion proteins between TrxA::PA44 and an antigen of interest is a useful approach for CaP NP delivery of antigens.

The CaP NP adjuvants were ineffective at increasing anti-OVA IgG antibody response in TrxA::PA44-OVA vaccines. CaP adjuvants are thought to function in a manner similar to aluminum adjuvants by acting as antigen depots that slowly release antigen from the site of injection. CaP NPs are likely to be rapidly cleared from the site of injection due to their small size, and the absence of a depot effect may explain the inability to elevate a T_H2 response.

Protective immunity was analyzed by challenging immunized mice 4 and 8-months post-vaccination with an influenza A strain expressing an OVA epitope on the phage surface (WSN)-OVA_I. One mouse from each group was challenged 4-months post vaccination, and higher levels of IFN-γ+ effector-memory T-cells were found at the challenge site (lungs) in the mouse immunized with the protein and CaP NP vaccine as compared to the mouse vaccinated with the protein only formulation. 8-months post immunization, the remaining mice from each group were challenged and mice immunized with the protein and CaP NP vaccine formulation had significantly higher levels of splenic antigen-specific effector-memory CD8+ T-cells as compared to mice immunized with protein-only vaccines. Also, addition of CaP NP adjuvant to vaccine formulations helped prevent weight loss in immunized mice after challenge.

Although IFN-γ T-cell response was only analyzed with one mouse per group after the 4-month challenge, the increased level of IFN-γ effector-memory T-cells in the mouse immunized with protein and CaP NP vaccines may help explain elevated antigen specific CD8 T-cell response. IFN-γ serves many biological functions, one of which is the upregulation and increased loading of MHC-I.[169] CD8 (cytotoxic) T-cells express receptors that recognize peptide:MHC-I

complexes presented on the surface of infected cells. Upon recognition and binding, CD8 T-cells induce apoptosis in the infected cell limiting the spread of intracellularly replicating pathogens.

Aluminum adjuvants are the most commonly used adjuvants in approved vaccine formulations. Although they are effective at increasing antibody responses, they elicit little to no cell-mediated or cytotoxic response.[83, 112] The elevated antigen-specific effector-memory CD8+ T-cell response after influenza challenge in mice immunized with a TrxA::PA44-OVA and CaP NP vaccine indicates that CaP NP adjuvant may be useful for increasing cytotoxic T-cell response in vaccines against intracellular pathogens.

Chapter 4: Ovalbumin Vaccines

4.1: Introduction

In Chapters 2 and 3, vaccinations were carried out using calcium phosphate (CaP) nanoparticles mineralized with thioredoxin A derivatives (TrxA::PA44)[27] or thioredoxin-ovalbumin fusion proteins (TrxA::PA44-OVA). While the thioredoxin derivatives and fusion proteins were able to effectively control CaP particle size in the sub-100nm size range, use of *E. coli* thioredoxin A as a scaffold or as a fusion protein in vaccines is problematic because of autoimmunity concerns.

Found in most living organisms, thioredoxin is a small (~12 kDa) redox protein that either reduces disulfide bonds or oxidizes sulfhydryls in a variety of proteins.[194] A previous study comparing antibodies raised against *E. coli* thioredoxin (trxA) and yeast thioredoxin (TRX2) showed cross reactivity between these antibodies.[85] Protein BLAST analysis (BLASTP 2.2.28+)[6, 7] reveals that trxA and TRX2 have a 34% protein identity, and trxA and human thioredoxin (TXN1) have a 35% protein identity. For this reason, thioredoxin is a poor choice as a vaccine carrier since any formulation containing TrxA has the potential to cause autoimmunity against endogenous thioredoxin in the immunized host.

As mineralization agents, cyclic peptides containing CaP binding motifs are alternatives to trxA derivatives. Binding ability of cyclic peptides containing binding motifs selected through phage display biopanning has been demonstrated with snake venom toxin.[8] The surface exposed dodecapeptides in the FliTrx™ Random Peptide Display Library are constrained by the trxA active site loop disulfide bond and disruption of that disulfide bond was previously shown to influence TrxA::PA44 CaP mineralization ability.[27] A cyclic peptide composed of a selected CaP

binding dodecapeptide flanked by Gly-Cys-Gly-Pro (GCGP) on the N-terminus and Gly-Pro-Cys (GPC) on the C-terminus and cyclized by a disulfide bond may maintain CaP binding motif conformational constraints similar to those found in trxA CaP binding derivatives. Additionally, endotoxin contamination is less likely for cyclic peptides constructed through solid-state synthesis as compared to proteins expressed in *E. coli*.

When tested for CaP mineralization ability, the cyclic peptides were able to influence CaP particle size. In Chap. 2, CaP precipitated in the absence of a capping agent formed large micrometer-sized polydisperse and polymorphous particles. When CaP was mineralized in the presence of ovalbumin (OVA) and cPN38, sub-100nm particles were formed that were stable for up to two hours after mixing. Vaccine formulations containing OVA and CaP nanoparticles (CaP NPs) were tested *in vivo*, and adjuvancy of CaP NPs was assessed by analyzing antibody and splenocyte cytokine response after vaccination.

4.2: Materials and Methods

4.2.1: Calcium phosphate nanoparticle formulation

For the CaP NP formulation used previously in TrxA::PA44 and TrxA::PA44-OVA experiments, a precursor solution containing 16.7mM $Ca(NO_3)_2$ (Fisher C-109-500) pH 7.4 is added dropwise while vortexing on a high setting to a solution containing $NH_4H_2PO_4/(NH_4)_2HPO_4$ (Sigma-Aldrich 216003 and Fisher BP361-500), pH 7.4 and cPN38 (GCGPEDIDAVSVGEVQGPC disulfide bond at 2^{nd} and 19^{th} residue, Genscript) at the indicated concentrations. Final concentrations of precursor salts are 1.67mM $Ca(NO_3)_2$ and 1mM $NH_4H_2PO_4/(NH_4)_2HPO_4$.

For CaP NP formulations used *in vivo*, CaP concentration was increased from 0.16mg/mL to 0.5mg/mL while keeping Ca^{2+} to PO_4^{3-} ratio constant. OVA and cPN38 were premixed with the PO_4^{3-} precursor solution and held at 4°C for 15 min. A 16.7mM $Ca(NO_3)_2$ precursor Ca^{2+} solution was held at 4°C for 15 min before mixing with the PO_4^{3-} precursor solution containing protein and peptide. Final concentrations were: 5.2mM $Ca(NO_3)_2$, 3.1mM $NH_4H_2PO_4/(NH_4)_2HPO_4$, 0.1mg/mL OVA, and 50µM cPN38.

4.2.2: Vaccine particle characterization

Particle size and zeta potential were determined by DLS using a Malvern Nano ZS zetasizer. Refractive index (RI) of CaP particles was assumed to be equal to tricalcium phosphate (RI=1.628). Absorbance was 0.01 according to manufacturer's instructions and dispersant was set to water at 25°C. Data collection was set to 10 runs per reading and particle size was presented as the mean of the maximum peak height from three readings.

OVA antigen loading was determined for nanoparticles by assaying the supernatant of samples by A280 for OVA concentration after separating nanoparticles by ultracentrifugation at 100,000g for 1 hr on a Beckman Coulter Optima TLX Ultracentrifuge with a Beckman Rotor TLA110#054798. Microparticles were pelleted with centrifugation at 16,000g for 30 min on a Spectafuge 16M microcentrifuge.

4.2.3: cPN38 conjugation to ovalbumin

Conjugation of cPN38 cyclic peptides to OVA was carried out using EDC/NHS chemistry which forms an amide bond between primary amines and carboxylate groups. To prevent polymerization of OVA, primary amines on OVA were irreversibly blocked with Sulfo-NHS Acetate (Thermo 26777). 2mL of 10mM Sulfo-NHS Acetate was added to 2mL OVA (2mg/mL) and incubated at RT for 1 hr in the dark. Reaction solution was dialyzed into 4L ddH_2O overnight at 4°C with buffer changes at 1 and 5 hrs using a 12,000-14,000 MWCO membrane (Fisher 21-152-14). The reaction solution was then dialyzed into 100mL of activation buffer (0.1M MES (Sigma M3671), 0.5M NaCl (Fisher BP358-212) pH 6.0) for 5 hrs at 4°C.

1.6mg EDC (Thermo 77149) and 4.4mg Sulfo-NHS (Thermo 24510B) were added to 4mL of the primary amine blocked OVA (1mg/mL) in activation buffer and reacted at RT for 15 min. 5.6 µL β-mercaptoethanol (BioRad 161-0710) was added to quench the reaction. Excess reagent and buffer was removed using a 7,000 MWCO desalting column (Thermo 89893) Two mL of cPN38 at a 1:1 or 8:1 molar ratio was added to 2 mL Sulfo-NHS activated OVA (1mg/mL=22.2µM) and the conjugation reaction mixture was held at RT for 2 hrs. The reaction mixture was then dialyzed into 4L ddH_2O overnight at 4°C with buffer changes at 1 and 5 hrs. Protein concentration determined by A280.

4.2.4: Immunizations with ovalbumin vaccines

All animal experiments adhered to federal guidelines and were approved by the University of Washington Animal Care and Use Committee. Groups of five C57Bl/6 mice (Jackson Laboratory, age 6-8 weeks) were immunized at day 0, 7, and 14 with 200uL of vaccine formulations split evenly between two lower abdominal subcutaneous sites. Mice were immunized with vaccine formulations (Tab. 4.1) prepared with endotoxin free water (Thermo SH30529).

Table 4.1: Immunization groups and vaccine formulations

Group	**Vaccine formulation**
CaP only	CaP (5.2mM $Ca(NO_3)_2$ and 3.1mM $NH_4H_2PO_4/(NH_4)_2HPO_4$)(0.5mg/mL) and cPN38 (50μM)
OVA only	OVA (0.1mg/mL) (Invivogen vac-efova) in PBS
OVA and CaP nanoparticles	OVA (0.1mg/mL), cPN38 (50μM) and CaP (0.5mg/mL) nanoparticles
OVA and CaP microparticles	OVA (0.1mg/mL) and CaP (0.5mg/mL) microparticles
OVA and aluminum hydroxide	OVA (0.1mg/mL) and aluminum hydroxide (0.5mg/mL) (Invivogen vac-alu-50)

For the “OVA and CaP microparticles” group, CaP particles were mineralized in the absence of a capping agent and left to ripen for 24hrs before mixing with OVA. For the “OVA and $Al(OH)_3$” group, OVA was mixed with preformed commercial aluminum hydroxide

adjuvant. OVA was adsorbed onto CaP microparticles or aluminum hydroxide for 30 min under gentle stirring prior to injection. For the "OVA and CaP nanoparticles" group, OVA and CaP NPs were mixed and injected within 30 min after mixing.

Mice were bled via submandibular veins on day 20 and 27. Blood was collected into capillary blood collection tubes with serum separator (BD 365959) and left at 4°C overnight before sera were separated by centrifugation at 16,000g. Sera were then aliquoted and stored at -80°C before assaying with ELISA.

4.2.5: Anti-ovalbumin IgG ELISAs

96-well maxisorp plates (Thermo 442404) were coated overnight with 100µL/well coating buffer [10µg/mL OVA (Invivogen vac-ova) in 1xPBS pH 7.4 (Thermo 28372), 0.1% [w/v] sodium azide (Sigma S-8032)] at 4°C. Plates were then washed 2x with 200µL/well wash buffer (1xPBS, pH 7.4 and 0.02% [v/v] Tween 20 (Fisher BP337-500). Plates were then blocked with 150µL/well block buffer (1% [w/v] bovine serum albumin (Sigma A7030-50g) in 1xPBS, pH7.4, 0.22µm filtered) for 1 hr at 37°C. Wells were washed twice. 100µL/well of diluted serum samples and standards (Anti-OVA IgG1 standard (Sigma A6075) and Anti-OVA IgG2a standard (Biolegend 520401)] in block buffer were added to plates and incubated for 1hr at 37°C. Wells were washed four times. 100µL/well secondary antibodies [goat anti-mouse IgG-HRP (Biolegend 405306), goat anti-mouse IgG1-HRP (Life Technologies A10551), goat anti-mouse IgG2a (Life Technologies M32207), and goat anti-mouse IgG2c (Thermo PA129288)] diluted in block buffer (2000x dilution for total anti-IgG, 0.4µg/mL for anti-IgG1, anti-IgG2a, and anti-IgG2c) followed by a 30min incubation at 37°C. Wells were washed four times. 100µL/well TMB substrate (Thermo 34021) added followed by a 10min RT incubation in the dark. Reaction

stopped with 100µL/well 2M sulfuric acid. Absorbance recorded at 450nm. Titers determined as the last dilution to have a reading higher than 3x the standard deviation of the blank wells after subtracting the average absorbance of blank wells.

4.2.6: Splenocyte IFN-γ secretion assay

Mice were sacrificed at day 28 and spleens were removed and placed in 1mL splenocyte medium [RPMI 1640 w/ 2mM L-glutamine (Gibco 11875-093) with 1x PenStrep (Gibco 15140), 10% heat inactivated FBS (Gibco 10082147) and 0.1% [v/v] beta-mercaptoethanol (Gibco 21985)] on ice. A 3mL syringe plunger (BC 309585) was used to force spleens through a 70µm cell strainer (BD 352350) pre-wetted with 1mL medium and the plunger and cell strainer were then washed with 10mL of medium. Suspended cells were pelleted at 500g for 5 min. The cell pellet was resuspended in 3mL ACK lysis buffer (Invitrogen A10492-01) and incubated at RT for 5 min. 12mL of medium was added to stop the reaction and cells were pelleted again. The cell pellet was resuspended with 10mL of medium and pelleted again. Finally, the cell pellet was resuspended in 1mL of medium and cells were counted.

Splenocytes were seeded at $1x10^6$ cells/well in 100µl medium in a 96-well TC-treated U-bottom plate (BD 353077) then stimulated by adding 20µg OVA (Invivogen vac-efova) per well in 100µL medium. Total cell culture volume after stimulation was 200µL/well. Stimulated splenocytes were then incubated for 16hrs at 37°C, 5% CO_2. After 16 hrs, plates were spun down at 500g for 5 min and 150µL splenocyte cell culture supernate aliquoted and stored at -80°C. IFN-γ concentration in splenocyte supernatants was analyzed with a commercial IFN-γ ELISA kit (Thermo ESS0020). ELISA carried out according to manufacturer's instructions.

4.3: Results

4.3.1: cPN38 calcium phosphate mineralization ability

A disulfide-constrained cyclic peptide (GCGPEDIDAVSVGEVQGPC) containing the previously identified PN38 CaP binding dodecapeptide (EDIDAVSVGEVQ)[27] was produced by solid-phase peptide synthesis (Genscript). This peptide was evaluated for its ability to control the size of CaP particles. When CaP was mineralized according the protocol previously used with the thioredoxin derivatives (see Chap. 2), particle sizes below 100 nm were observed 2hrs after mixing at cPN38 concentrations of 30uM and above (Fig. 4.2).

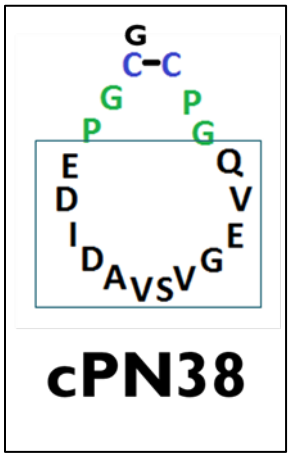

Fig 4.1: Schematic of cPN38 cyclic peptide. Disulfide bond indicated in blue. Flanking native active site sequence is indicated in green. The PN38 CaP binding dodecapeptide is boxed.

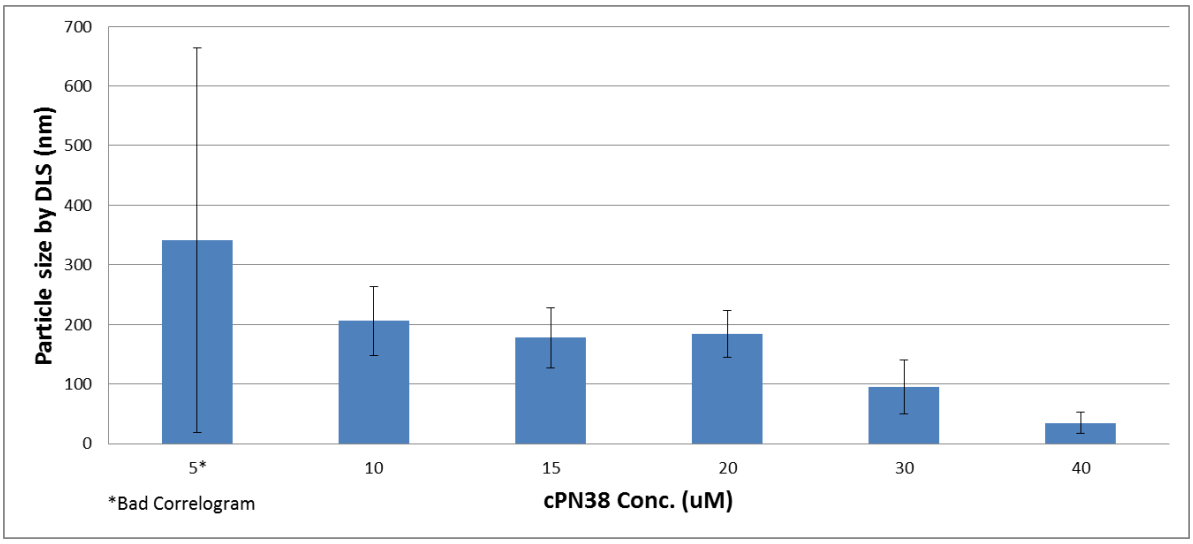

Fig. 4.2: Comparison of CaP [1.67mM $Ca(NO_3)_2$ and 1mM $NH_4H_2PO_4/(NH_4)_2HPO_4$, pH 7.4](0.16mg/mL CaP) particle size by DLS with the addition of increasing amounts of cPN38, 2 hrs after mixing.

4.3.2: Vaccine formulation characterization

Vaccine formulations containing ovalbumin protein (OVA) were characterized for particle size, zeta potential, and ovalbumin loading. For OVA vaccines, CaP concentration was increased to 0.5mg/mL from the concentration of 0.16mg/mL used in the thioredoxin immunizations. At an injection volume of 200µL and 0.5mg/mL CaP, mice received 100µg CaP per injection, matching the dose given in a previous study using CaP adjuvant.[76, 77]

Formulations containing CaP, OVA (0.1mg/mL), and varying concentrations of cPN38 (20-50µM) were analyzed by DLS after mixing to determine particle sizes. For CaP-OVA formulations containing less than 50µM cPN38, particles increased in size 1 hr after mixing (Fig. 4.3) and at 2 hrs post-mixing solutions all solutions except those containing 50µM cPN38 were turbid. Formulations containing 50µM cPN38 maintained a stable particle size (80 ± 10 nm) up to 2 hrs.

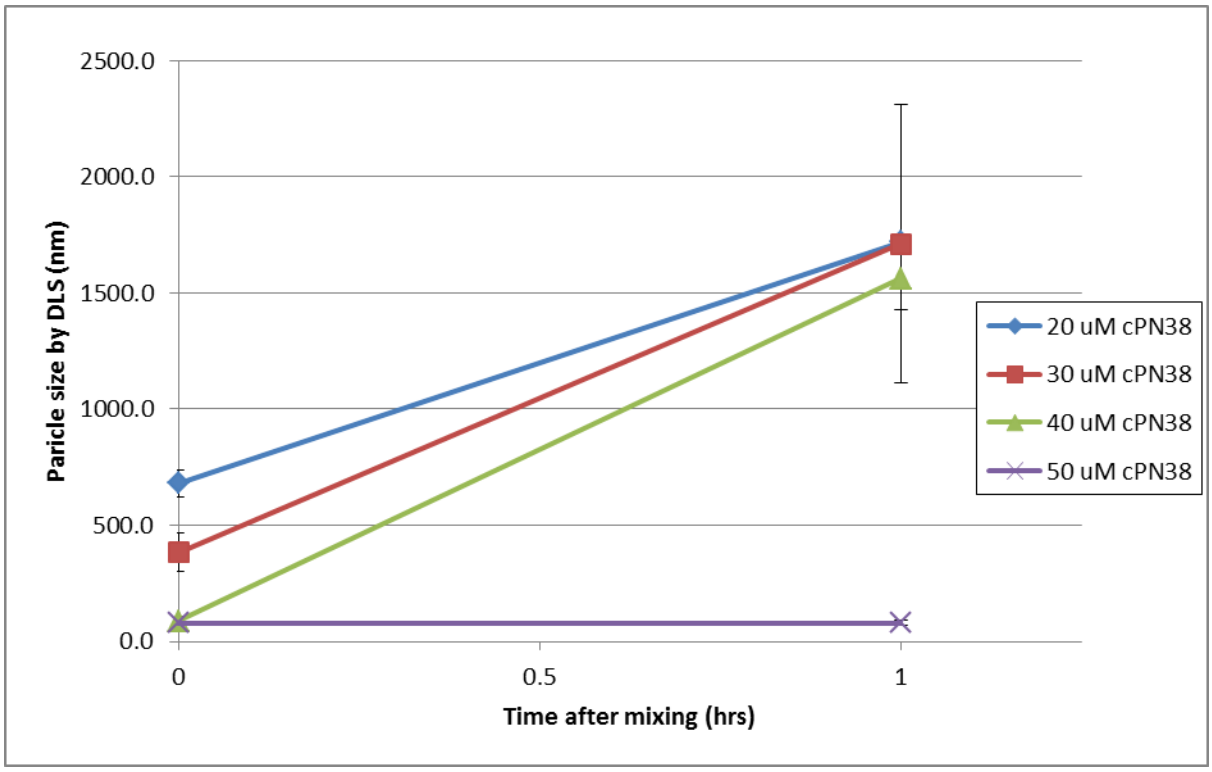

Fig. 4.3: Comparison of CaP [5.2mM $Ca(NO_3)_2$ and 3.1mM $NH_4H_2PO_4/(NH_4)_2HPO_4$, pH 7.4][0.5mg/mL CaP] particle size by DLS with ovalbumin (0.1mg/mL) and varying amounts of cPN38.

CaP particle size was also analyzed with and without OVA (0.1mg/mL) and/or cPN38 (50µM). After mixing Ca^{2+} and PO_4^{3-} precursor solutions, CaP will precipitate immediately forming a turbid solution in the absence of a capping agent. Decreased CaP particle sizes were seen relative to CaP only in formulations containing OVA or cPN38 2 hrs after mixing. When cPN38 and OVA were added to the precursor solutions, the smallest particle sizes were observed (80 +/- 10 nm) 2 hrs after mixing (Fig. 4.4). At 4 hrs after mixing, only the formulation containing both OVA and cPN38 was not turbid.

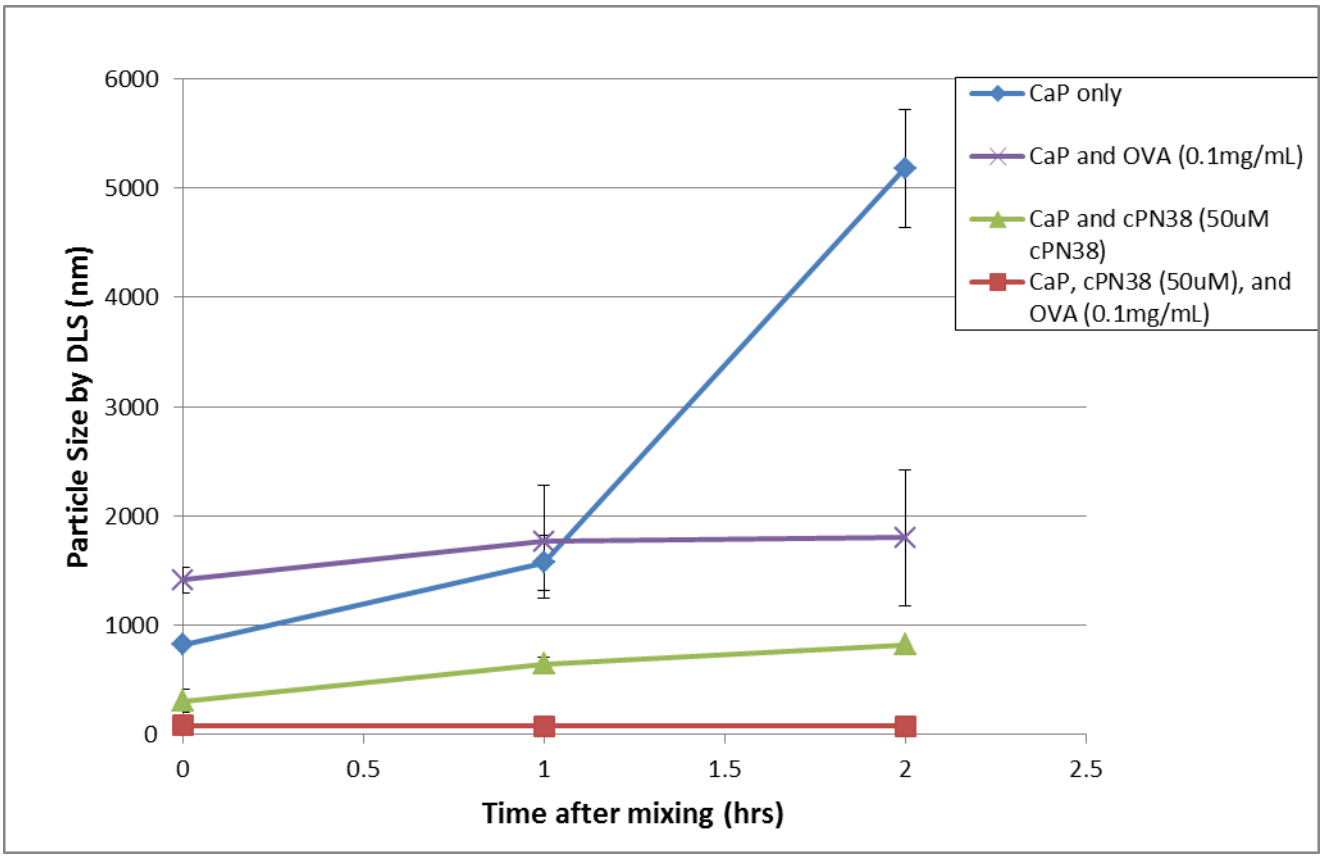

Fig. 4.4: Comparison of CaP [5.2mM $Ca(NO_3)_2$ and 3.1mM $NH_4H_2PO_4/(NH_4)_2HPO_4$, pH 7.4][0.5mg/mL CaP] particle size by DLS in the absence or presence of ovalbumin (0.1mg/mL) and/or cPN38 (50µM).

Tab. 4.1: CaP particle size by DLS for formulations containing CaP (0.5mg/mL), cPN38 (50µM) and OVA (0.1mg/mL)

CaP, cPN38, and OVA		
Time (hrs)	AVG (nm)	Stdev
0	83	7
1	79	12
2	76	13
4	311	4

The zeta potential of adjuvant particles was also analyzed by DLS (Fig. 4.5). Commercial aluminum phosphate and aluminum hydroxide had negative and positive zeta potentials, respectively. CaP particles had a positive zeta potential that shifted to a negative zeta potential with the addition of OVA and/or cPN38. The isoelectric points of OVA[109] and cPN38 are

respectively 4.5 and 3.4. Therefore, at a physiological pH of 7.4 ovalbumin and cPN38 will have a negative surface charge. These results indicate adsorption of negatively charged OVA and/or cPN38 to positively charged CaP particles.

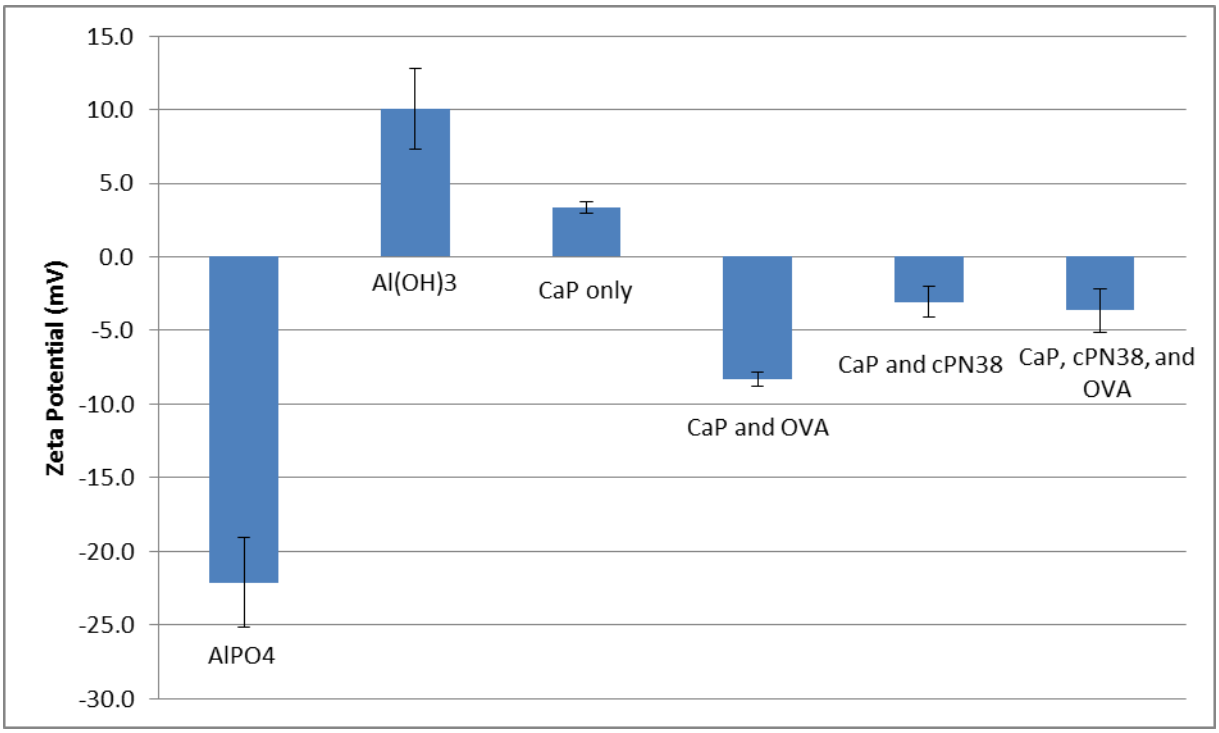

Fig. 4.5: Zeta Potential by DLS of commercial aluminum adjuvants and CaP formulations with cPN38 (50µM) and/or OVA (0.1mg/mL).

OVA loading onto aluminum phosphate, aluminum hydroxide, and CaP was determined by pelleting particles by ultracentrifugation (>100,000g) and assaying the resulting supernatant for the presence of OVA with A280 measurements (Fig. 4.6). Antigen loading onto aluminum phosphate was low possibly due to electrostatic repulsion of the negatively charged particles and OVA. Conversely, antigen loading onto positively charged aluminum hydroxide and CaP without cPN38 was high (>70%). As the concentration of cPN38 was increased, decreased OVA antigen loading onto CaP particles was observed. cPN38 may be displacing adsorbed OVA at higher cyclic peptide concentrations.

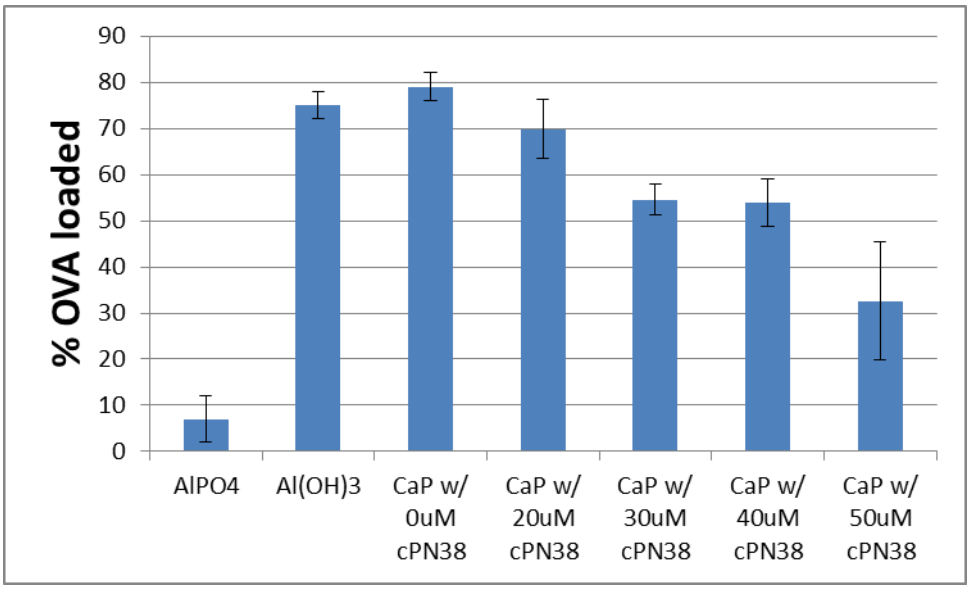

Fig. 4.6: Percent of OVA (0.1mg/mL) loaded onto particles.

In an attempt to increase antigen loading while maintaining small CaP particle size, cPN38 was conjugated to OVA using EDC/NHS chemistry. Conjugation reactions were carried out at 1:1 and 8:1 molar ratios of cPN38 to OVA. However, when CaP was mineralized in the presence of the cPN38-OVA conjugates (0.1mg/mL), the solutions became turbid immediately and particle sizes were greater than 800nm when measured by DLS (Fig. 4.7).

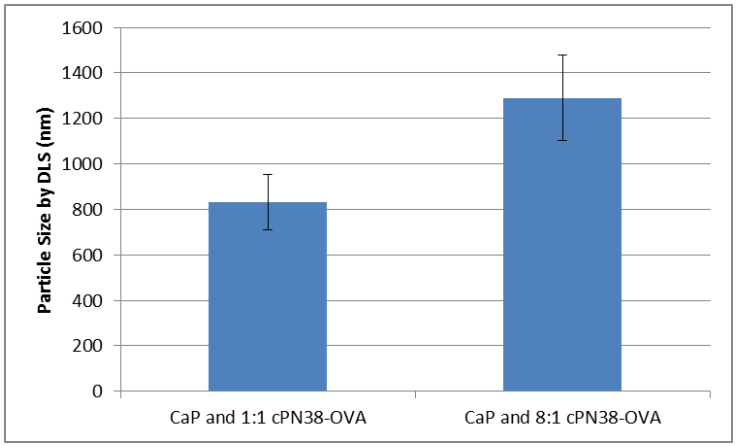

Fig. 4.7: Particle size by DLS of CaP mineralized in the presence of cPN38-OVA conjugates immediately after mixing.

4.3.3: Ovalbumin vaccinations

Groups of C57BL/6 mice were immunized with 200µL of vaccine formulations split evenly between two subcutaneous injection sites at day 0, 7, and 14. Splenocytes were harvested at day 28 and IFN-γ secretion 16 hrs after stimulation with OVA was analyzed. Mice received vaccines containing either: 1. CaP only, 2. OVA only, 3. OVA and CaP nanoparticles, 4. OVA and CaP microparticles, or 5. OVA and aluminum hydroxide. Mice vaccinated with OVA received 20 µg per injection and mice vaccinated with CaP or aluminum hydroxide received 100µg per injection.

Mice were bled at day 20 and 27. Total anti-OVA IgG concentration in serum was compared at day 20 and 27. Total IgG levels continued to increase between day 20 and 27 for all groups immunized with vaccines containing OVA protein (Fig. 4.8). Total IgG levels were significantly higher in the mice immunized with OVA and aluminum hydroxide adjuvant as compared to all other groups ($P<0.001$). These results are expected since aluminum hydroxide is known to stimulate strong T_h2 responses.[83,112] There were no significant differences ($\alpha=0.05$) in total IgG levels between mice receiving OVA only in PBS and mice receiving OVA and CaP nano or microparticles.

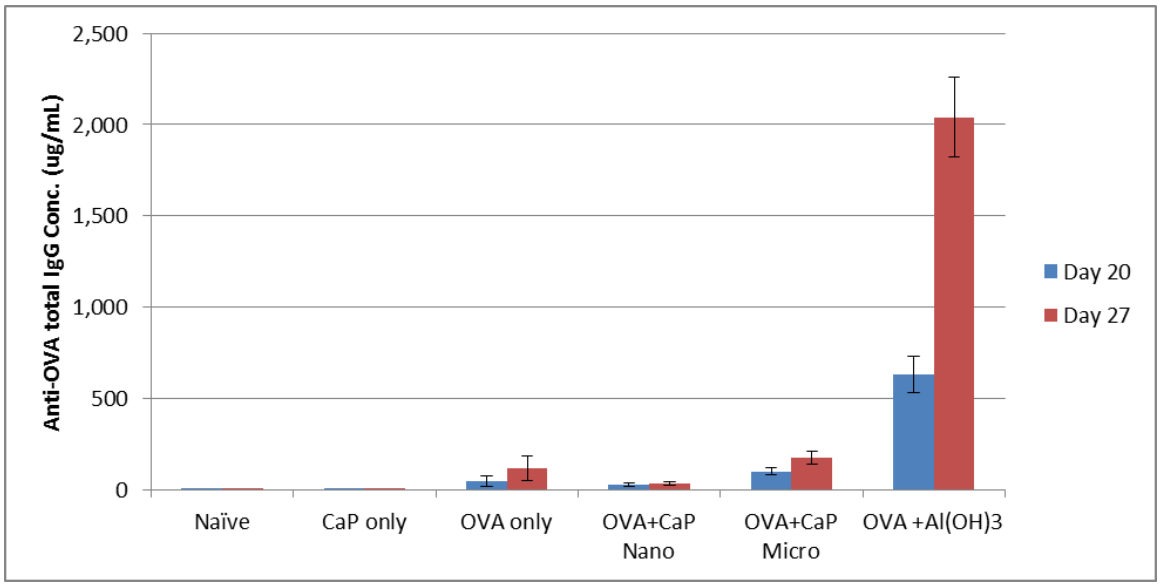

Fig. 4.8: Total anti-OVA IgG sera concentration in mice bled at day 20 and 27. Mean with SEM. Statistical significance determined by Student's t-test. All groups vaccinated with OVA were significantly higher at day 20 and 27 relative to both naïve and CaP only groups ($P<0.05$). No significant difference was seen between groups immunized with OVA only and OVA and CaP particles (nano or micro) ($\alpha=0.05$). The group immunized with aluminum phosphate and OVA was significantly higher than all groups at day 20 and 27 ($P<0.001$).

IgG isotypes were analyzed from the day 27 serum. Trends seen with the T_H2 isotype IgG1 matched those seen with total IgG. Mice vaccinated with OVA and aluminum hydroxide had the highest IgG1 levels (Fig. 4.9). Also, mice immunized with OVA and CaP microparticles displayed significantly higher IgG1 levels than the OVA only and OVA and CaP nanoparticle groups ($P<0.05$). The T_H1 antibody isotype IgG2a was only detectable in mice immunized with OVA and CaP particles (Fig. 4.10). Mice immunized with OVA and CaP microparticles had significantly higher IgG2a levels than all groups ($P<0.05$). IgG1/IgG2c titer ratio was analyzed in Day 27 sera and mice vaccinated with vaccine formulations containing aluminum hydroxide had the highest IgG1/IgG2c ratio (Fig. 4.11) indicating a T_H2 bias immune response consistent with findings in literature.

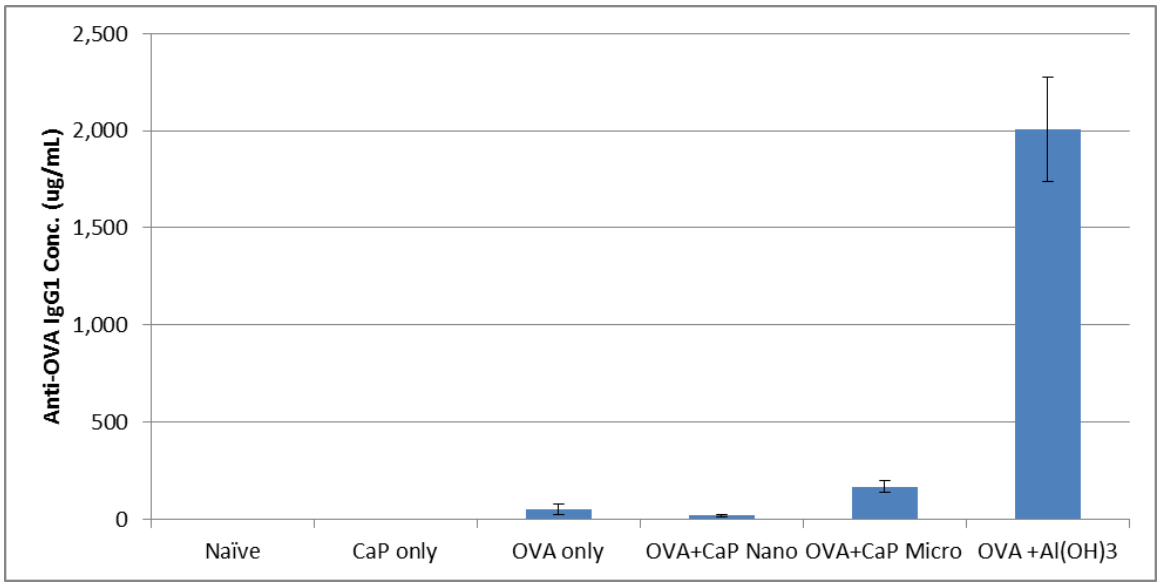

Fig. 4.9: Anti-OVA IgG1 isotype sera concentration from Day 27 bleeds. Mean with SEM. Statistical significance determined by Student's t-test. All groups vaccinated with OVA were significantly higher relative to both naïve and CaP only groups ($P<0.05$). No significant difference was seen between groups immunized with OVA only and OVA and CaP nanoparticles. The group immunized with OVA and CaP microparticles was significantly higher than both the OVA only and the OVA and CaP nanoparticle groups ($P<0.01$). The group immunized with aluminum hydroxide and OVA was significantly higher than all groups ($P<0.001$).

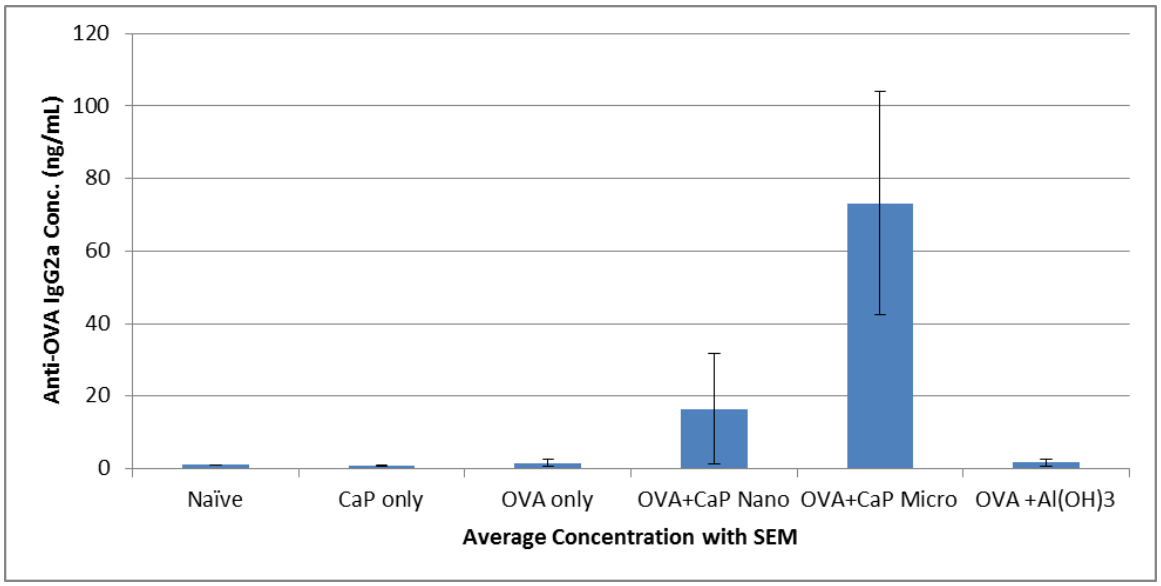

Fig. 4.10: Anti-OVA IgG2a isotype sera concentration from Day 27 bleeds. Mean with SEM. Statistical significance determined by Student's t-test. Presence of IgG2a was only detected in groups immunized with CaP particles. The OVA and CaP microparticle group had a significantly higher mean concentration relative to all groups ($P<0.01$ for all groups except OVA and CaP nanoparticles, $P<0.05$).

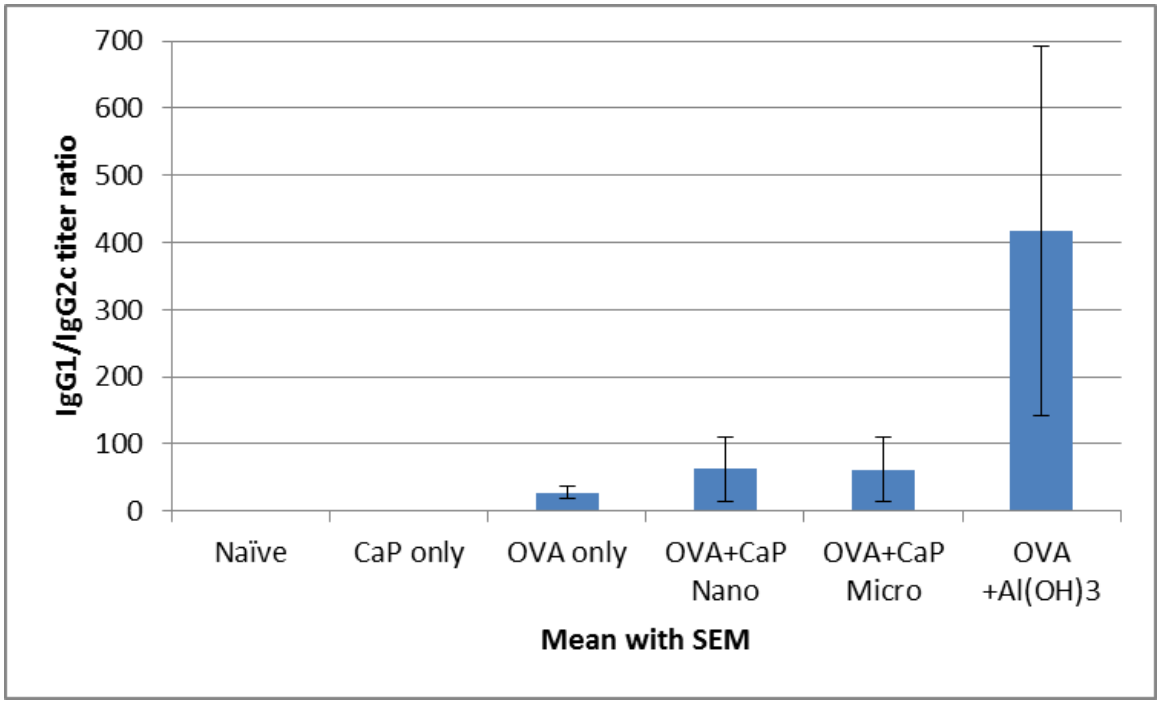

Fig. 4.11: Anti-OVA IgG1/IgG2c titer ratio from Day 27 bleeds.

At day 28, mice were sacrificed and spleens were extracted. Splenocytes ($1x10^6$ cells/well) were stimulated with 20µg OVA and 16 hrs after stimulation supernatant IFN-γ concentration was analyzed (Fig. 4.12). Mice immunized with OVA and CaP nanoparticles had the highest mean IFN-γ response. Although splenocytes from the OVA and CaP NP group secreted nearly twice as much IFN-γ on average after antigen stimulation as compared to splenocytes from the OVA only group, the increase was not statistically significant ($\alpha=0.05$, $P=0.12$) due to the large range of responses seen between individual mice within a group. At $\alpha=0.05$, $\beta=0.1$, power analysis reveals that approximately 30 mice would be required per group to determine significance. The small sample size n=5 may not be adequate to account for physiological differences in the immune response between mice. IL-4 concentration was also analyzed but no detectable IL-4 was present in supernatants of OVA stimulated splenocytes (data not shown).

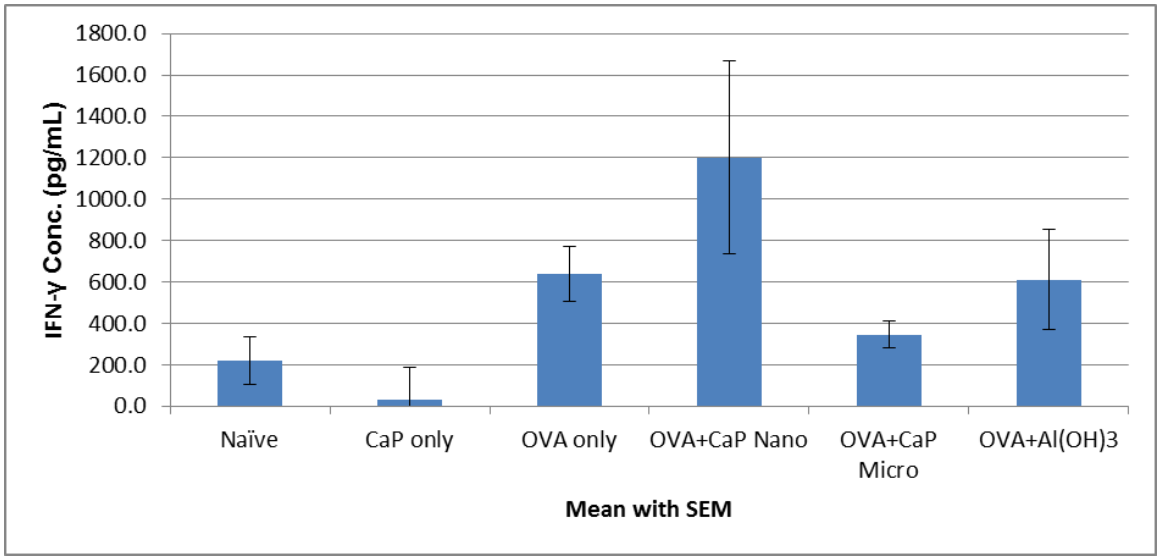

Fig. 4.12: Splenocyte IFN-γ secretion 16hrs after stimulation with 20ug of OVA. The highest mean response was seen in mice receiving OVA and CaP nanoparticle adjuvant. Statistical significance determined by Student's t-test. OVA only and OVA and CaP nanoparticle groups had a statistically significantly higher response than the naïve, CaP only, and OVA and CaP microparticle groups ($P<0.05$)

4.4: Summary

The cyclic peptide cPN38 was shown to mineralize sub-100nm CaP particles that were stable up to 2 hrs after mixing at peptide concentrations of 30μM and above. A positive to negative shift in zeta potential was also observed for CaP particles after the addition of OVA and/or cPN38 indicating adsorption of proteins/peptides to the negatively charged CaP surface.

Vaccine formulations containing OVA with and without adjuvants were tested in mice. Mice receiving OVA and aluminum hydroxide adjuvant had the highest anti-OVA IgG and IgG1 response. These findings were consistent with literature, since aluminum hydroxide has been shown to strongly stimulate Th2 responses when used as an adjuvant.[83, 112] Only mice vaccinated with OVA and CaP nanoparticles or microparticles had detectable amounts of IgG2a in serum. In mice, IgG1 facilitates opsonization of antibody coated pathogens and IgG2a activates antibody-dependent cellular cytotoxicity and complement dependent cytotoxicity. IgG2a/IgG1 ratio is typically used as a measure of T_H1/T_H2 response.

The type of mouse strain can also affect the observed antibody response. Igh-1 alleles differ between strains of mice with C57Bl/6 mice carrying the Igh-1b allele coding for IgG2c and BALB/c mice carrying the Igh-1a allele coding for IgG2a.[137, 206] It has been suggested that C57Bl/6 mice are incapable of producing IgG2a and instead produce IgG2c, while Balb/c mice produce IgG2a but no IgG2c.[126, 149] IgG1/IgG2a ratio is used to determine T_H2/T_H1 bias and IgG1/IgG2c ratio has been commonly used for the same purpose with C57Bl/6 mice. It remains unclear if IgG2c serves the same biological function as IgG2a,[126, 149] but C57Bl/6 mice deficient in the T_H1-associated cytokine IFN-γ have exhibited marked decreases in IgG2c response after infection with the extracellular rodent pathogen *C. rodentium* indicating that IFN-γ is necessary for IgG2c production.[21] Interestingly, many studies have detected IgG2a in the sera of C57Bl/6

mice.[139, 152, 170, 204] C57Bl/6 mice have also been shown to elicit different IgG isotype distribution after infection with viruses and IgG2a is the predominant IgG isotype expressed after infection with most viruses.[32] C57Bl/6 mice have also been shown to produce both IgG2a and IgG2c after infection with influenza.[78]

Anti-IgG2a antibody specificity can vary greatly between IgG2a allotypes expressed in different strains of mice[98] and the detection of IgG2a may depend upon which secondary antibody is used. Cross-reactivity of secondary antibodies with other IgG isotypes may explain why IgG2a has been detected in C57Bl/6 mice but the secondary antibodies for mouse IgG2a and IgG2c used in this chapter did not exhibit any cross-reactivity with the anti-OVA IgG1standard (data not shown).

Splenocytes from vaccinated mice were isolated, and IFN-γ response after OVA stimulation was analyzed. Splenocytes from mice immunized with OVA and CaP NPs had the highest mean IFN-γ response. IFN-γ is a cytokine involved in innate and adaptive immunity against intracellular infections and can be produced by CD4 T_H1 cells, CD8 T cells, natural killer cells, myeloid cells, dendritic cells, and macrophages. The effector functions of IFN-γ include: macrophage activation leading to intracellular antimicrobial activity by increased fusion of lysosomes with phagosomes, increased MHC-I expression in infected cells, increased expression of IgG2a and decreased production of IgG1, promotion of T_H1 cell differentiation and suppression of T_H2 growth.[169]

IL-4 splenocyte supernatant concentration was also analyzed after stimulation but no detectable amounts were found in any of the groups (data not shown). Immune responses to the same vaccine can also vary between different strains of mice and T_H1 and T_H2 bias has been

reported for C57Bl/6 and BALB/c mice. C57Bl/6 are considered a prototypical T_H1 strain with their lymphocytes producing mainly IFN-γ after stimulation with *Leishmania major*, whereas lymphocytes from BALB/c mice produce IL-4.[132] Therefore, it is not surprising that IFN-γ but not IL-4 was detected in stimulated splenocytes. It is apparent that mouse strain specific biases can impact the results of immunization studies and a better understanding of CaP NP adjuvancy may be gleaned from repeating *in vivo* studies with BALB/c mice.

Similar trends between the TrxA::PA44-OVA fusion protein immunization study detailed in Chap. 3 and the OVA protein immunization study were observed. In both studies, CaP NPs did not increase IgG responses but did increase either CD8+ T-cell response or antigen sensitization of IFN-γ producing splenocytes. The results from the OVA and OVA fusion protein vaccination studies indicate that CaP NP adjuvants may selectively increase cell-mediated T_H1 and cytotoxic T-cell responses over T_H2 antibody responses.

Chapter 5: Nucleic Acid Transfections and Vaccines

5.1: Introduction

In Chapters two through four, calcium phosphate (CaP) nanoparticles (NPs) were evaluated as adjuvants in vaccine formulations containing protein antigens. As an alternative to protein antigen vaccines, nucleic acid vaccines encoding genes for antigens may be useful for the following reasons. First, nucleic acids are easier to construct and purify than proteins. Second, nucleic acid vaccines can target MHC-I loading of peptides by synthesizing antigens in the cytosol. Third, nucleic acids themselves can act as adjuvants through activation of TLR-7 or TLR-9 by single stranded RNA or CpG motifs respectively. Finally, nucleic acid vaccines lack the MHC haplotype restrictions of peptide/protein antigens. Although no nucleic acid vaccines have yet to be licensed in humans, three DNA vaccines have been licensed for veterinary use showing promise for future development.[115]

Major histocompatibility complex (MHC) presentation of antigen epitopes by antigen presenting cells (APCs) after nucleic acid vaccine delivery can occur through the direct transfection and priming of somatic cells (myocytes, keratinocytes, or any MHC-II negative cells), direct transfection of APCs, and exogenous uptake of antigen released from transfected cells by APCs.[71]

The majority of nucleic acid vaccination studies have been carried out with plasmid DNA (pDNA) vaccines. Vaccine plasmids contain features necessary for replication (bacterial origin of replication and antibiotic resistance gene) and mammalian gene expression (viral promoter, insert containing the antigen, and transcription/termination sequences).[71]

mRNA vaccines are an alternative to pDNA vaccines. Although mRNA is less stable than pDNA and more difficult to synthesize, mRNA vaccines have several benefits over pDNA vaccines. Host cell chromosomal integration of pDNA is a potential safety concern with pDNA vaccines[42] and mRNA vaccines eliminate this concern. pDNA vaccines must also enter the nucleus in order for transcription to occur whereas mRNA vaccines only need to enter the cell cytoplasm for translation to occur. DNA entry into the nucleus is particularly difficult in nondividing cells like monocytes.[187] Also, antigen expression after RNA delivery is transient, peaking and decaying rapidly after administration, whereas DNA vaccines can cause antigen expression for many weeks at the site of injection.[150]

Effective cellular delivery and transfection are major barriers for naked nucleic acid vaccine efficacy.[71, 134] Mammalian cells transfected with viral vectors often have the highest rates of transfection but viral vectors are limited by safety concerns and difficulty of production[106]. Polymeric particles and liposomes have been explored for delivery of pDNA vaccines and show promise for enhancing delivery and immunogenicity of pDNA vaccines.[104]

As an alternative nucleic acid delivery vehicle, CaP NPs may be useful in nucleic acid vaccines formulations by acting simultaneously as an adjuvant and delivery vehicle. Transfection of mammalian cells with CaP was first discovered in 1973 by Graham and Van der Eb[62] and is frequently used to transfect a variety of cell types. By adding cPN38 and decreasing the Ca^{2+} to $PO4^{3-}$ ratio, CaP nanoparticles were formed using a modification of the standard CaP transfection method.[62] Transfection efficiency in RAW 264.7 mouse macrophage cells was evaluated *in vitro* with CaP particles and a plasmid encoding the green fluorescent protein (GFP) (gWiz-GFP). Transfection efficiencies were low in groups transfected with CaP (~3%) relative to

the PEI positive controls (~25%). CaP particle uptake was high (>70%) but endosomal escape of pDNA was not observed in RAW 264.7 macrophage cells.

CaP nanoparticles were also evaluated *in vivo* as adjuvants in mRNA and pDNA vaccines encoding ovalbumin (OVA) as the antigen. In mRNA vaccine formulations, CaP NPs did not have an adjuvant effect as measured by total anti-OVA IgG response and splenocyte IFN-γ secretion after OVA protein antigen stimulation. In contrast, the addition of CaP to pDNA vaccines significantly increased total anti-OVA IgG responses. Additionally, mean splenocyte IFN-γ response was higher in the group vaccinated with pDNA and CaP as compared to pDNA only vaccines suggesting that CaP nanoparticles may be useful adjuvants for increasing T_H1 and IgG responses in pDNA vaccines.

5.2: Materials and Methods

5.2.1: Calcium phosphate-DNA particle formulations for *in vitro* transfection

A modification of the CaP formulation, used in both the previous thioredoxin[27] and thioredoxin-ovalbumin fusion protein vaccinations, was evaluated for transfection efficiency *in vitro*. In the original formulation, a precursor solution containing 16.7mM $Ca(NO_3)_2$ (Fisher C-109-500), pH 7.4 and pDNA (gWiz-GFP, Aldevron 5006) is added dropwise while vortexing on a high setting into a solution containing $NH_4H_2PO_4/(NH_4)_2HPO_4$ (Sigma-Aldrich 216003 and Fisher BP361-500), pH 7.4 and cPN38 (GCGPEDIDAVSVGEVQGPC disulfide bond at 2nd and 19th residue, Genscript). Final concentrations were 1.67mM $Ca(NO_3)_2$, 1mM $NH_4H_2PO_4/(NH_4)_2HPO_4$, pH 7.4(0.16mg/mL CaP), 50µM cPN38 and 0.05mg/mL gWiz-GFP. This original CaP formulation was only used in section 5.3.1 for comparison and all other CaP formulations used in this chapter were formulated as described below.

A modification of the standard CaP transfection method[62] was evaluated for *in vitro* transfection efficiency. In the CaP standard transfection method, a solution of calcium chloride and DNA is added slowly dropwise to a 2x HEPES buffered saline (HBS) (50mM HEPES, 280mM NaCl, and 1.5mM Na_2HPO_4, pH 7.1) solution while vortexing at room temperature (Final Ca^{2+} and PO_4^{3-} concentrations: 125mM $CaCl_2$ and 0.75mM Na_2HPO_4). CaP is left to precipitate for 30min before addition to cells. For formulations containing cPN38, cPN38 was added to the HBS precursor solution. Some CaP formulations also contained lowered $CaCl_2$ concentrations as indicated.

5.2.2: Calcium phosphate particle characterization

Particle size and zeta potential were determined by DLS using a Malvern Nano ZS zetasizer. Refractive index (RI) of CaP particles was assumed to be equal to tricalcium phosphate (RI=1.628). Absorbance was 0.01 according to the manufacturer's instructions and dispersant was set to water at 25°C. Data collection was set to 10 runs per reading and particle size was presented as the mean of the maximum peak height from three readings.

Nucleic acid loading was determined for nanoparticles by assaying the supernatant of samples by A280 for nucleic acid concentration after separating nanoparticles by ultracentrifugation at 100,000g for 1 hr on a Beckman Coulter Optima TLX Ultracentrifuge with a Beckman Rotor TLA110#054798. Microparticles were pelleted with centrifugation at 16,000g for 30 min on a Spectafuge 16M microcentrifuge.

5.2.3: *In vitro* transfections

$2.0x10^5$ cells/mL RAW 264.7 mouse macrophage cells (ATCC TIB-71, passage number less than 15) or $5.0x10^4$ cells/mL NIH 3T3 mouse fibroblast cells (ATCC CRL-1658, passage number 40-45) were seeded in 1mL of complete medium [DMEM (Corning 50-013) with Pen/Strep (Gibco 15140) and 10% FBS (Gibco 10437)] per well in 24-well tissue culture treated plates (Corning 3527) and incubated for 24 hrs at 37°C and 5% CO_2. Wells were then washed 1x with PBS, pH 7.4, 0.22µm filtered (Thermo 28372) and 200µL of DMEM (no antibiotics or FBS) with transfection agents was added. PEI polyplexes were prepared according to the following protocol. Per well, a 10µL PEI solution (0.13mg/mL PEI for a 10 N/P ratio) (Sigma 408727) was added to a 10µL 0.1 mg/mL pDNA (gWiz-GFP) solution. Polyplexes were formed for 10-30 min at room temperature (RT). Immediately before addition to the wells polyplexes

were diluted with 180µL DMEM warmed to 37°C. Lipoplexes were formed with Lipofectamine 2000 (LF 2000) (Invitrogen 52758) according to the manufacturer's instructions. Per well, 10µL of a 0.1 mg/mL pDNA solution was added to 40µL DMEM and incubated for 5 min at RT. 3µL of LF 2000 was added to 47µL DMEM and incubated for 5 min at RT. pDNA and LF 2000 solutions were then gently mixed and incubated for 20 min at RT forming lipoplexes at a [3:1] LF 2000 volume to pDNA mass ratio. Immediately before addition to wells, lipoplexes were diluted with 100µL warmed DMEM. For CaP transfections, CaP particle solutions were prepared as previously described and 20µL of CaP particle solutions were added to 180µL warmed DMEM per well. CaP solutions contained 125mM $CaCl_2$ unless otherwise indicated and 0.05mg/mL pDNA. pDNA per well was normalized at 1µg per well and total volume per well was normalized at 200µL.

Transfection agents were left in wells for 4 hrs at 37°C and 5% CO_2, then wells were washed 1x with PBS and 500µL of complete medium was added to wells. 44 hrs after changing medium, cells were washed 1x with PBS and dissociated from wells with 100µL/well Cell Dissociation Buffer (Gibco 13151-014). Cells were pelleted at 500g for 5 min and resuspended in 200µL FACS buffer (1xPBS, pH 7.4 and 2% FBS) with 0.2µg/mL propidium iodide (PI) (Life Technologies P3566). Cells were then analyzed on a BD Facscan flow cytometer. 10,000 cells were gated and % GFP positive cells and PI+ cells (dead) were determined. Transfection efficiency presented as the percentage of GFP+, PI- cells. See supplemental data for flow cytometer gate settings.

5.2.4: RAW 264.7 cell viability assay

In a 96-well tissue culture treated plate (BD 353077), 200µL of $2.0x10^5$ cells/mL RAW 264.7 cells in complete medium were seeded for 24 hrs at 37°C and 5% CO_2. Wells were then washed 1x with PBS and 40µL of the previously described transfection agents in DMEM were added per well. Cells were incubated with transfection agents for 4 hrs at 37°C and 5% CO_2, and then wells were washed 1x with PBS, and 100µL of complete medium was added to wells. After 20 hr incubation, 10µL of Alamar Blue (Life Technologies DAL 1025) was added per well and incubated for an additional 3.5 hrs. Absorbance at 570nm normalized to 600nm was then read.

5.2.5: Mannosylation of cPN38

A primary amine reactive mannose precursor, α-D-mannopyranosylphenyl isothiocyanate (MIC) (Sigma M9271), was used to mannosylate the cyclic CaP binding peptide cPN38. 0.9mL of 0.3mg/mL cPN38 was mixed with 0.5mg MIC in 100uL DMSO (approximately 11-fold molar excess of MIC to cPN38). The reaction solution was held at 4°C for 16 hrs under gentle mixing. The reaction solution was then dialyzed with a 1,000 MWCO membrane (Spectrum Labs 132105) against ddH_2O at 4°C with buffer changes at 1, 4, and 16 hrs followed by overnight dialysis. The dialyzed reaction mixture was then filtered through a 0.22µm filter and analyzed for mannose using the resorcinol assay for detection of neutral sugars (Monsigny, 1988). In brief, 20µL of sample was added to 20µL of 6mg/mL resorcinol (Acros 132290500) and 100µL of 75% sulfuric acid (Mallinckrodt 2876). The sample mixture was then heated at 90°C for 30min then kept at RT for 30 min in the dark. Absorbance was then read at 430nm. The mannose concentration in samples was determined from a free mannose standard curve (R^2 =0.99).

5.2.6: *In vitro* uptake of Cy3 tagged pDNA

gWiz-GFP was labeled with Cy3 using the Mirus' Label IT® Nucleic Acid Labeling Kit, Cy™3 (Mirus MIR 3625) according to the manufacturer's instructions, which labels pDNA at a 1:1 [v:w] ratio of Label IT Reagent to nucleic acid. Labeled pDNA should have approximately one Cy3 molecule for every 20-60 bp.

CaP particles were prepared with Cy3-tagged gWiz-GFP and mineralized in the presence of cPN38 (25μM) or mannosylated cPN38 (cPN38-M) (25μM). RAW 264.7 cells were seeded at $2.0x10^5$ cells/mL in 1 mL of complete medium and incubated for 24 hrs at 37°C and 5% CO_2. Cells were then washed 1x with PBS and 20uL of the following CaP formulations were added to 180μL DMEM per well:

"*CaP microparticles*": 1xHBS, 125mM $CaCl_2$, and 0.05mg/mL gWiz-GFP-Cy3

"*CaP nanoparticles*": 1xHBS, 60mM $CaCl_2$, 25uM cPN38 and 0.05mg/mL gWiz-GFP-Cy3

"*CaP mannosylated nanoparticles*": 1xHBS, 60mM $CaCl_2$, 25uM cPN38-M and 0.05mg/mL gWiz-GFP-Cy3.

Mannose receptor specific uptake was blocked in cells by addition of 2.5mM mannose for 30 min before addition of mannosylated particles. After 24 hr incubation, cells were washed 1x with PBS, dissociated from plates, and resuspended in FACS buffer before analysis on a BD Facscan flow cytometer. Fluorescence from particles attached to the surface of cells was quenched by addition of Trypan Blue (Sigma D2650) at a final concentration of 20μg/mL. See supplemental data for flow cytometer gate settings.

5.2.7: Fluorescence microscopy of RAW 264.7 cells and calcium phosphate-DNA particles

gWiz-GFP was tagged with fluorescein using the Mirus' Label IT® Nucleic Acid Labeling Kit, Fluorescein (Mirus MIR 3225) according to the manufacturer's instructions. RAW 264.7 cells were seeded into 8-chamber coverglass slides (Nunc LabTek 155411) with 0.43 mL complete medium per well at a cell density of $2.0x10^5$ cells/mL. Cells were incubated for 24 hrs at 37°C and 5% CO_2. Wells were washed 1x with PBS and incubated with 86µL of DMEM without phenol red (Corning 90-013PB) containing an intracellular Ca^{2+} dye, 50nm X-Rhod-5F, Acetoxymethyl (AM) (Life Technologies X23985) for 1hr. Cells were then washed 1x with PBS and incubated in 86µL dye free DMEM without phenol red for 30 min. Cells were then washed 1x with PBS and the following CaP formulations were added: CaP standard (125mM $CaCl_2$) and 0.05mg/mL tagged pDNA; CaP nanoparticles (60mM $CaCl_2$ and 50uM cPN38); or mannosylated CaP particles (60mM $CaCl_2$ and 50uM cPN38-M). 8.6µL of CaP particle dispersions were added to 77.4 µL DMEM without phenol red per well. Fluorescent microscopy images were taken on an Axio Observer inverted microscope (Zeiss) 5 hours after addition of CaP-DNA particles.

For imaging at 24 hrs, X-Rhod-5F was not added until 24 hrs after addition of CaP. After 24 hrs cells were washed 1x with PBS, and incubated with 50nm X-Rhod-5F, AM (Life Technologies X23985) in 86µL DMEM without phenol red for 1hr. Cells were then washed 1x with PBS and incubated in 86µL dye free DMEM without phenol red for 30 min. Cells were then washed 1x with PBS and 86µL DMEM without phenol red was added before imaging.

5.2.8: Immunizations with pVAX-OVA vaccines

The plasmid used for *in vivo* vaccinations was pVAX-OVA [Cheng, 2012], which contains the ovalbumin cDNA EcoRI fragment from pAc-neo-OVA subcloned into Invitrogen's

pVAX1 (Life Technologies V260-20), which is a specialized vector for DNA vaccines that contains the cytomegalovirus immediate-early (CMV) promoter, bovine growth hormone (BGH) polyadenylation signal, and minimal DNA sequences not necessary for replication in *E. coli* or expression in mammalian cells. pVAX-OVA was harvested from Top10 *E. coli* cells using Qiagen's EndoFree Plasmid Mega Kit (Qiagen 12381).

All animal experiments adhered to federal guidelines and were approved by the University of Washington Animal Care and Use Committee. Groups of C57Bl/6 mice (Jackson Laboratory, age 6-8 weeks) (n=10) were immunized at day 0, 7, and 14 with 200µL of vaccine formulations split between two lower abdominal subcutaneous sites. Mice received vaccine formulations containing either pVAX-OVA only (0.1mg/mL pVAX-OVA in 0.1xHBS) or pVAX-OVA with CaP nanoparticles (0.1mg/mL pVAX-OVA, 0.5mg/mL CaP and 20µM cPN38). Serum was collected at day 20 via submandibular vein bleeds. Mice were sacrificed at day 28 and the spleens were removed aseptically.

5.2.9: Immunizations with OVA mRNA Vaccines

mRNA encoding OVA was transcribed from a template plasmid pGEM4z-OVA-A64 [Cheng, 2012] [Boczkowski 2000] derived from Promega's pGEM-4z commercial cloning vector. pGEM4z-OVA-A64 is harbored in *E. coli* Top 10 cells with the plasmid conferring ampicillin (Amp) resistance. The template plasmid was purified using Qiagen's EndoFree Plasmid Mega Kit (Qiagen 12362).

In a total reaction volume of 0.5mL, 50µg of purified pGEM4z-OVA-A64 was linearized with 100U SpeI in 1xNEB4 buffer and 100µg/mL BSA. The digestion was carried out at 37°C then terminated after 4 hrs by adding 25µL of 0.5M EDTA, 50µL of 3M sodium acetate, and

1mL of 95% ethanol. The reaction mixture was then mixed and chilled at -20°C for 15 min. DNA was pelleted for 15min in a microcentrifuge at 16,000g. Supernatant was removed and the DNA pellet was resuspended in molecular biology grade water (Corning 46-000-CM). Linearized plasmid purity and concentration was evaluated with A280 and A280/260 measurements. OVA mRNA transcripts were transcribed from the linearized pGEM4z-OVA-A64 template with Ambion's mMessage mMachine T7 kit (Life Technologies AM 1344) according to the manufacturer's instructions. mRNA transcripts were purified using Ambion's MEGAclear Kit (AM1908). mRNA purity and concentration were determined with A280 and A280/260 measurements.

Groups of C57Bl/6 mice (Jackson Laboratory, age 6-8 weeks) (n=5) were immunized at day 0, 7, and 14 with 200µL of vaccine formulations split equally between two lower abdominal subcutaneous sites. Mice received vaccines containing either OVA mRNA only (0.025mg/mL OVA mRNA in 0.1xHBS) or OVA mRNA and CaP (0.1mg/mL pVAX-OVA, 0.5mg/mL CaP and 20uM cPN38). Serum was collected at day 17, 20, and 27 via submandibular vein bleeds. Mice were sacrificed at day 28 and spleens were removed aseptically.

5.2.10: Anti-OVA IgG ELISAs

Ninety-six-well maxisorp plates (Thermo 442404) were coated overnight with 100µL/well coating buffer [10µg/mL OVA (Invivogen vac-ova) in 1xPBS pH 7.4 (Thermo 28372), 0.1% [w/v] sodium azide (Sigma S-8032)] at 4°C. Plates were then washed 2x with 200µL/well wash buffer (1xPBS, pH 7.4 and 0.02% [v/v] Tween 20 (Fisher BP337-500). Plates were then blocked with 150µL/well block buffer (1% [w/v] bovine serum albumin (Sigma A7030-50g) in 1xPBS, pH7.4, 0.22µm filtered) for 1 hr at 37°C. Wells were then washed twice.

100µL/well of diluted serum samples and standards [Anti-OVA IgG1 standard (Sigma A6075)] in block buffer were added to plates and incubated for 1hr at 37°C. Wells were then washed four times. 100µL/well secondary antibody [goat anti-mouse IgG-HRP (Biolegend 405306)] diluted 2000x in block buffer were added per well followed by a 30min incubation at 37°C. Wells were again washed four times. 100µL/well TMB substrate (Thermo 34021) was added followed by a 10 min RT incubation in the dark. The reaction was stopped by adding 2M sulfuric acid at 100µL/well. Absorbance was recorded at 450nm. Titers were determined as the last dilution to have a reading higher than 3x the standard deviation of the blank wells after subtracting the average absorbance of blank wells.

5.2.11: Splenocyte IFN-γ secretion assay

IFN-γ secretion was analyzed after stimulation with OVA in the spleens of mice from each group (n=5). Spleens were removed aseptically from mice sacrificed by CO_2 asphyxiation and placed in 1mL splenocyte medium [RPMI 1640 w/ 2mM L-glutamine (Gibco 11875-093) with 1x PenStrep (Gibco 15140), 10% heat inactivated FBS (Gibco 10082147) and 0.1% [v/v] beta-mercaptoethanol (Gibco 21985)] on ice. A 3mL syringe plunger (BC 309585) was used to force spleens through a 70um cell strainer (BD 352350) pre-wetted with 1mL medium and the plunger and cell strainer were then washed with 10mL of medium. Suspended cells were pelleted at 500g for 5 min. Cell pellets were resuspended in 3mL ACK lysis buffer (Invitrogen A10492-01) and incubated at RT for 5 min. Then, 12mL of medium was added to stop the reaction and cells were pelleted again. Cell pellets were resuspended with 10mL of medium and pelleted again. The cell pellet was finally resuspended in 1mL of medium. Live cell density was determined by counting cells diluted 1:20 with a 1:10 dilution of Trypan Blue (Sigma T8154) using a Bright-Line™ Hemacytometer (Sigma Z359629).

Splenocytes were seeded at $1x10^6$ cells/well in 100µl medium in a 96-well TC-treated U-bottom plate (BD 353077). Splenocytes were stimulated by adding 200µg OVA (Invivogen vac-ova) per well in 100µL medium. Total medium volume after stimulation was 200µL/well. Stimulated splenocytes were then incubated for 16 hrs at 37°C, 5% CO_2. After 16 hrs, plates were centrifuged at 500g for 5 min and 150µL splenocyte cell culture supernate was aliquoted and stored at -80°C. IFN-γ concentration in splenocyte supernatants was analyzed with a commercial IFN-γ ELISA kit (Thermo ESS0020). ELISAs were carried out according to manufacturer's instructions.

5.3: Results

5.3.1: Evaluation of previously used calcium phosphate formulation for transfection efficiency

The previous CaP formulation used for the thioredoxin immunization experiments[27] was evaluated for use as a transfection agent. Precursor Ca^{2+} and $PO4^{3-}$ concentrations remained the same but cPN38 (50µM) was used as a capping agent instead of Trx::PA44, and pDNA (0.05mg/mL gWiz-GFP) was also added to the Ca^{2+} precursor solution. Up to 24hrs after mixing of precursor solutions, CaP particle size remained at 40 ± 10nm in the presence of cPN38 and pDNA (Table 5.1). However, when pDNA loading onto CaP particles was evaluated, poor pDNA loading was observed with this formulation (Fig. 5.1). When tested as a transfection agent, these CaP formulations had little to no transfection efficiency in RAW 264.7 cells (Fig. 5.2).

Table 5.1: Size by DLS of CaP particles [1.67mM $Ca(NO_3)_2$ and 1mM $NH_4H_2PO_4/(NH_4)_2HPO_4$, pH 7.4](0.16mg/mL CaP) with cPN38 (50µM), and pDNA (0.05mg/mL).

CaP, cPN38 and DNA		
Time (hrs)	AVG (nm)	Stdev
0	26	9
1	31	14
2	20	16
4	27	14
24	41	12

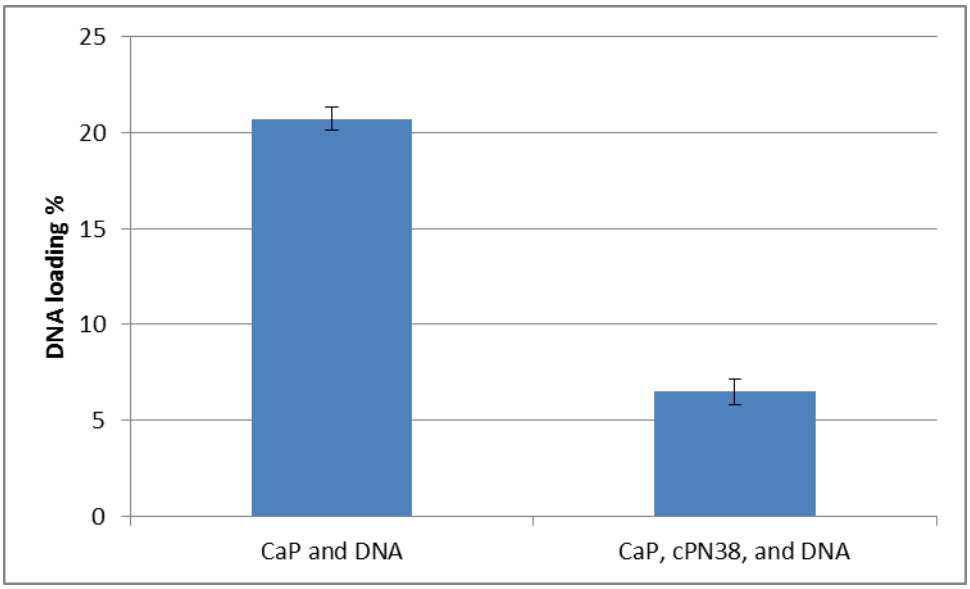

Fig. 5.1: gWiz-GFP (0.05mg/mL) loading onto CaP particles [1.67mM $Ca(NO_3)_2$ and 1mM $NH_4H_2PO_4/(NH_4)_2HPO_4$, pH 7.4](0.16mg/mL CaP) with and without 50µM cPN38.

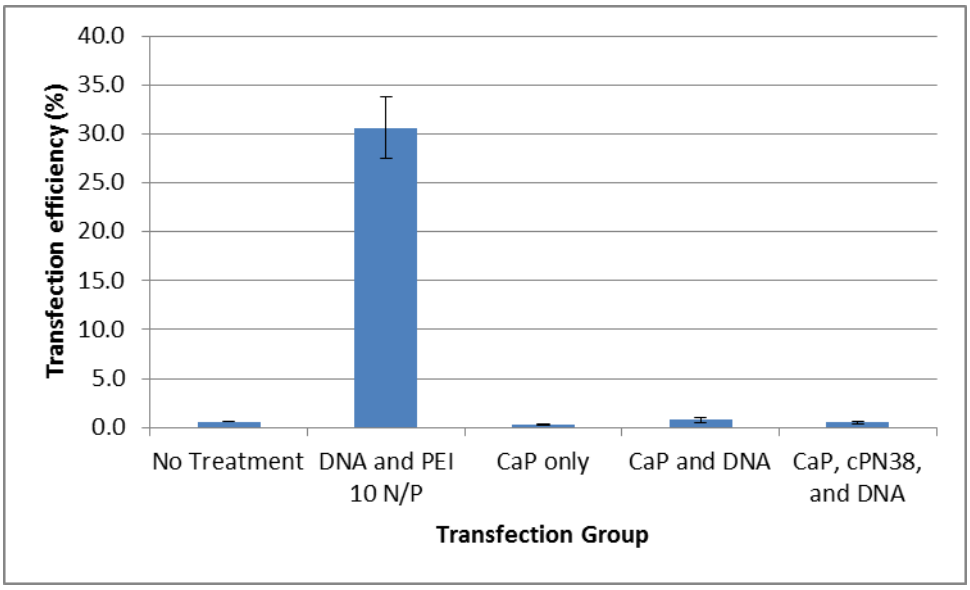

Fig. 5.2: Transfection efficiency in RAW 264.7 cells with PEI (10 N/P, 0.05mg/mL gWiz-GFP) and CaP-DNA particles [0.16mg/mL CaP (1.67mM $Ca(NO_3)_2$ and 1mM $NH_4H_2PO_4/(NH_4)_2HPO_4$, pH 7.4), 0.05mg/mL gWiz-GFP) with and without 50µM cPN38.

5.3.2: Evaluation of a modified calcium phosphate formulation

Another CaP formulation modified from the commonly used standard CaP transfection method[62] was also evaluated for transfection efficiency. In this method, a solution of calcium chloride and DNA or RNA is added slowly dropwise to a 2x HEPES buffered saline (HBS) (50mM HEPES, 280mM NaCl, and 1.5mM Na_2HPO_4, pH 7.1) solution while vortexing at room temperature (Final Ca^{2+} and PO_4^{3-} concentrations: 125mM $CaCl_2$ and 0.75mM Na_2HPO_4). CaP-DNA particles are then left to ripen for 30min before addition to cells. Although this method of CaP transfection is widely used, reproducibility can vary due to differences in nucleic acid concentration and mixing technique resulting in variations in particle size and morphology.[11, 92, 118] The Ca^{2+} to PO_4^{3-} molar ratio in the standard CaP tranfection method is a hundredfold higher (167) than the previously described formulation used for the protein vaccinations (1.67). In the following sections, all CaP formulations used for nucleic acid *in vitro* and *in vivo* work will refer to the standard CaP transfection formulation or the modified protocol unless indicated.

CaP particle size was evaluated immediately after mixing CaP precursor solutions. Standard CaP transfection formulations (1xHBS, 125mM $CaCl_2$ and 50µg/mL gWiz-GFP) exhibited small particle sizes (sub-200nm) but with the addition of 50µM cPN38, a decreased CaP particle size was observed at all concentrations of calcium chloride. At a calcium chloride concentration below 70mM, CaP particles were below 100nm in size with the addition of 50µM cPN38 (Fig. 5.3). When left at room temperature for 30min, the standard CaP transfection formulation consisted of particles 1400 +/- 100 nm in size as determined by DLS. Zeta potential of CaP particles without DNA or cPN38 showed a strongly positive zeta as expected from the high Ca^{2+} to PO_4^{3-} ratio (Fig. 5.4). Upon addition of pDNA, the zeta potential shifted to a negative value indicating adsorption of the polyanionic pDNA.

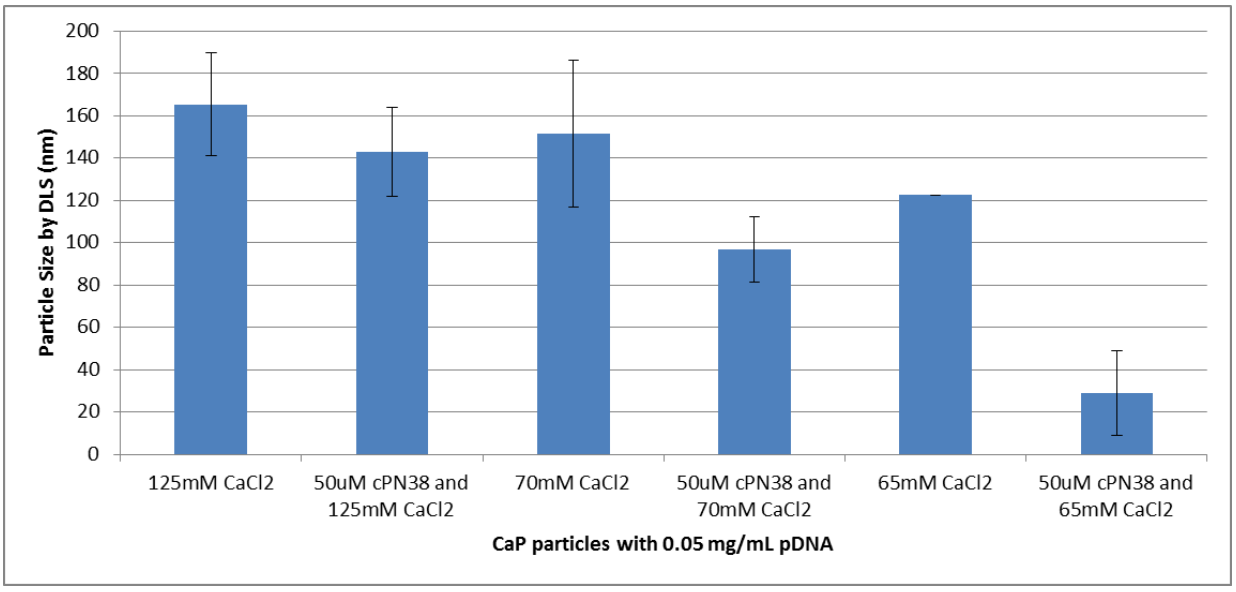

Fig. 5.3: Comparison of CaP-pDNA (1xHBS, $CaCl_2$, and 0.05mg/mL gWiz-GFP) particle size with and without cPN38 (50µM) at varying $CaCl_2$ concentrations by DLS immediately after mixing.

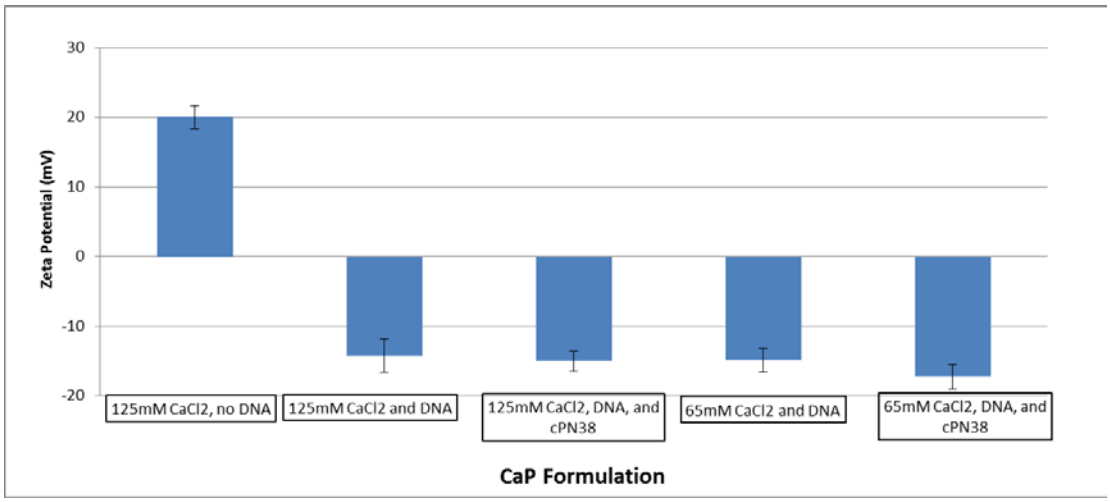

Fig. 5.4: Zeta potential by DLS of CaP particles (1xHBS and $CaCl_2$) at varying $CaCl_2$ concentrations with and without pDNA (0.05mg/mL) and cPN38 (50µM).

RAW 264.7 mouse macrophage cell viability was analyzed after addition of various transfection agents (Fig. 5.5). Lipofectamine 2000 ([3:1][v:w] Lipofectamine to pDNA ratio) was the least toxic and PEI (10 N/P) was found to be the most toxic of the transfection agents evaluated.

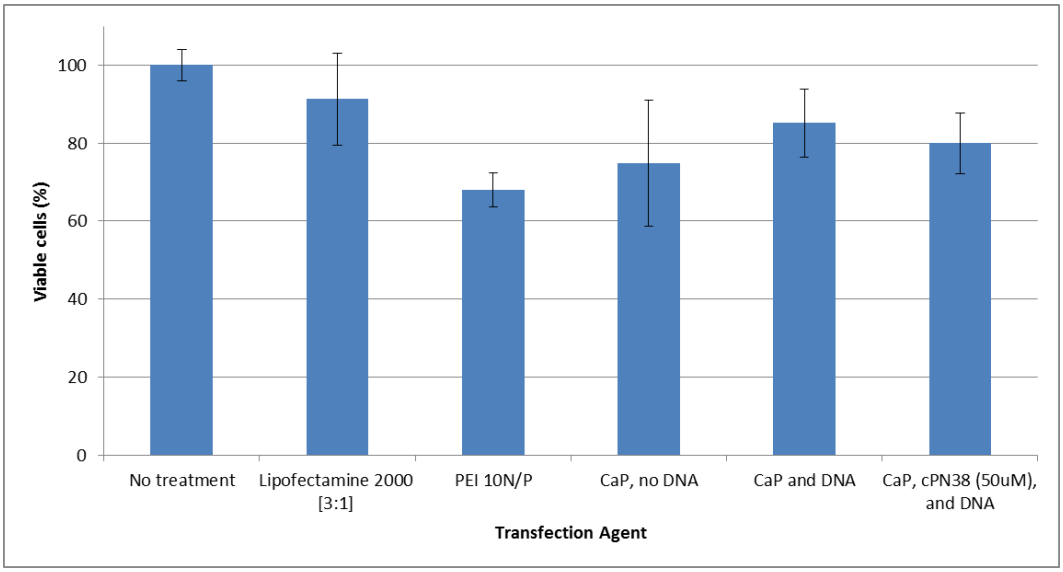

Fig. 5.5: Cell viability by Alamar Blue assay of RAW 264.7 cells in the presence of various transfection agents. pDNA (1µg) was added to all wells except the "No Treatment" and "CaP (1xHBS and 125mM $CaCl_2$) no DNA group".

GFP transfection efficiency was evaluated in RAW 264.7 cells with various CaP formulations (Fig. 5.6). Lipofectamine [3:1] and PEI 10 N/P were used as positive controls. CaP formulations described in other CaP NP studies[93, 176] were also evaluated for transfection efficiency as a comparison. These formulations were prepared according to the methods described with the exception of pDNA concentration which was normalized for all CaP formulations. The standard CaP transfection method and modifications thereof did show higher transfection efficiencies than the previous CaP formulations modified from the protein studies (Fig. 5.2). However, overall transfection efficiencies using CaP particles were much lower as compared to the positive controls. CaP formulations modified from Sokolova, et. Al.[176] and Joyappa, et. Al.[93] did not show any transfection efficiency in the RAW 264.7 cells. CaP standard and NP formulations had comparable levels of transfection. pDNA loading onto CaP particles was high for CaP standard particles (99.1 ± 0.5%) and CaP NPs (86.6 ± 0.9%) at a pDNA concentration of 0.05mg/mL.

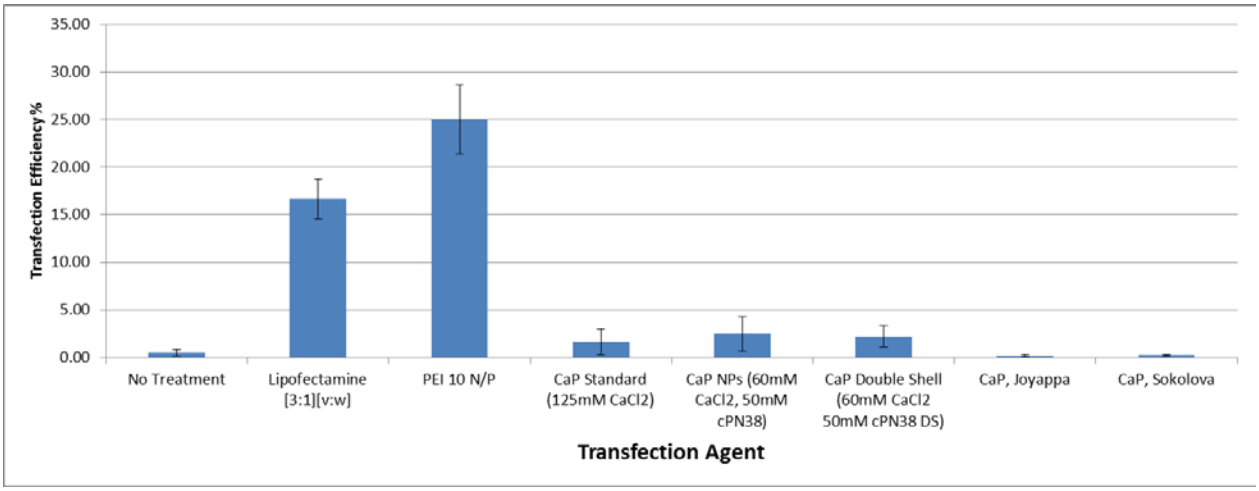

Fig. 5.6: GFP transfection efficiency of RAW 264.7 cells with various transfection agents.

5.3.3: Calcium phosphate transfection efficiency in NIH 3T3 cells

Transfection efficiency with CaP particles can vary greatly with cell type. CaP transfection is commonly evaluated using Human Embryonic Kidney (HEK) 293 cells,[92,94, 117] Chinese Hamster Ovary (CHO) cells,[11] and Hela cells.[14, 56, 144, 148, 176] Increased transfection efficiency in NIH 3T3 cells has also been reported with CaP nanoparticles as compared to larger CaP microparticles.[117]

GFP transfection efficiency was evaluated in NIH 3T3 mouse fibroblast cells with various transfection agents (Fig. 5.7). Of the CaP formulations tested, the highest transfection efficiency was observed in cells receiving CaP microparticles (Table 5.2). Use of smaller CaP particles did not increase transfection efficiency, and the transfection efficiency with CaP microparticles (11 +/- 2%) was higher than the highest transfection efficiency reported (4.71%) with CaP nanoparticles in NIH 3T3 cells by Liu, et. Al.[117]

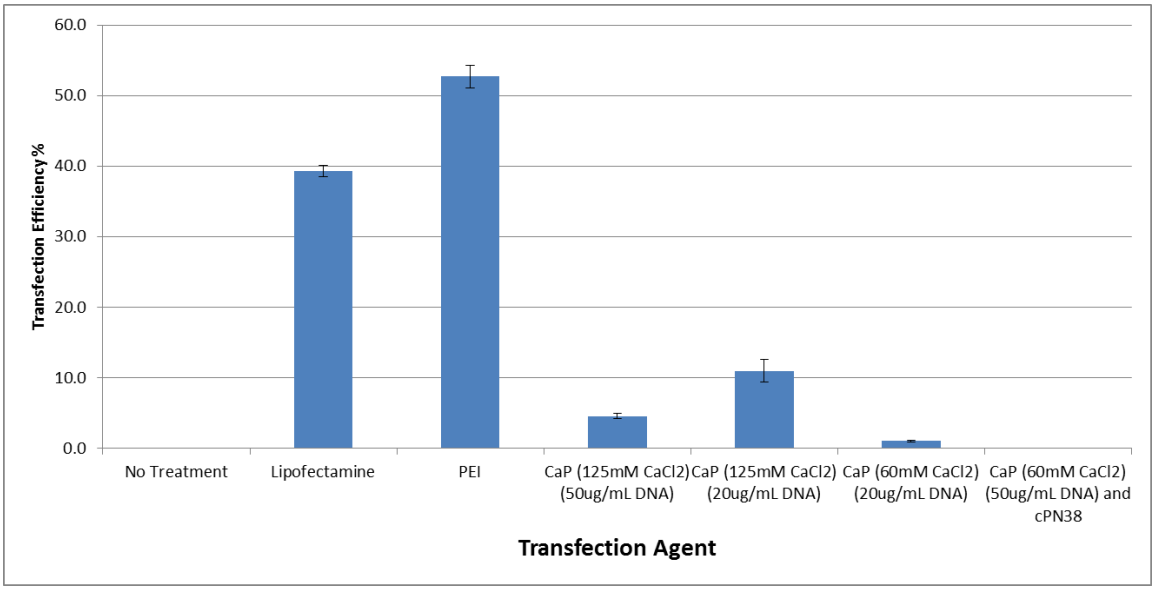

Fig. 5.7: GFP transfection efficiency of NIH 3T3 cells with various transfection agents.

Table 2: Particle size by DLS of CaP particles used in NIH 3T3 transfections.

Transfection Agent	AVG (nm)	Stdev
CaP (125mM CaCl2) (50ug/mL DNA)	212	37
CaP (125mM CaCl2) (20ug/mL DNA)	2126	490
CaP (60mM CaCl2) (20ug/mL DNA)	181	15
CaP (60mM CaCl2) (50ug/mL DNA) and cPN38	37	8

5.3.4: Mannosylation of cPN38

Macrophage and dendritic cells express mannose receptors that recognize, bind, and initiate endocytosis and phagocytosis of infectious agents displaying repeated mannose patterns.[178] Increased uptake of mannosylated liposomes,[48, 188] PEI,[40] and proteins[17] has been demonstrated in macrophages and dendritic cells.

A primary amine reactive mannose precursor, α-D-mannopyranosylphenyl isothiocyanate (MIC), was used to mannosylate the cyclic CaP binding peptide cPN38 resulting in cPN38-M. Mannosylation of cPN38 was verified using a resorcinol sulfuric acid assay.[136] Approximately two mannose residues were found per cPN38 peptide (2.03 molar ratio of mannose to cPN38) most likely attaching at the N-terminus of cPN38 and with the glutamine side chain present within the CaP binding dodecapeptide. CaP (1xHBS and 60mM $CaCl_2$) particle sizes with 50ug/mL gWiz-GFP and cPN38-M (170 +/- 30nm) were similar to CaP and gWiz-GFP particle sizes (170 +/- 30nm) without protein. No significant increase in transfection efficiency was seen with RAW 264.7 cells transfected with CaP-DNA particles when cPN38-M was added to formulations (data not shown).

5.3.5: Uptake of calcium phosphate-DNA particles *in vitro*

pDNA uptake in RAW 264.7 cells was quantified by fluorescently tagging gWiz-GFP with Cy3 prior to CaP particle incorporation. Uptake of tagged pDNA was evaluated with CaP microparticles, nanoparticles and mannosylated nanoparticles (Fig.5.8). 24 hrs after addition of CaP-DNA particles, Cy3+ RAW 264.7 cells were detected by flow cytometry. Extracellular fluorescence from CaP-DNA particles bound to the surface of cells was quenched with Trypan Blue.

pDNA uptake was the highest (>90%) in cells treated with CaP nanoparticles, both mannosylated and non-mannosylated particles. pDNA uptake was also high with CaP microparticles (>70%). Uptake of mannosylated particles did not appear to be mannose receptor mediated as the addition of free mannose did not inhibit uptake of particles. The high uptake of CaP-DNA particles suggests that low transfection efficiencies are not limited by delivery of pDNA into macrophages.

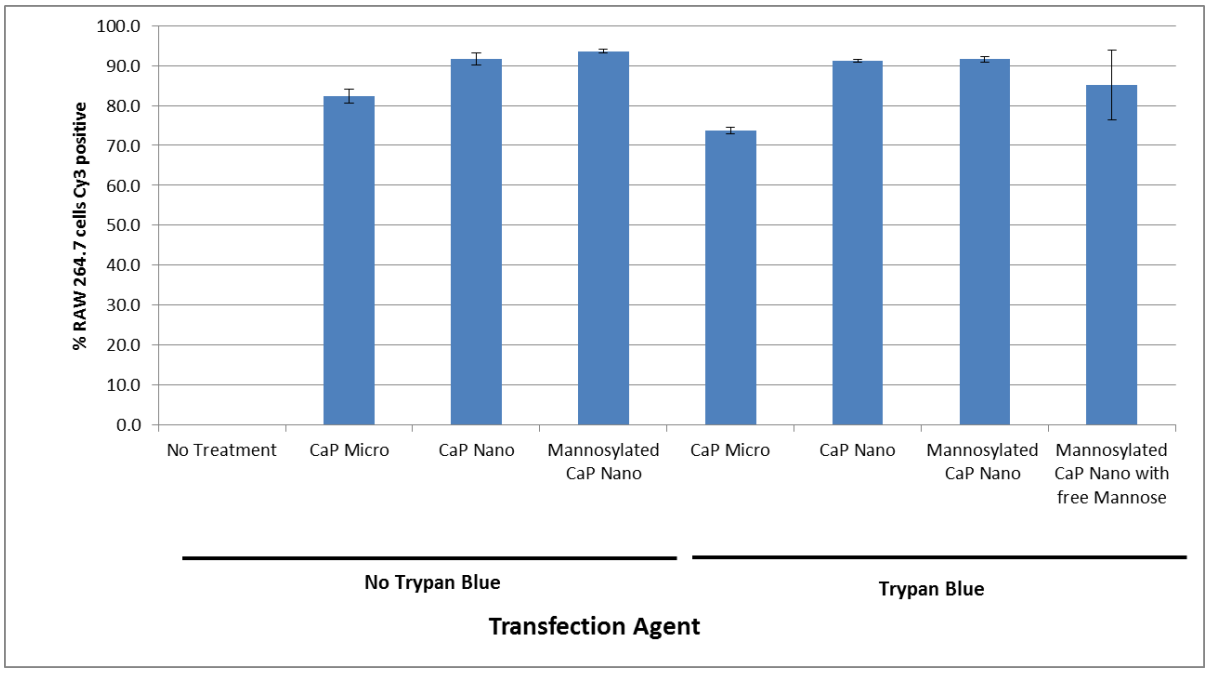

Fig. 5.8: Uptake of Cy3 tagged gWiz-GFP in RAW 264.7 cells with and without extracellular fluorescence quenching by addition of Trypan Blue.

Endosomal escape of pDNA into the cytoplasm is thought to occur via the following process when CaP is used as a transfection agent. 1. Uptake of CaP-DNA into early endosomes, 2. As pH drops CaP dissolves releasing ions, 3. Osmotic pressure from a sudden increase in ion concentration disrupts the endosome and free pDNA escapes.[108]

Fluorescence microscopy was carried out to determine whether endosomal escape was limiting CaP transfection in RAW 264.7 macrophage cells. Delivery of CaP-DNA particles was observed by labeling pDNA with fluorescein and intracellular Ca^{2+} release was detected with X-Rhod-5F. CaP particles were added to RAW 264.7 cells for 4 hrs followed by washing and staining with X-Rhod-5F. X-Rhod-5F was only observed in a small percentage of cells following staining indicating poor acidification of CaP particles (Fig. 5.9). In a separate experiment, CaP-DNA uptake and intracellular Ca^{2+} release was observed 24hrs after addition of CaP-DNA (Fig. 5.10). No increase in frequency of X-Rhod-5F fluorescence was observed between cells with and

without CaP-DNA particles, indicating poor acidification of particles. There did appear to be binding or uptake of Cy-3 tagged pDNA and CaP particles in RAW 264.7 cells 24 hrs after addition of CaP but intracellular Ca^{2+} release did not appear to be occurring.

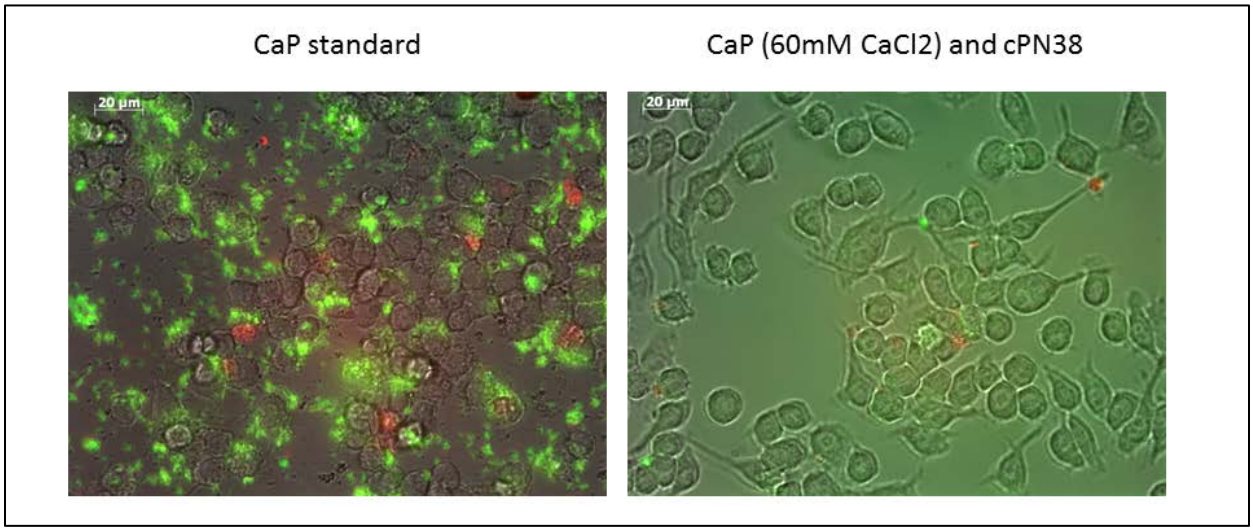

Fig. 5.9: RAW 264.7 cells with CaP and gWiz-GFP tagged with fluorescein (green) and stained with an intracellular Ca^{2+} stain X-Rhod-5F (red). Images were taken 5 hrs after addition of CaP. 40x magnification.

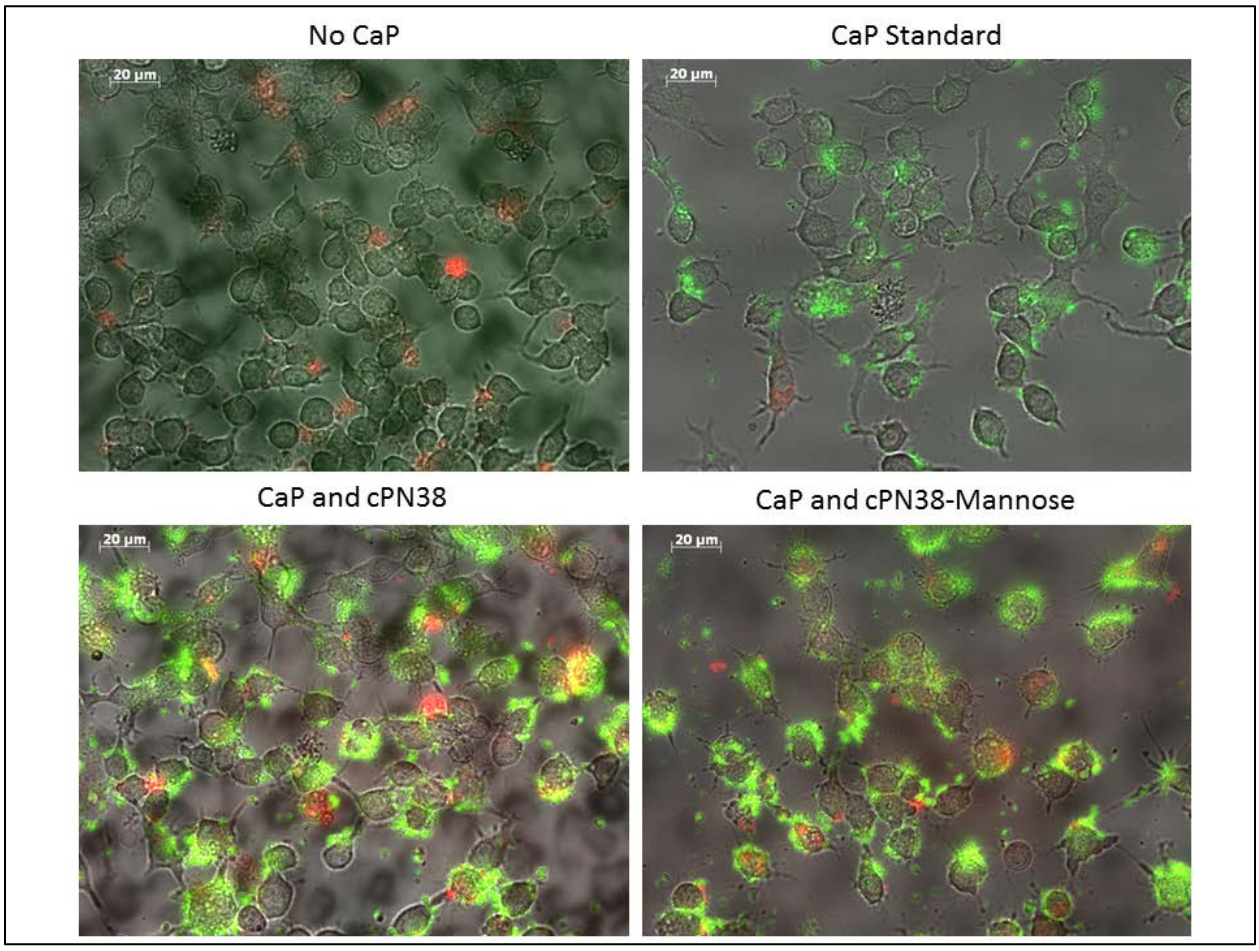

Fig. 5.10: RAW 264.7 cells with CaP and gWiz-GFP tagged with fluorescein (green) and stained with an intracellular Ca^{2+} stain X-Rhod-5F (red). Images taken 24 hrs after addition of CaP. 40x Magnification.

5.3.6: Immunizations with pVAX-OVA and calcium phosphate

Immunizations with pDNA vaccines were carried out using the plasmid encoding the OVA gene, pVAX-OVA, under control of the cytomegalovirus immediate-early (CMV) mammalian promoter. For CaP-DNA formulations used *in vivo*, CaP concentration was lowered

from the standard CaP transfection concentration of 5mg/mL to 0.5mg/mL for a CaP adjuvant dose of 100ug per 200uL injection. The Ca^{2+} to PO_4^{3-} ratio remained unchanged at 167.

The CaP (0.5mg/mL), cPN38 (20μM), and pVAX-OVA (0.1mg/mL) particles used for the immunization studies formed stable CaP NPs 40 +/- 10nm by DLS up to 4hrs after mixing. pVAX-OVA loading onto particles was also high, 80.9+/-0.5%.

Mice were immunized with 200μL of vaccine formulations split equally between two abdominal subcutaneous sites at day 0, 7, and 14. Groups received vaccines containing either pVAX-OVA only (20μg per injection) or pVAX-OVA and CaP NPs (20μg pVAX-OVA, 100μg CaP and 3.7μg cPN38 per injection). Mice were bled at day 20 and splenocytes were extracted at day 28.

Mice immunized with pVAX-OVA and CaP NPs had a significantly higher total anti-OVA IgG levels ($P<0.01$) than the naïve group and the group immunized with pVAX-OVA only (Fig. 5.11). Overall, serum total anti-OVA IgG levels were low compared to responses seen in mice immunized with protein vaccines (see Fig. 4.8). Sera IgG1 and IgG2c isotype concentrations were below detectable values in all groups.

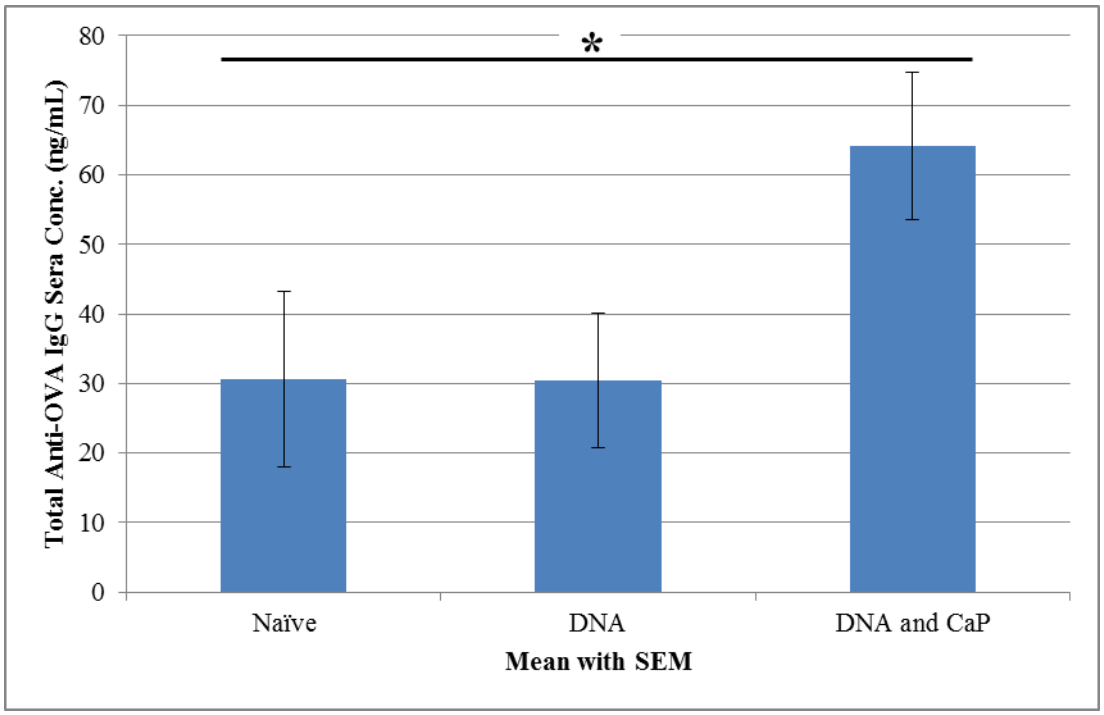

Fig. 5.11: Total anti-OVA IgG concentration in sera at day 20 from mice vaccinated with pDNA vaccines. Statistical significance determined using Student's t-test. (*P<0.01, "DNA and CaP" group relative to other groups).

Splenocytes were extracted at day 28 and cell culture supernatant was analyzed 16hrs after OVA stimulation for IFN-γ concentration by ELISA (Fig. 5.12). The highest IFN-γ response was observed in splenocytes from mice immunized with pVAX-OVA and CaP NP adjuvant. Due to variability in the response between individual mice (n=5) within each group, the differences between groups was not significant at α=0.5 (p=0.07 DNA and CaP group relative to Naïve and DNA only groups). At α=0.5, β=0.1, approximately 20 mice would be required per group to determine significance. When compared to a study by Boyle *et al*. under similar conditions,[20] the IFN-γ concentration of the naïve group was 5 times higher than the highest IFN-γ concentration reported in their study. High IFN-γ response may be due to endotoxin contamination in the lower grade OVA (Invivogen vac-ova) used for stimulation.

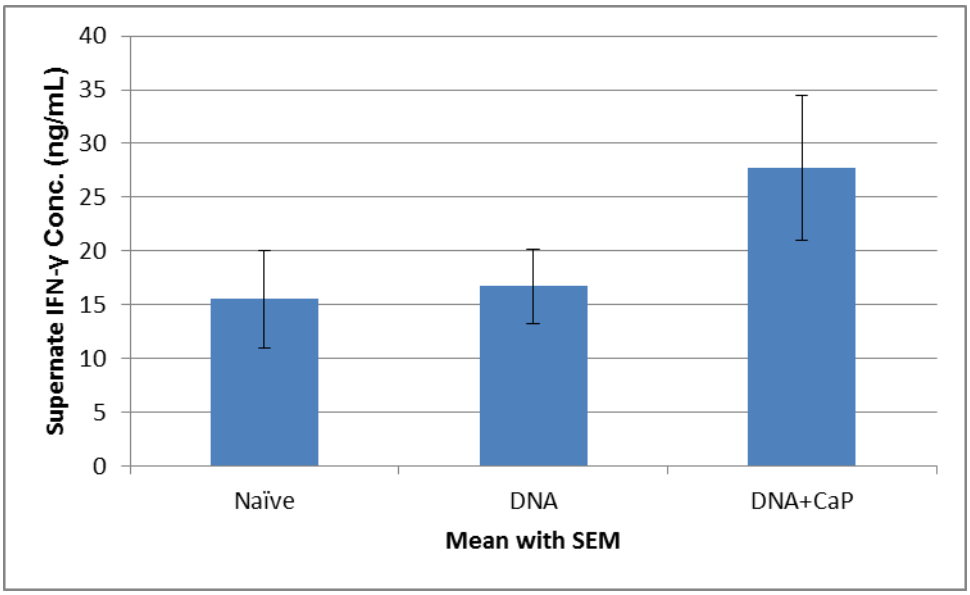

Fig. 5.12: Splenocyte supernatant IFN-γ concentration 16 hrs after stimulation with OVA. Statistical significance determined using Student's t-test. (Data not significant between groups, α=0.05)

5.3.7: Immunizations with OVA mRNA and calcium phosphate

Adjuvancy of CaP particles was also evaluated with vaccines containing mRNA encoding OVA. pGEM4z-OVA-A64[26] was linearized with SpeI and used as a template for mRNA transcription using Ambion's mMessage mMachine T7 kit.

CaP (0.5mg/mL), cPN38 (20µM), and OVA mRNA (0.025mg/mL) particles used *in vivo* formed stable CaP nanoparticles (30 +/- 10nm) up to 4hrs after mixing and OVA mRNA loading onto particles was 89.9+/-0.8%.

Groups of C57Bl/6 mice were immunized with 200µL of vaccine formulations split equally between two abdominal subcutaneous sites at day 0, 7, and 14. Groups received vaccines containing either OVA mRNA only (0.025mg/mL OVA mRNA in

0.1xHBS) or OVA mRNA and CaP (0.1mg/mL pVAX-OVA, 0.5mg/mL CaP and 20uM cPN38). Mice were bled at day 17, 20, and 27 and splenocytes were extracted at day 28.

Similar to the DNA vaccines, overall total anti-OVA IgG levels were low relative to OVA protein vaccinations (Fig. 5.13). Mice immunized with naked OVA mRNA had significantly higher IgG levels than mice immunized with OVA mRNA and CaP at day 17 and 27 ($P<0.05$).

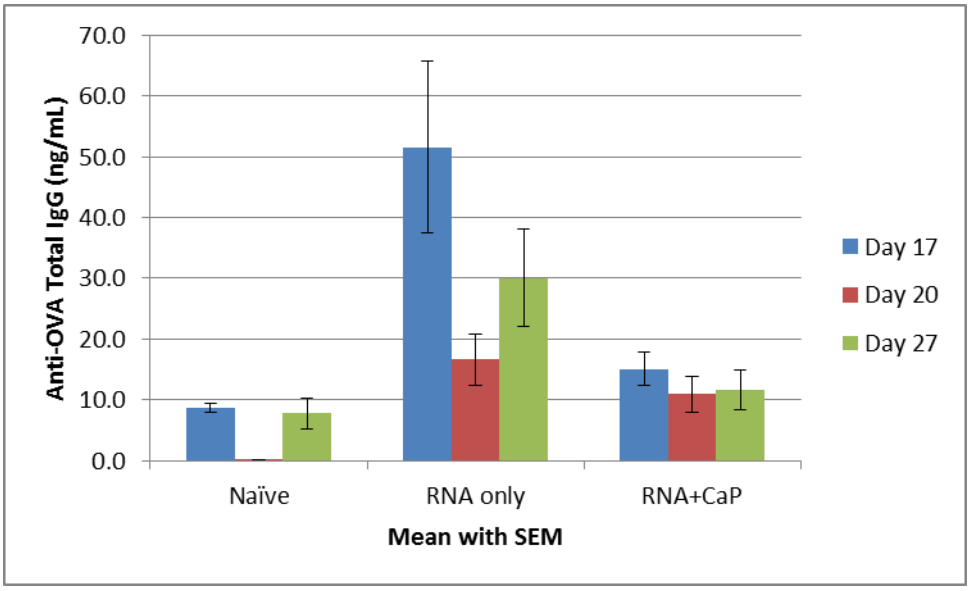

Fig. 5.13: Total anti-OVA IgG concentration in sera from mice immunized with mRNA vaccines. Statistical significance determined using Student's t-test. Mice receiving RNA only vaccines had significantly higher levels as compared to the Naïve group at all days tested ($P<0.01$) and the RNA and CaP group at day 17 and 27 ($P<0.05$).

Splenocytes were extracted at day 28 and cell culture supernatant was analyzed 16hrs after OVA stimulation for IFN-γ concentration by ELISA (Fig. 5.14). The highest IFN-γ response was seen in mice immunized with naked OVA mRNA. p-values relative to the Naïve group ($P=0.058$) and RNA and CaP group ($P=0.048$) were close to the $\alpha=0.05$ cutoff for significance.

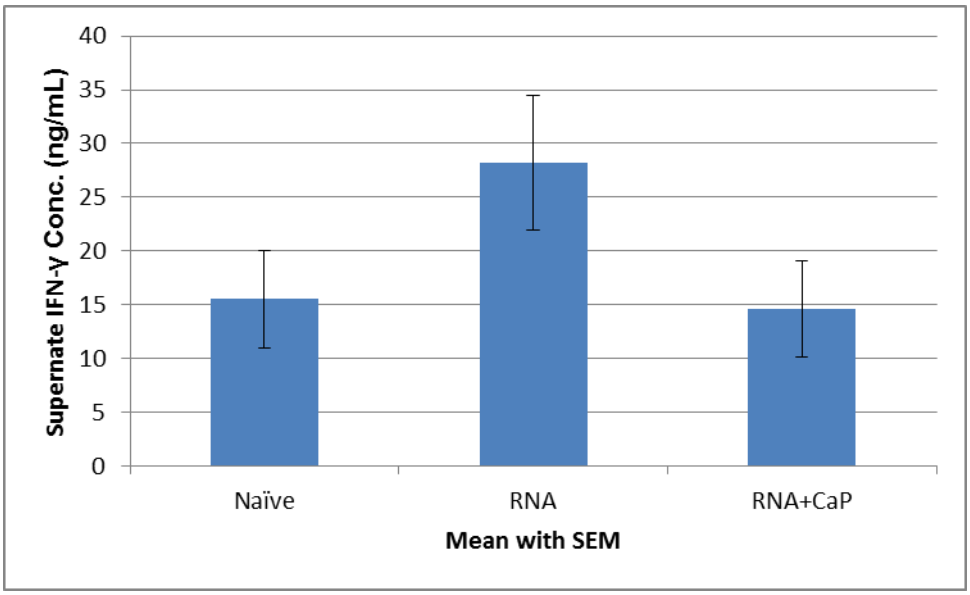

Fig. 5.14: Splenocyte supernatant IFN-γ concentration 16 hrs after stimulation with OVA. Statistical significance determined using Student's t-test. Mice immunized with RNA only had significantly higher levels than the mice immunized with RNA and CaP ($P<0.05$) but when compared to the Naïve group the results were insignificant ($\alpha=0.05$)

5.4: Summary

Effective transfection of host cells is a barrier for nucleic acid vaccine efficacy.[71, 134] CaP NP transfection efficiency with pDNA in RAW 264.7 mouse macrophage cells was analyzed prior to use in pDNA vaccines. pDNA transfection efficiency with CaP NPs was poor (<5%) as compared to positive controls PEI and Lipofectamine 2000. Also, no correlation between CaP particle size and transfection efficiency was observed in RAW 264.7 cells. Analysis of fluorescently labeled pDNA adsorbed to CaP particles revealed that uptake of CaP particles was high but pDNA was not escaping from the endosomes of macrophages. Increased transfection efficiency with CaP NPs has been reported in literature.[14, 56, 144, 148, 176] However, none of these studies analyzed macrophage cells and macrophages are typically more difficult to transfect than other cell types when using standard transfection agents.[41, 47, 183]

In vitro transfection results are not necessarily predictive of *in vivo* results. *In vitro,* transfection efficiencies with naked pDNA are low or absent[120] but when pDNA is administered *in vivo,* transfection at the site of injection has been observed.[115] PEI is considered a gold standard for transfection agents and when used *in vitro* high transfection efficiencies are observed[58]. When used *in vivo,* PEI transfection is often low due to interactions with extracellular matrix components or negatively charged serum glycoproteins.[162]

Although CaP NPs were poor transfection agents *in vitro* with RAW 264.7 cells, CaP nanoparticles elevated immune responses when used as adjuvants in pDNA vaccines. Higher anti-OVA total IgG levels were observed in mice vaccinated with pDNA and CaP NPs as compared to pDNA only. However, total anti-OVA IgG levels were low as compared to previous vaccination studies with protein OVA (Chap. 4). When splenocytes from immunized mice were

stimulated with OVA, the highest splenocyte IFN-γ response after stimulation was observed in the mice immunized with pDNA and CaP nanoparticle adjuvants. In contrast to pDNA vaccines, no adjuvant affect was observed when CaP NPs were added to OVA mRNA vaccine formulations. No *in vitro* transfection experiments were carried out with mRNA and CaP NP formulations may need to be optimized for delivery of mRNA.

For future nucleic acid vaccine studies, changing the route of administration from subcutaneous to intramuscular may increase immune responses. In mice, intramuscular injection of naked pDNA or pDNA encapsulated in liposomes has been shown to elicit elevated antibody responses to pDNA vaccines as compared to subcutaneous injection.[89, 130]

Nucleic acid vaccines have several advantages over protein antigen vaccines. These include ease of production, targeting of MHC-I loading through intracellular antigen expression, and inherent immunogenicity of foreign nucleic acids. Nucleic acid vaccines may be particularly useful for vaccines against intracellular pathogens since nucleic acid vaccines are able to target the MHC-I loading pathway. Nucleic acid delivery vehicles can increase *in vivo* transfection and immunogenicity by protecting nucleic acids from extracellular degradation and increasing nucleic acid delivery into cells.[10, 117, 187] CaP NPs increased IgG and splenocyte IFN-γ response when added to OVA pDNA vaccine formulations showing promise as an adjuvant in pDNA vaccines.

Chapter 6: Discussion and Future Research Directions

6.1: Discussion

As a vaccine adjuvant, calcium phosphate (CaP) has been evaluated in vaccines against diphtheria,[1-3] tetanus,[61, 69] herpes simplex virus 2,[76, 77] influenza,[99] hepatitis B, bacterial meningitis,[175] and HIV.[158] The most commonly used adjuvants in human vaccines are aluminum compounds.[65, 112] When CaP has been compared to aluminum adjuvants, adjuvancy has varied depending upon the type of vaccine antigen and animal model used. In a comprehensive study, Singh *et al.*[175] compared CaP and aluminum hydroxide adjuvancy for tetanus, diphtheria, hepatitis B, and group C Meningococcal antigens. In mice, aluminum hydroxide elicited higher antigen-specific antibody responses than CaP with every antigen tested except for group C Meningococcal antigen. In mice and guinea pigs, aluminum phosphate and aluminum hydroxide elicited higher IgG response to tetanus and diphtheria toxoids as compared to CaP.[2, 61, 69] However, in one human study, CaP was found to be more effective than aluminum hydroxide at eliciting antibodies against diphtheria and tetanus toxoids.[1] Also, in an inactivated herpes simplex virus type 2 vaccine CaP elicited higher IgG and IgG2a responses in mice as compared to aluminum hydroxide.[76]

While aluminum adjuvants have proven to be safe and effective at raising antibody responses in some vaccines, disadvantages of aluminum adjuvants include elevated IgE production, inability to stimulate cell-mediated and cytotoxic T-cell responses, and weak or no adjuvant effect with certain vaccine candidates.[65, 112] These drawbacks necessitate the exploration of alternative adjuvants for new vaccines.

CaP nanoparticles (NPs) with diameters less than 100nm are of particular interest as vaccine adjuvants. Different studies have found that sub-100nm particles stimulate elevated B and T-cell responses as compared to larger particles.[50, 141, 146, 155] When CaP is mineralized in the absence of a capping agent, large polydisperse and polymorphous micro-sized particles are formed. Several non-collagenous proteins, including osteocalcin, fibronectin, and osteonectin, are thought to play a role in the formation of vertebrate bone.[24] Autoimmunity concerns preclude the use of these proteins or CaP binding motifs derived from these proteins as CaP capping agents in vaccines. As an alternative biomimetic approach, random CaP dodecapeptides with binding affinity to CaP were selected through biopanning using a cell-surface display library.[27] Interestingly, identified CaP binding dodecapeptides exhibited a wide range of isoelectric points and hydrophobicity. CaP binding motifs presented within an *E. coli* thioredoxin A scaffold (TrxA::CaP) were evaluated for CaP NP mineralization ability.[27] Of the CaP binders tested, only dodecapeptides that contained negatively charged residues and isoelectric points below pH 7 were able to effectively mineralize CaP NPs below 100nm in size. This suggests that the CaP binding motifs are controlling CaP particle growth through electrostatic interactions with calcium ions on the particle surface. These findings are in agreement with those in literature since anionic capping agents including citrate,[76, 77, 116, 128, 203] phosphate-functionalized porphyrin,[52] and oligonucleotides[144, 176, 198] are frequently used to control CaP particle size.

In a preliminary *in vivo* study, CaP NP adjuvant was compared against commercial aluminum phosphate adjuvant in trxA vaccines.[27] Twenty-eight days after a single dose vaccination, the anti-trxA IgG sera concentration was approximately three times higher in mice receiving CaP NPs as compared to aluminum phosphate establishing CaP NP adjuvant potential.

Unfortunately, this study failed to assess the immune response of trxA vaccines without the CaP NPs.

Applications of a trxA vaccine are limited and only a few studies detailing trxA immunogenicity exist in literature. In contrast, ovalbumin (OVA) is a frequently used and well characterized model antigen. A fusion protein (TrxA::PA44-OVA) between a trxA CaP binding derivative (TrxA::PA44) and OVA was constructed to present OVA while still maintaining the CaP mineralization ability of TrxA::PA44. When evaluated as a CaP mineralization agent, the fusion protein maintained the ability to mineralize sub-100nm CaP NPs. CaP NP adjuvancy was evaluated in mice with vaccines containing TrxA::PA44-OVA. CaP NPs did not elevate antibody response to OVA after immunization with the vaccines tested. However, mice immunized with fusion protein vaccine formulations containing CaP NPs had elevated levels of splenic antigen-specific CD8+ effector-memory T-cells after challenge with an influenza strain expressing an OVA T-cell epitope on the phage surface relative.

The use of trxA as a scaffold for CaP binding motif presentation is problematic in vaccines since thioredoxin is a ubiquitous redox protein found in most organisms.[194] trxA and human thioredoxin (TXN1) share a 35% protein identity (BLASTP 2.2.28+)[6, 7] limiting the use of trxA derivatives in human vaccines. A cyclic peptide containing a selected CaP binding dodecapeptide and lacking the trxA scaffold (cPN38) was found to influence CaP particle size. Sub-100nm CaP particles were formed in the presence of OVA and cPN38. CaP NP adjuvancy in mice was evaluated here with OVA vaccines. CaP NPs did not elevate total anti-OVA IgG response in mice, but mice immunized with vaccines containing CaP NP adjuvant had ~90% higher mean splenocyte IFN-γ response after *in vitro* antigen stimulation as compared to mice vaccinated with protein only formulations. IFN-γ is a cytokine involved in innate and adaptive

immunity against intracellular infections. IFN-γ effector functions include: activation of macrophage intracellular antimicrobial activity, increased MHC-I expression in infected cells, increased expression of IgG2a, decreased production of IgG1, promotion of T_H1 T-cell differentiation and suppression of T_H2 T-cell growth.[169]

As an adjuvant in vaccines containing OVA protein, CaP NPs induced higher antigen-specific CD8+ T-cells after influenza challenge and increased antigen sensitization of IFN-γ producing splenocytes. T_H2-associated IgG1 antibody response was not elevated by CaP NPs. In stark contrast to the trends observed with CaP NPs, aluminum adjuvants typically elicit a very strong T_H2-antibody mediated response and do not increase T_H1 cell-mediated or CD8+ cytotoxic T-cell responses.[65, 112] Immune responses can be skewed towards a T_H1 or T_H2 response and the T_H1-associated cytokine IFN-γ and the T_H2-associated cytokine IL-4 have opposite roles in stimulating and suppressing T_H1/T_H2 T-cells.[132, 139, 170]

CaP NPs were also evaluated here as adjuvants in nucleic acid vaccines. Nucleic acid vaccines have several advantages over protein vaccines. Nucleic acids are easier to produce and purify as compared to proteins and nucleic acids can target the MHC-I loading pathway by expressing antigens endogenously in transfected cells. A disadvantage of nucleic acid vaccines is that host cells must be transfected for antigen expression to occur. Effective delivery of intact nucleic acid and transfection of host cells is a barrier for nucleic acid vaccine efficacy. CaP pDNA transfection efficiency was extensively evaluated here *in vitro* with the RAW 264.7 mouse macrophage cell line and CaP NP transfection efficiency was found to be low (3 ± 2%) when compared to the standard polycationic polyethylenimine (PEI) (25 ± 4%) and liposomal Lipofectamine® 2000 transfection agents (17 ± 2%). Use of smaller CaP NPs did not increase transfection efficiency in RAW 264.7 cells and no transfection was observed when CaP NP

formulations described in literature were evaluated.[93, 176] Uptake of pDNA-CaP NPs in RAW 264.7 cells was high (~90% uptake) indicating that low transfection efficiencies were not limited by uptake as is the case with naked pDNA *in vitro*.[120]

When pDNA-CaP is endocytosed, pDNA is thought to escape the endosome when the endosome is ruptured due to osmotic pressure from the rapid ion release caused by dissolution of CaP particles in the acidic environment of the late endosome.[108] Analysis of fluorescently tagged pDNA and intracellular calcium ions in RAW 264.7 cells indicated that pDNA-CaP particles were not escaping the endosome suggesting endosomal escape may be the limiting factor in CaP pDNA transfection of RAW 264.7 cells. *In vitro* pDNA transfection results are not necessarily predictive of *in vivo* results. *In vitro*, transfection efficiencies with naked pDNA are very low but transfection has been observed at the site of injection when naked pDNA is delivered *in* vivo.[115] Conversely, PEI *in vitro* transfection is typically high[58] but *in vivo* transfection is often low due to interactions with extracellular matrix components or negatively charged serum glycoproteins.[162]

pDNA vaccine formulations containing plasmids encoding the OVA gene were evaluated *in vivo*. Addition of CaP NP adjuvant increased anti-OVA total IgG response in mice as compared to naked pDNA vaccines. However, anti-OVA total IgG serum levels after OVA pDNA vaccination were approximately three orders of magnitude lower than serum levels observed after OVA protein vaccination.

The mechanism of adjuvancy for CaP and aluminum compounds is thought be due to a "depot effect" where adsorbed antigen is slowly released from adjuvants at the site of injection. However, a depot effect alone is insufficient to explain mineral compound adjuvancy since CaP

microparticles and aluminum hydroxide bound similar amounts of OVA antigen but generated significant differences in antibody response.

CaP NP adjuvants may potentiate immune responses by increasing intracellular concentrations of free Ca^{2+}. Intracellular calcium ion levels are tightly controlled in vertebrates and increases in calcium ion concentration are used as intracellular signals for a range of cellular processes.[13] The activation of T-cell receptors generates an increase in intracellular calcium ions[59] which act as second messengers to amplify the initial recognition signal by stimulating NF-kB, NF-AT and CREB transcription factors involved in T-cell proliferation.[13] T-cells can also be stimulated artificially *in vitro* in a manner similar to T-cell receptor-antigen binding by activating protein kinase C with phorbol 12-myristate 13-acetate (PMA), an analog diacylglycerol, and ionomycin, an ionophore which increases intracellular Ca^{2+} levels.[88, 142] Disruption of calcium dependent phosphatases can inhibit T-cell receptor signaling and the immunosuppressive drugs cyclophilin and FKBP have been shown to interact with calcineurin, a calcium/calmodulin dependent serine phosphatase.[114]

Adjuvants are evaluated and approved by the FDA as components of an entire vaccine formulation. Therefore, a new adjuvant could be approved in a vaccine as long as the entire vaccine is proven to be safe. The approval of monophosphoryl lipid A (MPLA) in combination with aluminum hydroxide in the HPV vaccine Cervarix® represents a significant milestone in adjuvant research as MPLA is the first non-aluminum adjuvant to be approved by the FDA for use in human vaccines.[36]

The development of new vaccines is currently hindered by a narrow range of adjuvant options. Aluminum adjuvants are the most common but are unable to elevate cell-mediated and

cytotoxic T-cell responses that may be critical for protective immunity in vaccines against intracellular pathogens. CaP NPs elevated CD8+ T-cell responses after influenza challenge and T_H1-associated IFN-γ splenocyte antigen response in vaccines containing OVA protein. The adjuvant effects of CaP NPs observed here indicate that CaP NPs have potential as effective adjuvants in intracellular vaccines. Immune stimulation by adjuvants can vary greatly depending upon the antigen used[175] and the failure or success of an adjuvant with one antigen may not necessarily translate to all antigens. Antibody response is a key indicator for adjuvancy but evaluating adjuvancy by antibody response alone may fail to account for increases in cell-mediated and cytotoxic T-cell response. As one of the few adjuvants to be previously used in human vaccines, CaP adjuvants have an established safety profile and CaP NPs adjuvants may be useful for eliciting immune responses that are not elevated by aluminum adjuvants.

6.2 Future Research Directions

Addition of phagocytic cell targeting motifs may increase CaP NP adjuvancy. Macrophages and dendritic cells express mannose receptors that recognize repeated mannose patterns on the surface of pathogens.[178] Mannosylation of liposomes,[48, 188] PEI,[40] and proteins[17] has been shown to increase macrophage and dendritic cell uptake. cPN38 was successfully mannosylated but CaP particles with the mannosylated cyclic peptide have yet to be evaluated *in vivo* and may increase CaP NP adjuvancy by increasing delivery of adsorbed antigens to macrophages and dendritic cells.

Another option for phagocytic cell targeting is conjugation of cPN38 to the tetrapeptide tuftsin (TKPR), an opsonin isolated from the Fc fragment of IgG.[140] Tuftsin can increase immunostimulation when conjugated to liposomes[4] and peptides.[192] Additionally, tuftsin has been shown to increase antimicrobial, antiviral, and antitumor responses.[174]

Adjuvancy of CaP NPs may be further increased by combination with TLR agonists like CpG or monophosphoryl lipid A (MPLA). Combination of CpG with various adjuvants (including aluminum hydroxide) increased total IgG response and also increased IgG2a/IgG1 ratios in mice vaccinated with hepatitis B antigen.[193] Mice immunized with vaccines containing an influenza antigen and a combination of CaP and CpG adjuvants had significantly increased populations of antigen specific splenic CD8 T-cells and splenic IFN-γ producing CD4 and CD8 T-cells after antigen stimulation as compared to mice vaccinated with antigen and CpG formulations. In this same study, the CaP and CpG combination adjuvant did not increase serum IgG responses[99] showing a similar immune response profile observed with the OVA protein vaccinations (Chap. 3 and 4). Addition of CpG to polymeric nanoparticles covalently conjugated

to antigen has been shown to increase antigen-specific CD8 and CD4 T-cell responses as compared to free antigen and CpG.[141, 199] MPLA is another option for CaP combination adjuvants. In human papillomavirus (HPV) vaccines, MPLA in combination with aluminum hydroxide has also been shown to elicits higher humoral responses than aluminum hydroxide alone in mice, monkeys, and humans.[55]

Since they are negatively charged, CpG and MPLA may also provide additional benefits to CaP particle size control. Oligonucleotides are well known to influence CaP particle size and short CpG oligonucleotides have been used as CaP capping agents.[177] Although CpG and MPLA may be able to influence CaP particle size, the concentration of CpG and MPLA required for effective size control of CaP NPs may be above the optimal dosage and addition of the cyclic CaP binding peptide cPN38 could allow for CaP NP formation at lower concentrations of CpG and MPLA.

Appendix A

*Revised Manuscript
Click here to download Revised Manuscript: Text_Re_revised2.docx

Just-in-time vaccines: Biomineralized calcium phosphate core-immunogen shell nanoparticles induce long-lasting CD8$^+$ T cell responses in mice

Weibin Zhou[†,a], Albanus Moguche[‡,a], David Chiu,[†,§] Kaja Murali-Krishna[‡,b], and François Baneyx[†,§,*]

Departments of [†]Chemical Engineering, [‡]Immunology, and [§]Bioengineering, University of Washington, Seattle, WA 98195

[a]Contributed equally to this work

[b]Current address: Department of Pediatrics, Emory University School of Medicine, Atlanta, GA 30322

Key words: Nanovaccine; Nanocarrier; Biomineralization; Solid binding peptide

*Corresponding author

E-mail address: baneyx@uw.edu (F. Baneyx)

This work was supported by a Grand Challenge Exploration grant from the Bill and Melinda Gates Foundation and by NIH awards U19ES019545 and R01AI086133.

Conflict of Interest: The authors have no conflict of interest.

WORD COUNT
Abstract: 148
Body text and figure legends: 4223
Number of references: 42
Number of figures/tables: 5

Abstract

Distributed and on-demand vaccine production could be game-changing for infectious disease treatment in the developing world by providing new therapeutic opportunities and breaking the refrigeration "cold chain". Here, we show that a fusion protein between a calcium phosphate binding domain and the model antigen ovalbumin can mineralize a biocompatible adjuvant in a single step. The resulting 50 nm calcium phosphate core-immunogen shell particles are comparable to soluble protein in inducing ovalbumin-specific antibody response and class switch recombination in mice. However, single dose vaccination with nanoparticles leads to higher expansion of ovalbumin-specific $CD8^+$ T cells upon challenge with an influenza virus bearing the ovalbumin-derived SIINFEKL peptide, and these cells produce high levels of IFN-γ. Furthermore, mice exhibit a robust antigen-specific $CD8^+$ T cell recall response when challenged with virus 8 months post-immunization. These results underscore the promise of immunogen-controlled adjuvant mineralization for just-in-time manufacturing of effective T cell vaccines.

The next generation of vaccines should provide potent and long-lasting immune responses, have minimal side effects, and be safe, stable and easy to manufacture. This means moving from attenuated or killed pathogens towards purer, protein-based subunit vaccines. It also means compensating for the fact that subunit vaccines are less effective than traditional ones by including macromolecules or particles in the formulation to enhance, sustain and/or direct antigen immunogenicity.[1] These added compounds are known as adjuvants and function either as immunostimulants that are bound by pathogen-recognition receptors (e.g., Toll-like receptors) to boost immune responses, or as vehicles that optimize antigen delivery and presentation to the immune system.[1, 2]

Delivery vehicles are amenable to engineering design (which includes changes in structure, composition, morphology, physicochemical properties and conjugation of immunostimulatory or targeting molecules)[1, 3] and they hold potential for single dose, needle-free vaccination.[4] Aside from liposome-based and virus-like particles antigen delivery systems, several of which are already licensed or undergoing clinical studies, considerable attention has been paid to nanoparticles in the 20-100 nm size range because they freely enter the lymphatic system following subcutaneous or intramuscular injection.[5, 6, 2] Once these nanoparticles reach the lymph nodes, antigens coupled to their surface or entrapped within their cores have the opportunity to directly activate follicular B cells (which drive antibody-mediated responses), and to be efficiently taken up by dendritic cells which are powerful inducers of the T cell responses required for long-lasting humoral and cell-mediated immunity.[5, 7, 6, 8, 9] To date, such vaccinating nanoparticles have been made from polyesters (PLA/PLGA), polyanhydride (PVM/MA), and polysaccharides (inulin, alginate, hyaluronic acid and chitosan) which have a long record of biocompatibility (see ref. [2] and references within). However, while polymeric-based nanocarriers

decorated with immunogens can induce robust antibody-mediated responses, achieving the robust $CD8^+$ T cell responses and memory that are critical to the development of therapeutic vaccines against viral infections and cancer[7, 8] can require considerable engineering (e.g., ref. [10]).

Another major challenge in vaccinology is that immunogens are often proteins which are prone to degradation, aggregation, oxidation or deamidation and that particulate vaccines are susceptible to colloidal instability.[9] This translates into limited shelf life and a need for stabilizing excipients and refrigeration. We believe that a solution to breaking the cold chain is distributed and just-in-time vaccine manufacturing. In this concept, a limited number of vaccine doses sufficient to treat the affected population are rapidly produced in rudimentary facilities at the time and place where they are most needed.

Solid binding peptides (SBPs) selected by combinatorial techniques for their ability to bind inorganic surfaces can be used to control materials nucleation, growth, crystallography, shape, size and function.[11-15] By engineering SBPs within larger protein frameworks, it is further possible to combine inorganic- and protein-associated activities, as we have for example demonstrated by using a fusion protein between a zinc sulfide binding peptide and an antibody-binding module to produce immunoglobulin-binding luminescent nanocrystals.[16, 17] The approach is appealing because an inorganic core-protein shell nanostructure of defined dimension can be produced in a single step and in aqueous solvents by the simple expedient of mixing protein with precursor salts.

Previously, we reported on the construction, expression and purification of TrxA::PA44, a derivative of *E. coli* thioredoxin A (TrxA) containing a 12 residues-long calcium phosphate (CaP) binding peptide called PA44 in place of the protein's native Cys-Gly-Pro-Cys active site loop. We used this fusion protein for the one-pot mineralization of sub-100 nm particles

consisting of an amorphous calcium phosphate core stabilized by a capping protein shell. We further demonstrated that the resulting nanoparticles were slightly more effective than alum-adjuvanted TrxA::PA44 at eliciting a humoral response in C57BL/6 mice vaccinated subcutaneously as there was an about 3-fold increase in anti-TrxA IgG titers 21 days post-injection.[18] Here, we amplify on the just-in-time vaccine manufacturing concept by showing that a fusion protein between TrxA::PA44 and the model antigen ovalbumin (OVA) is suitable for the production of ≈ 50 nm CaP core-immunogen shell nanoparticles that support antibody class switch recombination and are potent inducer of antigen-specific $CD8^+$ T cell responses and memory.

Materials and methods

DNA Manipulations

Plasmid pTrxA::PA44-OVA which encodes a fusion protein between a calcium binding variant of thioredoxin called TrxA::PA44 [18] and chicken ovalbumin (OVA) was constructed as follows. A DNA cassette encoding OVA was PCR-amplified from plasmid pAc-neo-OVAl,[19] a kind gift from Mike Bevan (University of Washington), using primers 5′-CAACTCAGACCTAGGCATGGGCTCC-3' and 5′-TCAGCTCTCTTCTTCTTAAGGGGAAACACAT-3′ to introduce *Avr*II and *Afl*II restriction sites. Plasmid pTrxA::PA44,[18] and primers 5'-GCGTCGACCTTAAGTAATCGTACAGGGTAGT-3' and 5'-GCAAGCCTAGGTTAGCGTCGAGGAAC-3' were used to introduce the same restriction sites in a large DNA fragment specifying most of pTrxA::PA44. Amplified DNAs were digested with *Avr*II and *Afl*II and the cassette encoding OVA was ligated to the pTrxA::PA44 backbone that

had been dephosphorylated with shrimp alkaline phosphatase. Construct integrity was verified by DNA sequencing. A plasmid encoding an OVA-TrxA::PA44 fusion protein was also built but no protein expression was detected (presumably due to the fact that a stem-loop structure at the 5' end of the ovalbumin mRNA interferes with transcription)[20] and the construct was abandoned.

Protein expression, refolding and purification

BL21(DE3) cells harboring pTrxA::PA44-OVA were grown to $A_{600} \approx 0.5$ at 37°C in 500 mL of LB medium supplemented with 34 µg/mL chloramphenicol. Flasks (2L) were transferred to a water bath held at 25°C for 10 min and protein synthesis was induced by addition of 1 mM of isopropyl β-D-thiogalactopyranoside (IPTG). After 4h, cells were harvested by centrifugation at 3,000 *g* for 15 min, and resuspended in 20 mM Tris-HCl, pH 7.5 supplemented with 2.5 mM EDTA and 1 mM PMSF to an A_{600} of 50. Cells were disrupted by three cycles of homogenization on a French pressure cell operated at 10,000 psi and the lysate was separated into soluble and insoluble fractions by centrifugation at 14,000 *g* for 15 min.

Pellets containing the inclusion body material were resuspended by vortexing into 5 mL of buffer A (20 mM Tris-HCl, pH 7.5, 2.5 mM EDTA, 1 mM PMSF) supplemented with 1% (v/v) Triton X-100. Following centrifugation at 14,000 *g* for 10 min, the supernatant was discarded and the wash step was repeated once as above and twice more using buffer A alone. Washed inclusion bodies were resuspended in 15 mL of buffer A supplemented with 6 M of guanidium hydrochloride and incubated at room temperature for 1h with gentle shaking. After removing any remaining insoluble material by centrifugation at 14,000 *g* for 10 min, unfolded protein aliquots (5 mL) were refolded by dropwise addition into 95 mL of buffer A with gentle stirring. The remaining guanidium hydrochloride was removed by 16 h dialysis against 2L of buffer A,

with buffer changes at 1h and 4h. The refolded protein was filtered through a 0.45 μm cartridge and loaded on a 1 cm column packed with 5 g of DE52 Cellulose (Whatman) pre-equilibrated in buffer A. The column was developed at 1 mL/min in buffer A and TrxA::PA44-OVA was eluted with 200 mM NaCl after a 50 mM NaCl step to remove contaminants. Protein concentrations were determined using the Thermo Bradford assay with BSA as a standard, and lack of endotoxin contamination was confirmed using the Pyrogent-5000 LAL assay kit (Lonza).

Nanoparticle mineralization and characterization

Calcium phosphate (CaP) nanoparticles were produced essentially as described.[18] Briefly, 200 μL of a 16.7 mM $Ca(NO_3)_2$ solution were added dropwise to 1.8 mL of a well-stirred mixture of 1.11 mM $(NH_4)_2HPO_4/NH_4H_2PO_4$, pH 7.5 supplemented with 4.44 μM TrxA::PA44-OVA that had been previously incubated at 4°C for 30 min. After addition of the calcium, the mixture was allowed to age at 4°C for 2 h with high-speed stirring with a small magnetic bar. Endotoxin-free water and disposable glassware cleaned with acetic acid, acetone and water was used in all steps.

Hydrodynamic diameters were measured by dynamic light scattering (DLS) on a Nano-ZS Zetasizer (Malvern). For SEM imaging, samples (≈ 100 μL) were allowed to contact a clean, ≈ 1 cm^2 silicon wafers for 30 min and excess fluid was removed by wicking with a laboratory tissue. The substrate was rinsed with ddH_2O to remove salts, air dried and coated with a 7-10 nm Au/Pd film. Micrographs were taken with a FEI Sirion SEM at 10 keV acceleration voltage.

Mice, immunization and challenge

All mice were used in accordance with the guidelines of the Institutional Animal Care and Use Committees of the University of Washington. A total of 24 C57BL/6J mice were purchased from Jackson Laboratory. One group (n=8) was immunized with 18 μg of TrxA::PA44-OVA in 1 mM ammonium phosphate. A second group (n=8) was immunized with 18 μg of TrxA::PA44-OVA@CaP in 1.67 mM calcium nitrate and 1 mM ammonium phosphate. The final group (n=8) was left unimmunized to serve as a control. A total volume of 200 μl of control protein or nanoparticles (≈ 0.005% v/v) was administered by sub-cutaneous injection. Mice were challenged at 4 months (n=1 animal per cohort) or 8 months (n=6 animals per cohort) post-immunization with 1000 plaque forming units (PFU) of a recombinant influenza virus A/WSN/1933 (WSN) carrying the transgene for chicken ovalbumin (WSN-OVA).[21] Following viral challenge, spleens were extracted from half of the animals on day 7 while the remaining mice were monitored for weight loss every other day. Animals were sacrificed if they lost more than 20% of their starting body weight.

Antibody titration

At 1, 2 and 4 weeks post-vaccination, mice were bled and serum was analyzed for ovalbumin specific antibodies. In brief, 96-well micro-plates (Corning #3369) were coated overnight at 4°C with chicken ovalbumin (Fisher Scientific #BP2535-5) in 0.2M anhydrous sodium carbonate, 0.2M sodium bicarbonate, pH 9.2. Non-specific binding was blocked using 5% fat free milk in 0.05% Tween Tris-buffered saline at 4°C overnight. After discarding the blocking buffer, twofold serial dilutions of serum samples (or for standards curve, titrated anti-chicken ovalbumin monoclonal antibody; Gene Script #A00852) were added to the plates. After 2h incubation at 37°C, the plates were washed 3 times with 0.5% fat free milk in 0.05% Tween Tris-buffered

saline. Anti-mouse IgG or anti-mouse IgM conjugated to Horseradish Peroxidase (Millipore) were added and plates were incubated at 37°C for 1h. After 3 wash cycles, plates were developed with TBM reagent (Fisher Scientific) for 20 min. Reactions were stopped by addition of 2 M sulfuric acid and absorbance was read at 450 nm using a plate reader (Molecular Devices).

Flow cytometry analysis

Spleen, lung, blood or pulmonary training lymph nodes single cell suspensions were prepared essentially as reported.[22] In brief, single cell suspensions of intra-parenchymal lung lymphocytes were prepared by Liberase-Blendzyme (Roche) digestion of perfused lungs in the presence of DNAse (Sigma-Aldrich). Single cell lymphocyte cell suspensions were also made from spleen and lung draining lymph node by crushing the tissues between two frosted glass slides. Red blood cells in the above single cell suspensions were lysed using the ACK RBC lysis buffer (Invitrogen). The cells were subsequently stained for surface markers using anti-mouse monoclonal antibodies against CD3 (clone 145-2C11), CD4 (clone RM4-5), CD8 (clone 53-6.7), CD44 (clone IM7) and CD62L (clone MEL-14) obtained from Biolegend. Ova-specific $CD8^+$ T cells were detected using the major histocompatibility complex class I ($H2K^b$) restricted SIINFEKL tetramer (OVA 257-264) tetramerized to APC or PE-conjugated streptavidin. The antibodies and tetramer were diluted in a buffer containing 0.1% sodium azide and 2.5% fetal bovine serum and Fc receptor blocking antibodies (anti-mouse CD16/32). All stains were done at saturating concentrations and 4°C for 30 min. To detect IFN-γ, aliquots of single cell lymphocytes suspensions were stimulated with SIINFEKL peptide and incubated for 4 h in complete RPMI (RPMI 1640 supplemented with 10% FCS, 2 mM L-glutamine, 10 mM Hepes, 0.5 μM 2-mercaptoehtanol, 100 U/ml penicillin, and 100 μg/ml streptomycin) in the presence of

monensin (BD Golgi-Stop). Cells were then stained for surface markers as above and, after permeabilization, stained for IFN-γ (XMG1.2, BD) and incubated at 4°C for 30 min. Cells were fixed in 1% paraformaldehyde solution in PBS and analyzed on a LSRII flow cytometer (BD) and the FlowJo software (Tree Star).

Results

Construction and purification of a calcium phosphate-binding ovalbumin variant

To further explore the potential of CaP core-protein shell nanoparticles for vaccine formulation, we fused TrxA::PA44 to ovalbumin (OVA), thus combining a domain capable of producing CaP nanoparticles by surface capping[18] with a model antigen (Fig. 1A). Because the resulting fusion protein accumulated as inclusion bodies when overexpressed in *E. coli* (Fig. 1B), we purified TrxA::PA44-OVA by unfolding it in guanidium hydrochloride, refolding it by dilution, and removing trace contaminants and endotoxins by ion exchange chromatography as detailed in Materials and Methods.

Protein-aided fabrication of calcium phosphate core immunogen shell nanoparticles

We first sought to determine how the presence of the 45-kDa OVA extension would affect the ability of TrxA::PA44 to control the mineralization of CaP nanoparticles. To this end, 4 μM of fusion protein in calcium nitrate buffer was added dropwise and with high agitation to a sodium phosphate solution essentially as described[18] and the mixture was allowed to age for 2h. SEM imaging of gold-palladium coated samples (Fig. 2A) revealed the presence of well-dispersed spheroids that were 75 ± 12 nm in diameter based on manual measurement of n = 50 particles. This size is in good agreement with a hydrodynamic diameter of 44 ± 3 nm obtained by

dynamic light scattering (DLS) once the 7-10 nm thickness of the Au/Pd coating used for SEM visualization is taken into account. It is also comparable to the size of particles that we previously obtained with unfused TrxA::PA44 (70 ± 15 nm by SEM and 60 ± 20 nm by DLS).[18] Inspection of higher resolution SEM images (Fig. 2B) suggests that each nanoparticle is formed by the agglomeration of nanometer size CaP clusters whose accretion is quenched upon adsorption of the fusion protein. We conclude that the presence of a full-length OVA domain does not interfere with the ability of TrxA::PA44 to prevent bulk CaP precipitation and to stabilize colloidal suspensions of ≈ 50 nm particles by surface capping.[18]

Biomineralized nanoparticle induce antibody class-switch recombination

Class switch recombination (CSR) occurs in B cells after they have been exposed to antigen and costimulatory signals, proliferated, differentiated and migrated to the germinal centers of secondary lymphoid organs (spleen, lymph nodes and tonsils).[23, 24] CSR is typically dependent upon $CD4^+$ T helper cells[25, 26] and involves deletional recombination events that target the heavy chain constant region of immunoglobulins and redirect antibody production from IgM and IgD classes to the IgG, IgA and IgE isotypes. To determine if TrxA::PA44-OVA-mineralized nanoparticles (thereafter referred to as TrxA::PA44-OVA@CaP) would induce CSR, C57BL/6 mice were injected subcutaneously with the nanomaterial (Figure 3, closed symbols) or the same amount of purified TrxA::PA44-OVA (open symbols) and serum ovalbumin-specific antibodies were quantified. Figure 3A shows that both formulations induced comparable levels of ovalbumin-specific pentameric IgM, the first antibody produced, with a production peak at 7 days post-immunization followed by a rapid decline in serum levels. As expected for a typical CSR process, the concentration of OVA-specific IgG and IgG1 subclass antibodies started to rise

at day 7 in both populations, reached a plateau at day14 and remained elevated after 4 weeks (Figures 3B-C). Clearly, the TrxA::PA44-OVA@CaP formulation does not interfere with CSR which implies that the particles are capable of inducing antigen-specific $CD4^+$ T cell responses. Nonetheless, the lack of difference in the levels or dynamics of IgM, IgG and IgG1 accumulation indicates that there is no distinct advantage in using the nanoparticle formulation over free protein if one seeks to induce humoral immunity. Why we did not observe a small increase in antigen-specific IgG titers as we previously did when using TrxA::PA44-mineralized particles remains unclear but may be related to differences in immunization protocol, more efficient uptake of the larger TrxA::PA44-OVA by dendritic cells, or to the higher immunogenicity of the OVA domain relative to TrxA.

Biomineralized nanoparticle are more efficient than free protein at inducing antigen-specific $CD8^+$ T cell responses

Protein immunogens that have been uptaken by antigen presenting cells (e.g., dendritic cells) are processed into peptides in the endolysosome, loaded onto major histocompatibility complex (MHC) class II molecules, and exported to the cell surface for stimulation of $CD4^+$ T helper cells. The latter collaborate with activated B cells to generate antibody-producing plasma cells and memory B cells. In a process known as cross-presentation, antigens may also be loaded onto MHC class I molecules to prime $CD8^+$ T cells which produce immune cytokines such as interferon (IFN)-γ and tumor necrosis factor (TNF)-α, play prominent roles in clearing viral infections and eradicating tumors.[8]

Most of the currently licensed vaccines confer protection through the induction of antigen specific antibody responses.[7] However, some infections are not easily controlled by antibodies

and require the induction of antigen specific $CD4^+$ T cells and cytotoxic $CD8^+$ T cells for protection. Because soluble and nanoparticle-bound TrxA::PA44-OVA induce similar antibody

responses and support CSR (Figure 3), both formulations likely activate similar $CD4^+$ T cell responses. To determine if antigen-specific $CD8^+$ T cells responses would be different, we performed a preliminary challenge experiment at 4 months in which one mouse from the groups immunized with TrxA::PA44-OVA, TrxA::PA44-OVA@CaP or left unimmunized, was subjected to intranasal administration of WSN-OVA. This recombinant influenza virus contains the ovalbumin-derived (OVA 257-264) SIINFEKL peptide in the stalk of the neuraminidase capsid protein.[21] Mice were sacrificed 12 days after viral infection and their lungs were analyzed for antigen specific $CD8^+$ T cell responses against OVA by flow cytometry. Figure 4A shows that the mouse vaccinated with TrxA::PA44-OVA@CaP induced a 2.5 fold higher expansion of antigen (SIINFEKL)-specific $CD8^+$ T cell relative to the animal immunized with free protein, and a 40-fold higher expansion compared to the unimmunized animal. Furthermore, when these cells were re-stimulated *in vitro* with the SIINFEKL peptide, they produced twice as much IFN-γ than those from the animal vaccinated with free protein (Figure 4B). On the other hand, while lung cells from both immunized animals produced significantly more TNF-α upon peptide stimulation relative to cells from naïve mice, the vaccine formulation had no influence on the levels of this cytokine (Figure 4C). Although conducted on a single mouse per group, these experiments revealed an encouraging trend: immunization with the nanoparticle formulation leads to larger numbers of antigen specific $CD8^+$ T cells at the infection site and these cells are capable of producing high-levels of the antiviral cytokine IFN-γ.

Nanoparticle-induced $CD8^+$ T cells are long-lived and undergo enhanced recall responses

A critical concern for vaccine development is the longevity of antigen-specific responses which often wane after 6 months.[27] To determine how long nanoparticle-induced $CD8^+$ T cell memory would last, we waited an additional four months to repeat the intranasal WSN-OVA challenge. In this 8 months study, we measured OVA-specific $CD8^+$ T cells in the spleen 7 days post-infection and monitored mice for weight loss. We used three animals per group for each of these two experiments. Figure 5A shows that antigen-specific T cells could be detected in the spleen of mice from each of the three groups. However, expansion was highest in mice immunized with TrxA::PA44-OVA@CaP. Further underscoring the performance of nanoparticles in eliciting T-cell memory, there were 4-times more SIINFEKL tetramer-binding cells in the spleen of animals immunized with TrxA::PA44-OVA@CaP compared to those vaccinated with free protein (Fig. 5B). These results are comparable to, and in complete agreement with, the preliminary data of Fig. 4 in which mice were challenged at 4 months post immunization. Finally, although infected animals immunized with TrxA::PA44-OVA@CaP lost weight at an initial rate that was comparable to that of control mice, we observed a small but statistically significant difference in weights at day 8 (Fig. 5C). Moreover, whereas two animals from the unimmunized group and two animals from the TrxA::PA44-OVA-vaccinated group were sacrificed at day 9 because they had lost over 20% of their original weight, all mice from the TrxA::PA44-OVA@CaP-immunized group retained 85 to 90% of their original weight at day 10.

Discussion

In this study, we have shown that *ca*. 50 nm calcium phosphate core-immunogen shell nanoparticles fabricated in a single-pot reaction using a fusion protein between a CaP-binding moiety and OVA are effective elicitors of cell mediated immunity. More specifically, we found that immunization with this formulation is vastly superior to the use of free protein in eliciting long-lasting $CD8^+$ T cell responses with high-level IFN-γ production and enhanced recall responses. This may be due to the fact that the mean hydrodynamic diameter of our nanoparticles falls within the 40-50 nm size that has been determined to be optimal for delivery to dendritic cells in the lymph nodes[28, 29, 10, 30] and for antigen cross-presentation in mice[31]. In addition, the presence of multiple immunogens on each nanoparticle is likely to improve loading on class I MHC molecules as cross-presentation of antigens attached or adsorbed to particles in the 20 nm to 3 μm size range is more efficient than with soluble proteins.[32, 33] The role of the inorganic core is less clear. A possible explanation is that the kinetics of dissolution of amorphous CaP nanoparticles[34] and the associated rate of antigen release in the acidic phagosomes where 50 nm diameter particles are preferentially transported[35] are optimal for antigen cross-presentation.[36]

He and coworkers have previously entrapped/adsorbed viral proteins within micrometer-sized CaP aggregates by co-precipitation and reported that this formulation induces a robust antibody response in mice.[37, 38] By analogy to aluminum-based adjuvants,[39] this is likely due to the ability of the CaP aggregates to function as immunogen depots that enhance T helper cell responses through long-lasting antigen release. The small nanoparticles that we produce through our biofabrication scheme are morphologically very different. They are expected to readily drain to the lymph nodes[5] and are thus unlikely to function as antigen depots. In addition, while multiple epitopes decorate each nanoparticle, they are not presented in the repetitive geometry that is necessary for efficient cross-linking of B cell receptors and strong B cell activation.[6, 40] It

is therefore not surprising that the antibody response observed with the TrxA::PA44-Ova@CaP is comparable to that obtained with the soluble protein. Nevertheless, our nanoparticle formulation activates $CD4^+$ T helper cell responses since it supports CSR.[25, 26] If a strong antibody-mediated response is desired, it should be straightforward to modify the design by tethering or adsorbing Toll-like receptor (TLR) ligands such as CpG-containing oligodeoxynucleotides since these molecules have proven quite effective at enhancing humoral immunity.[41, 42]

Conclusions

Just-in-time vaccine manufacturing requires simple production schemes with rudimentary equipment and an end-product efficacy comparable to, or superior to that of conventionally manufactured vaccines. Here, we have shown that a model immunogen consisting of a fusion protein between a calcium phosphate-binding segment and OVA can be used to mineralize its own adjuvant in a single mixing step. In mice, the resulting 50 nm CaP core-immunogen shell nanoparticles induce an OVA-specific antibody response and CSR comparable to the free protein. However, they are much more powerful at inducing OVA-specific $CD8^+$ T cell populations that secrete high levels of IFN-γ, are long-lived and exhibit enhanced recall responses. The strategy described here should prove useful for the distributed and on-demand production of T cell mediated therapeutic vaccines that hold great promise for the treatment of infectious diseases but have so far been very challenging to produce.

Acknowledgments

We are grateful to Sathana Kitayaporn for help with SEM imaging. Part of this work was conducted at the University of Washington Nanotech User Facility, a member of the NSF National Nanotechnology Infrastructure Network.

References

1. Reed SG, Bertholet S, Coler RN, Friede M, New horizons in adjuvants for vaccine development. *Trends Immunol*. 2009;**30**:23-32
2. Correia-Pinto JF, Csaba N, Alonso MJ, Vaccine delivery carriers: insights and future perspectives. *Int J Pharm*. 2013;**440**:27-38
3. Joshi MD, Unger WJ, Storm G, van Kooyk Y, Mastrobattista E, Targeting tumor antigens to dendritic cells using particulate carriers. *J Control Release*. 2012;**161**:25-37
4. Giudice EL, Campbell JD, Needle-free vaccine delivery. *Adv Drug Deliv Rev*. 2006;**20**:68-89
5. Swartz MA, The physiology of the lymphatic system. *Adv. Drug Deliv. Res.* 2001;**50**
6. Bachmann MF, T. JJ, Vaccine delivery: a matter of size, geometry, kinetics and molecular patterns. *Nat Rev Immunol*. 2010;**10**:787-796
7. Salerno-Gonçalves R, Sztein MB, Cell-mediated immunity and the challenges for vaccine development. *Trends Microbiol*. 2006;**14**:536-542
8. Yewdell JW, Designing CD8+ T cell vaccines: it's not rocket science (yet). *Curr Opin Immunol*. 2010;**22**:402-410
9. Amorij J-P, Kersten GFA, Saluja V, Tonnis WF, Hinrichs WLJ, Slütter B, et al., Towards tailored vaccine delivery: needs, challeges and perspectives. *J Control Release*. 2012;**161**:363-376
10. Reddy ST, van der Vlies AJ, Simeoni E, Angeli V, Randolph GJ, O'Neil CP, et al., Exploiting lymphatic transport and complement activation in nanoparticle vaccines. *Nat Biotechnol*. 2007;**25**:1159-1164
11. Sarikaya M, Tamerler C, Jen AK, Schulten K, Baneyx F, Molecular biomimetics: nanotechnology through biology. *Nat Mater*. 2003;**2**:577-585
12. Sarikaya M, Tamerler C, Schwartz DT, Baneyx F, Materials assembly and formation using engineered polypeptides. *Annu Rev Mater Res*. 2004;**34**:373-408
13. Dickerson MB, Sandhage KH, Naik RR, Protein- and peptide directed synthesis of inorganic materials. *Chem Rev*. 2008;**108**:4935-4978
14. Briggs BD, Knecht MR, Nanotechnology meets biology: peptide-based methods for the fabrication of functional materials. *J Phys Chem Lett*. 2012;**3**:405-418
15. Coyle BL, Zhou W, Baneyx F, 2013. Protein-aided mineralization of inorganic nanostructures in Rehm, BHA (ed) *Bionanotechnology: biological self-assembly and its applications*, Caister Academic Press, Norwich, U.K.
16. Zhou W, Schwartz DT, Baneyx F, Single pot biofabrication of zinc sulfide immuno-quantum dots. *J. Am. Chem. Soc.* 2010;**132**:4731-4738
17. Zhou W, Baneyx F, Aqueous, protein-driven synthesis of transition metal-doped ZnS immuno-quantum dots. *ACS Nano*. 2011;**5**:8013-8018
18. Chiu D, Zhou W, Kitayaporn S, Schwartz DT, Murali-Krishna K, Kavanagh TJ, et al., Biomineralization and size control of calcium phosphate core-protein shell nanoparticles: potential for vaccine applications. *Bioconjug. Chem.* 2012;**23**:610-617
19. Moore MW, Carbone FR, Bevan MJ, Introduction of soluble proteins into the class I pathway of antigen processing and presentation. *Cell*. 1988;**54**:777-785

20. Kopper RA, Stallcup T, Hufford G, Liakaros CD, The 5'-end structure of ovalbumin mRNA in isolated nuclei and polysomes. *Nucleic Acids Res*. 1994;**22**:4504-4509
21. Topham DJ, Castrucci MR, Wingo FS, Belz GT, Doherty PC, The role of antigen in the localization of naïve, acutely activated, and memory $CD8^+$ T cells to the lung during influenza pneumonia. *J Immunol*. 2001;**167**:6983-6990
22. Urdahl KB, Liggitt D, Bevan MJ, $CD8^+$ T cells accumulate in the lungs of *Mycobacterium tuberculosis*-infected $K^{b-/-}D^{b-/-}$ mice, but provide minimal protection. *J Immunol*. 2003;**170**:1987-1994
23. Peled JU, Kuang FL, Iglesias-Ussel MD, Roa S, Kalis SL, Goodman MF, et al., The biochemistry of somatic hypermutation. *Annu Rev Immunol*. 2008;**26**:481-511
24. Stavnezer J, Guikema JEJ, Schrader CE, Mechanism and regulation of class switch recombination. *Annu Rev Immunol*. 2008;**26**:261-292
25. MacLennan ICM, Gulbranson-Judge A, Toellner KM, Casamayor-Palleja M, Chan E, Sze DMY, et al., The changing preference of T and B cells for partners as T-dependent antibody responses develop. *Immunol Rev*. 1997;**156**:53-66
26. MacLeod MKL, David A, McKee AS, Crawford F, Kappler JW, Marrack P, Memory CD4 T cells that express CXCR5 provide accelerated help to B cells. *J Immunol*. 2011;**186**:2889-2896
27. Flynn KJ, Belz GT, Altman JD, Ahmed R, Woodland DL, Doherty PC, Virus-specific CD8+ T cells in primary and secondary influenza pneumonia. *Immunity*. 1998;**8**:683-691
28. Reddy ST, Rehor A, Schmoekel HG, Hubbell JA, Swartz MA, In vivo targeting of dendritic cells in lymph nodes with poly(propylene sulfide) nanoparticles. *J. Control. Release*. 2006;**112**:26-34
29. Reddy ST, Swartz MA, Hubbell JA, Targeting dendritic cells with biomaterials: developing the next generation of vaccines. *Trends Immunol.* 2006;**27**:573-579
30. Manalova V, Flace A, Bauer M, Schwarz K, Saudan P, Bachman MF, Nanoparticles target distinct dendritic cell populations according to their size. *Eur. J. Immunol.* 2008;**38**:1404-1413
31. Fifis T, Gamvrellis A, Crimeen-Irwin B, Pietersz GA, Li J, Mottram PL, et al., Size-dependent immunogenicity: therapeutic and protective properties of nano-vaccines against tumors. *J Immunol*. 2004;**173**:3148-3154
32. Pfeifer JD, Wick MJ, Roberts RL, Findlay K, Normark SJ, Harding CV, Phagocytic processing of bacterial antigens for class I MHC presentation to T cells. *Nature*. 1993;**361**:359-362
33. Harding CV, Song R, Phagocytic processing of exogenous particulate antigens by macrophages for presentation by class I MHC molecules. *J Immunol*. 1994;**153**:4925-4933
34. Sun L, Chow LC, Frukhtbeyn SA, Bonevich JE, Preparation and properties of nanoparticles of calcium phosphate with various Ca/P ratios. *J Res Natl Inst Stand Technol*. 2010;**115**:243-255
35. Tran KK, Shen H, The role of phagosomal pH on the size-dependent efficiency of cross-presentation by dendritic cells. *Biomaterials*. 2009;**30**:1356-1362
36. Howland SW, Wittrup KD, Antigen release kinetics in the phagosome are critical to cross-presentation efficiency. *J Immunol*. 2008;**180**:1576-1583
37. He Q, Mitchell AR, Johnson SL, Wagner-Bartak C, Morcol T, Bell SJD, Calcium phosphate nanoparticle adjuvant. *Clin Diagn Lab Immunol*. 2000;**7**:899-903

38. He Q, Mitchell A, Morcol T, Bell SJD, Calcium phosphate nanoparticles induce mucosal immunity and protection against herpes simplex virus type 2. *Clin Diagn Lab Immunol*. 2002;**9**:1021-1024
39. Tritto E, Mosca F, Gregorio E, Mechanism of action of licensed vaccine adjuvants. *Vaccine*. 2009;**27**:3331-3334
40. Rudra JS, Tian YF, Jung JP, Collier JH, A self-assembling peptide acting as an immune adjuvant. *Proc Natl Acad Sci U S A*. 2010;**107**:622-627
41. Ishii KJ, Akira S, Toll or toll-free adjuvant path toward the optimal vaccine development. *J Clin Immunol*. 2007;**27**:363-371
42. Vollmer J, Krieg AM, Immunotherapeutic applications of CpG oligodeoxynucleotide TLR9 agonists. *Adv Drug Deliv Rev*. 2009;**28**:195-204

Figure 1: (**A**) Schematic structure of the TrxA::PA44-OVA fusion protein. (**B**) SDS polyacrylamide gel analysis of soluble (Sol) and insoluble (Ins) cellular fractions and of washed inclusion bodies (IB) and refolded material (Refold). Lane M contains molecular mass markers.

Figure 2. SEM images of CaP nanoparticles produced in the presence of 4 µM of TrxA::PA44-Ova at low (**A**) and high (**B**) magnification.

Figure 3. Age and sex-matched wild type C57BL/6 mice (n = 8 in each group) were immunized with 18 µg of soluble TrxA::PA44-OVA protein (O) or mineralized TrxA::PA44-OVA@CaP nanoparticles ( ). Mice were bled at the indicated times and the concentration of ovalbumin specific IgM (**A**), IgG (**B**) and IgG1 (**C**) antibodies was determined. Horizontal bars correspond to mean values and shaded boxes to standard errors.

Figure 4. Age and sex matched WT C57BL/6 were left un-immunized (n = 8) or were immunized with 18 µg of soluble TrxA::PA44-OVA (n = 8) or TrxA::PA44-OVA@CaP nanoparticles (n = 8). Four months post-immunization, one mouse per group was challenged with WSN-OVA, a recombinant influenza virus carrying ovalbumin transgene. (**A**) Lungs were excised after 12 days and single cell suspensions were analyzed for OVA-specific $CD8^+$ T cells by flow cytometry using a monoclonal antibody against the CD44 antigen (a marker for effector-memory T cells) and $H2K^b$-restricted SIINFEKL tetramer. (**B**) Lung cells were re-stimulated *in vitro* with the SIINFEKL peptide or left un-stimulated and IFN-γ (B) or TNF-α production (**C**) was determined using monoclonal antibodies against these cytokines.

Figure 5. Unimmunized mice (n=6) or animals from groups immunized with TrxA::PA44-OVA (n=6) or TrxA::PA44-OVA@CaP (n=6) were challenged with WSN-OVA 8 months post-vaccination. (**A**) Spleens were excised from three mice in each group after 7 days. Single cell suspensions were analyzed for OVA-specific $CD8^+$ T cells by flow cytometry using anti-CD44 antibody and $H2K^b$-restricted SIINFEKL

tetramer. (B) Quantification of $H2K^b$-restricted SIINFEKL tetramer binding $CD8^+$ T cells from the spleen of the mice. (C) The remaining 3 animals in each cohort were monitored for weight loss.

Figure 1
Click here to download high resolution image

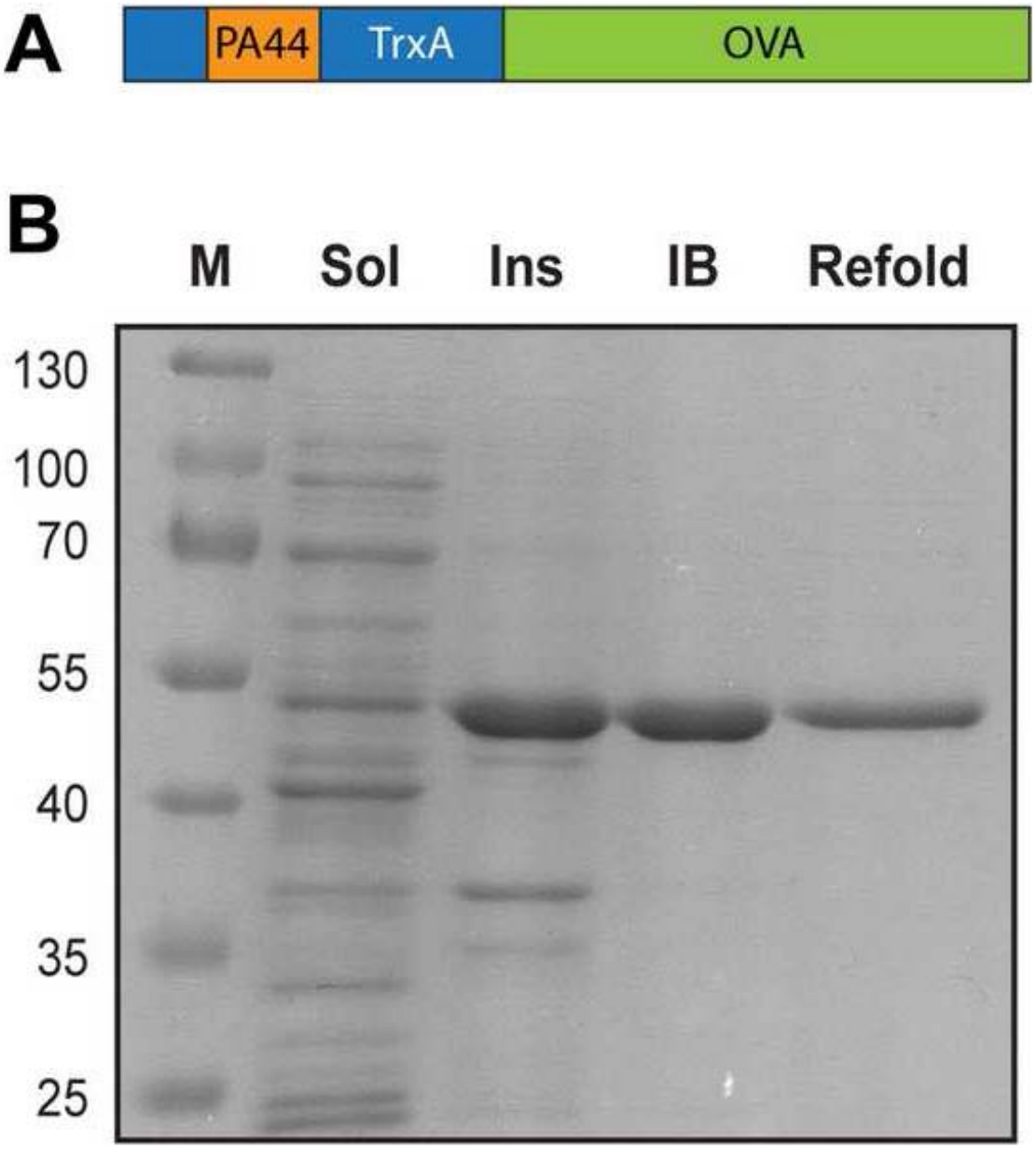

Figure 2
Click here to download high resolution image

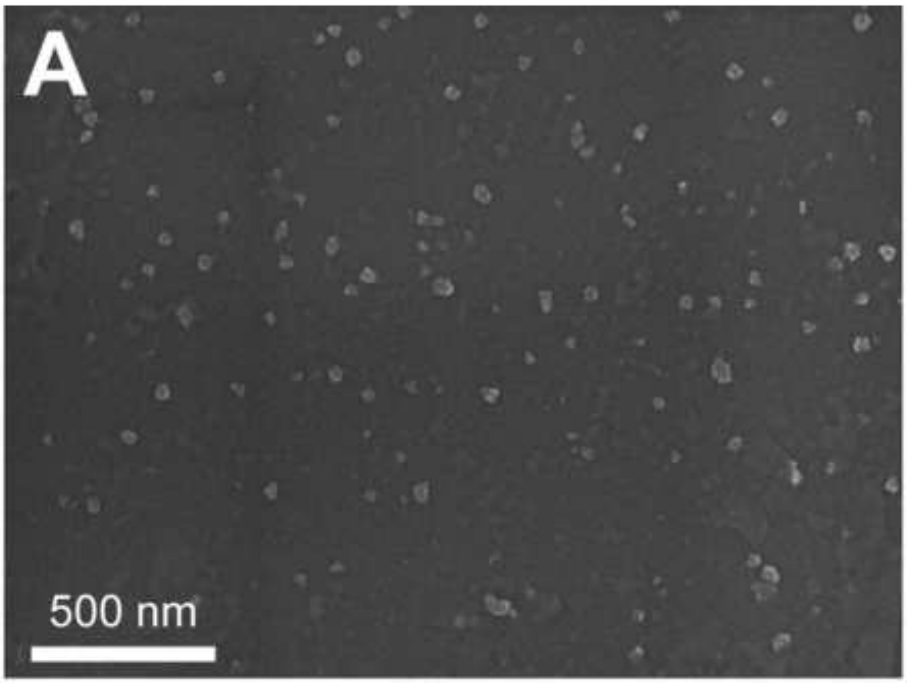

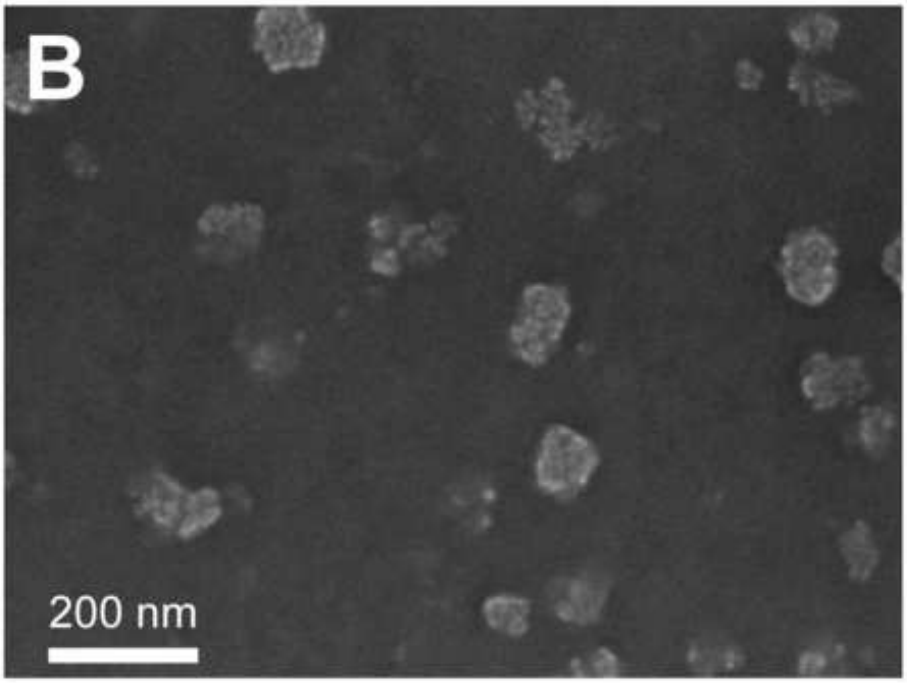

Figure 3
Click here to download high resolution image

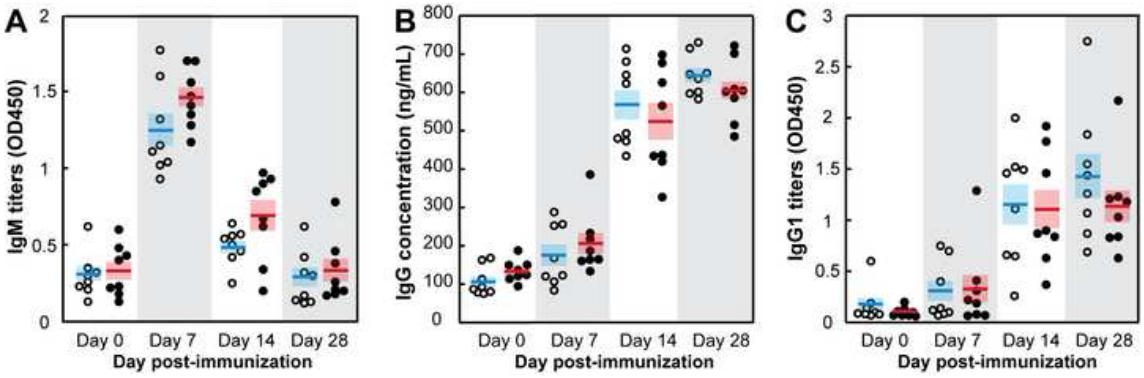

Figure 4
Click here to download high resolution image

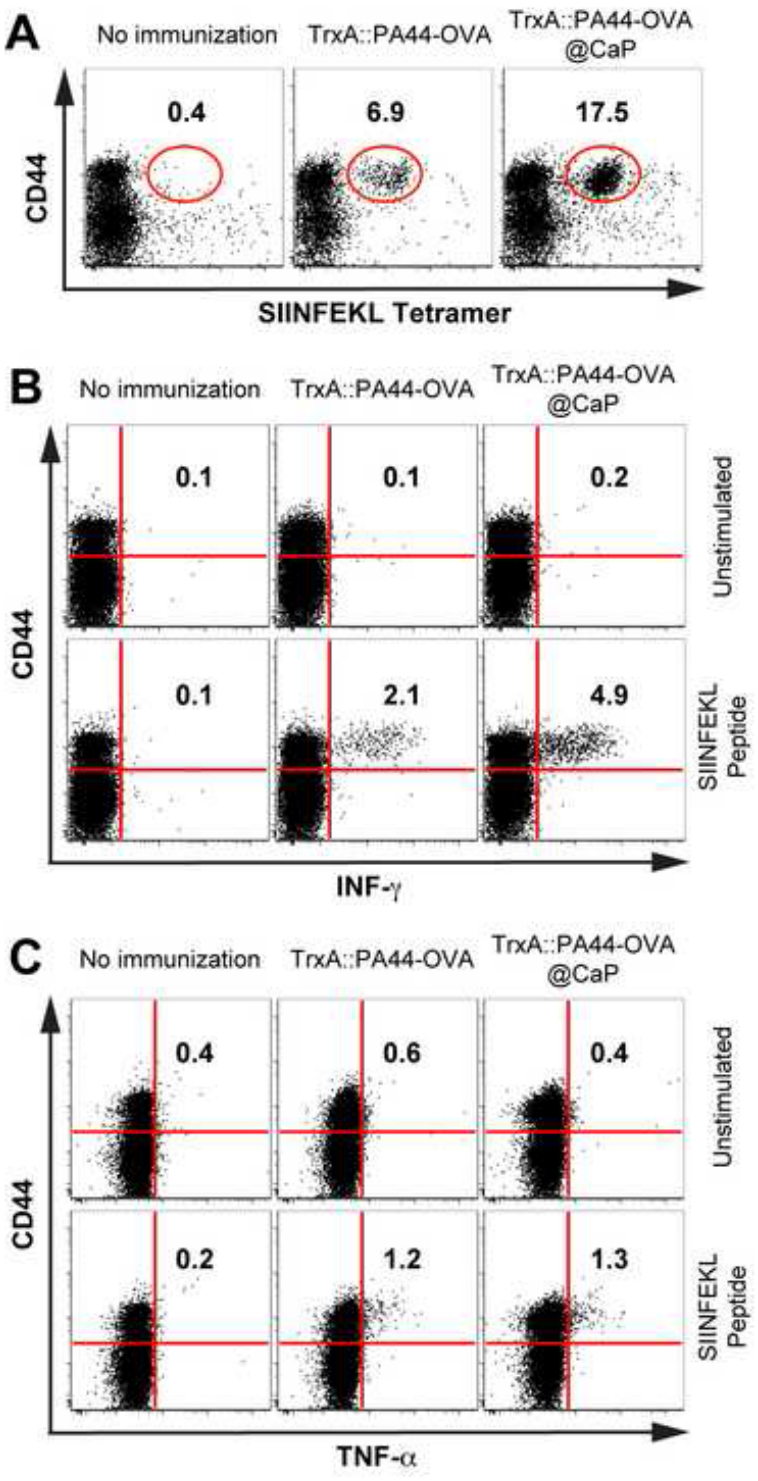

Figure 5
Click here to download high resolution image

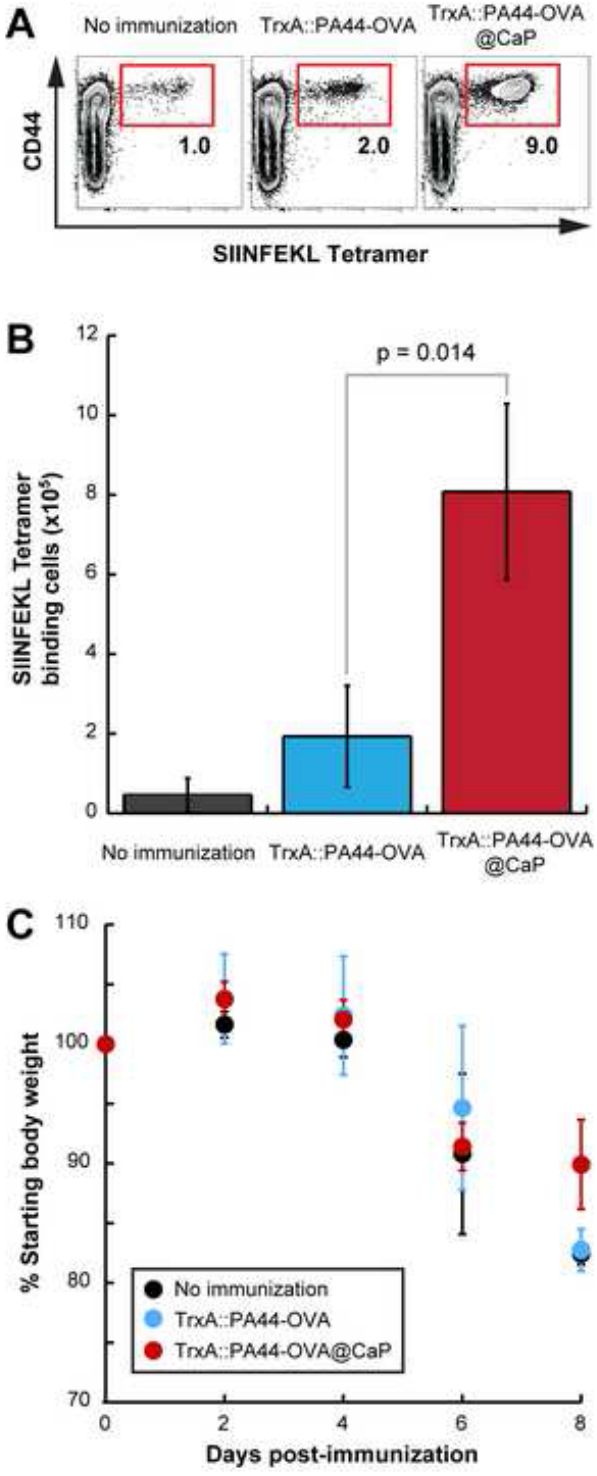

Appendix B: Monosodium Urate Binders

B.1 Introduction

Gout is an inflammatory arthritic condition caused by the deposition of monosodium urate (MSU) crystals in joints and soft tissue and is the most common form of inflammatory joint disease in men over 40 years old.[97] Uric acid is a byproduct of purine metabolism and hyperuricemia is a major risk factor for gout.[19] Phagocytosis of MSU crystals by polymorphonuclear leukocytes can cause lysis of leukocytes releasing lysosomal enzymes into serum causing localized pain and inflammation.[102] Gout is typically treated with nonsteroidal anti-inflammatory drugs, colchicine, corticosteroids, and corticotropin.[97]

Heptapeptides with binding affinity to MSU were identified by phage display library biopanning against a MSU substrate. Solid-binding peptides have been shown to nucleate and control the growth of a wide variety of inorganic and organic materials.[9] Uncharacterized biological factors derived from subcutaneous fluid in rats after MSU injection have been shown to decrease phagocytosis of MSU crystals and inflammation after injection into separate rats.[145] Identification of MSU peptide binding motifs may aid in the design of protein therapeutics designed to limit the growth and uptake of MSU crystals in patients afflicted with gout.

B.2 Materials and Methods

B.2.1 Preparation of monosodium urate Crystals

Procedure modified from "Ortiz-Bravo, E and Schumacher, R, Components Generated Locally as Well as Serum Alter the Phlogistic Effect of Monosodium Urate Crystals *in vivo*, *The Journal of Rheumatology* 1993;20:1162-6."

A 20 mL solution of 0.2 M NaOH (JT Baker 3722-05) was placed in a 50 mL beaker, covered with a glass lid and heated to 70°C while stirred with a small stirring bar. Approximately 400 mg of uric acid (Sigma U2625-25g) was added while stirring until no more salt could be dissolved. The saturated solution was then poured into a syringe, filtered through a 0.22 µm cellulose acetate filter, and rocked at 100 rpm at 22^{o}C for 24 h in a 60 mm x 16 mm covered polystyrene petri dish. On the next day, most of the supernatant was slowly decanted and seed crystals were allowed to grow in about 3 mL of leftover fluid in the uncovered dish for 24 hrs under a hood. The dried crystals attached to the bottom of the dish were washed 3x with 5 mL EtOH and allowed to airdry for another 24 hrs. Crystals were then washed 3x with 5 mL ddH_2O and left to airdry for 24 hrs. Approximately 1 mL of fluid remained in the dish before the air-drying step.

B.2.2 Biopanning against monosodium urate crystal substrates

(See NEB's PhD phage display libraries- Instruction Manual for additional information)

NEB's Phage Display Peptide Library, Ph.D. c7c (E8120S) was used to screen disulfide constrained heptapeptides exhibiting affinity for the MSU substrate. For the first round of biopanning, MSU plates were incubated with 3 mL of blocking buffer (0.1 M NaHCO3 (pH 8.6), 5 mg/mL BSA) at 4°C for 1 h. The blocking buffer was then decanted and the dish inverted onto a clean laboratory tissue. Next the plates were washed 6x with 3 mL of TBST buffer (50 mM

Tris-HCl (pH 7.5), 150 mM NaCl, with 0.1% [v/v] Tween-20) as above. Some crystal loss occurred during this step. The phage library was diluted 100x with TBST buffer to a final volume of 1 mL and a phage titer of 2.7×10^{11} Pfu/mL. The phage solution was added to the MSU plates that were covered and rocked at RT and 100 rpm for 1 h. The phage solution was then discarded and nonbinding phages were removed by washing plates 10x with 3 ml of TBST buffer as above. Bound phages were eluted with 1 mL of 0.2 M Glycine-HCl, pH 2.2, 1 mg/mL BSA.

The phage eluate titer was then analyzed (2.4×10^6 PFU/ml). Phage amplification was carried out by infecting a 20 mL culture containing a 100x dilution of an overnight culture of E. *coli* ER2738 in LB followed by incubation at 37°C for 4.5 h. The culture was then spun down at 12,000 g for 10 min at 4°C. The supernatant was transferred to fresh tube and centrifuged again. The upper 80% of the supernatant was transferred to a fresh tube and 3 mL of 20% [w/v] PEG-8000, 2.5 M NaCl was added. The tube was then vortexed briefly to mix the PEG/NaCl and phages were precipitated with an overnight hold at 4°C.

The PEG precipitation was spun at 12,000 g for 15 min at 4°C. The supernatant was decanted and discarded. The tube was respun and the residual supernatant was removed with a pipet. The phage pellet was resuspended in 1mL of TBS and then transferred to a 1mL microcentrifuge tube. The tube was spun down at 18,000 g for 5 min and the supernatant was transferred to a new tube. Phages were reprecipitated by adding 200 uL of 20% PEG/2.5M NaCl and incubated on ice for 45 min. Tubes were then respun at 18,000 g for 10 min and the supernatant was decanted and discarded. The tubes were respun and the residual supernatant was removed by pipetting. The remaining phage pellet was then resuspended in 200 uL TBS and

spun at 18,000 g for 1 min. The supernatant was removed and transferred to a new tube. The amplified phage eluate was then titered (1.0×10^{13} Pfu/mL).

The 2nd and 3rd rounds of biopanning were conducted in the same manner as listed above with the following exceptions. The amplified eluate from the previous round was used instead of NEB's Ph.D. c7c library, and amplified eluate was diluted to the same order of magnitude as was used in the first round (1.0×10^{11} Pfu/mL for the 2nd round and 1.6×10^{11} Pfu/mL for the 3rd round). For wash steps, Tween-20 concentration was increased to 0.5% [v/v] in TBST buffer.

3rd round eluate was titered (4.4×10^{7} Pfu/mL) and 10 plaques were picked for sequencing. Plaques were amplified by incubating at 37°C for 4.5 hrs in 1 mL of an overnight culture of *E. coli* ER2738 diluted 100x in LB. Phages were purified by 20% [w/v] PEG-8000, 2.5 M NaCl precipitation. pM13KE was extracted from phage pellets by precipitation for 15 min at RT in Iodide buffer (10mM Tris-HCl (pH 8.0), 1mM EDTA, 4 M sodium iodide) and ethanol. Plasmid purity was verified by agarose gel electrophoresis and c7c inserts were sequenced with the -96 gIII sequencing primer, 5´- ^{HO}CCC TCA TAG TTA GCG TAA CG –3´.

B.3 Results

The MSU substrate prepared for biopanning was imaged by optical microscopy before and after biopanning. MSU crystals formed in single needles or radial clusters (Fig. B.1). Dissolution of MSU crystals did occur but MSU crystals still remained after three rounds of biopanning (Fig. B.2). MSU biopanning eluate phage titers were above $2.2x10^6$ Pfu/mL for all biopanning rounds (Tab. B.1). After the third round of biopanning, plaques containing MSU binders were sequenced. Of the ten MSU binding heptapeptides identified, nine had isoelectric points (pIs) above pH 7 and eight were hydrophilic (Tab. B.2).

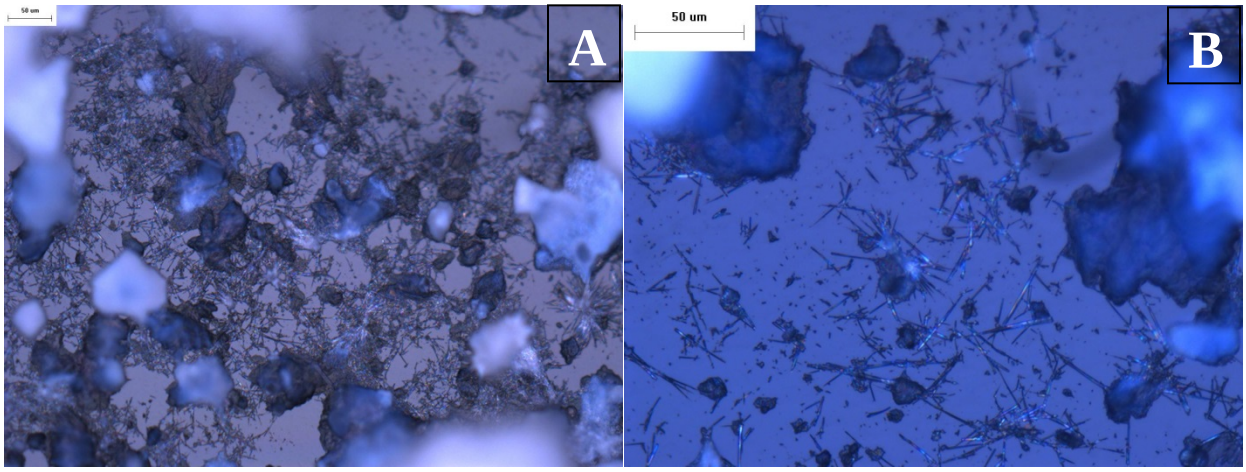

Fig. B.1: MSU plate before washing at (A) 20x magnification and (B) 50x magnification.

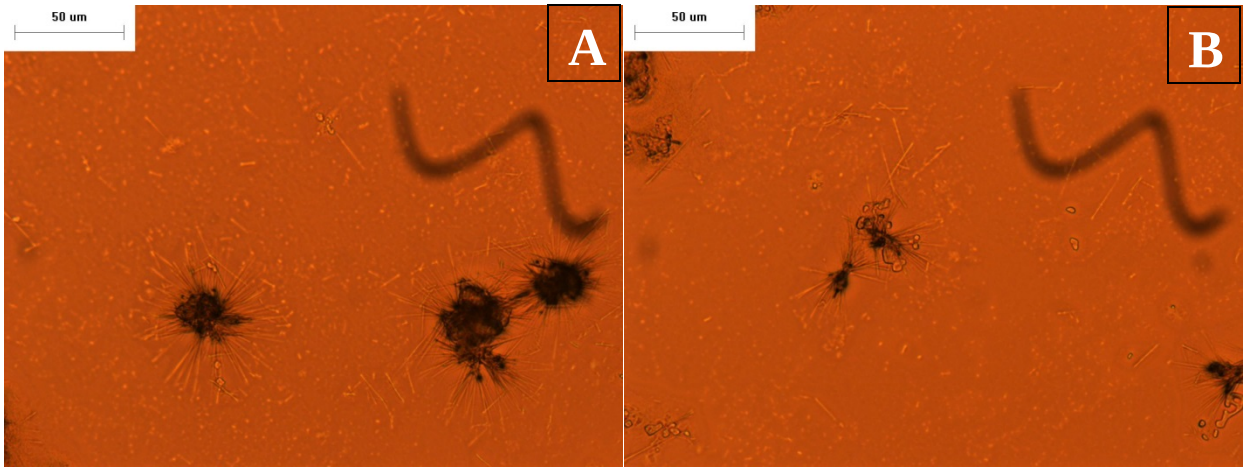

Fig. B.2: MSU plate after biopanning at (A) 20x magnification and (B) 50x magnification. An artifact is present in the top right quadrant of the images.

Table B.1: MSU biopanning eluate phage titers

Biopanning round		Pfu/mL
1	Eluate	4.0E+07
	Amplified Eluate	8.8E+13
2	Eluate	1.0E+08
	Amplified Eluate	1.6E+14
3	Eluate	2.2E+06

Table B.2: Monosodium Urate (MSU) c7c Binders

Name	Sequence	MW	pI	GRAVY
MSU1	ILMPQLS	801.0	5.52	1.157
MSU2	RIMSMPK	862.1	11.00	-0.357
MSU3	QPPRIRI	879.0	12.00	-.957
MSU4	TTQQRMR	920.0	12.00	-2.214
MSU5	IPRIRRQ	938.1	12.3	-1.371
MSU6	MIQILKL	858.1	8.50	1.586
MSU7	RLPLKSS	799.9	11.00	-0.571
MSU9	HLQPRIR	919.1	12.00	-1.286
MSU10	PRKPHTR	891	12.01	-2.857

Sequence: **Basic** **Acidic** **Hydrophobic** **Hydroxyl** **Amide**

pI: **Highly basic** **Moderately basic**

Moderately acidic **Highly Acidic**

GRAVY: **Highly hydrophobic** **Moderately hydrophobic**

Moderately hydrophilic **Highly hydrophilic**

B.4 Discussion

Analysis of optical microscopy images of MSU substrates revealed that MSU crystals were formed as single needles or radial clusters and similar MSU crystal morphology has been found in gouty individuals.[111] Crystallography analysis of MSU crystals revealed that MSU crystals are triclinic needles.[122]

Ten disulfide constrained heptapeptides with binding affinity to MSU were identified after three rounds of phage display biopanning. The majority of identified MSU binders shared similar properties. Positively charged residues seemed to play an important role in binding since 9/10 binders had basic pIs and 8/10 had pIs at or above pH 11. Also, the identified MSU binders were mostly hydrophilic with 8/10 binders having negative grand average of hydropathy indices (GRAVY).

These findings are in agreement with theorized MSU binding sequences based upon the crystal faces of MSU.[122] Exposed crystal MSU faces are rich in hydrogen and oxygen atoms and hydrogen bonding between the MSU binders and the MSU crystal face explains the prevalence of hydrophilic MSU binders (8/10). The oxygen atoms in the urate molecule may also contribute to electrostatic interactions between the MSU crystals and peptide binders. The prevalence of positively charged residues (Lys, His, and Arg) in the identified MSU binders indicates electrostatic interactions are involved in MSU crystal-peptide binding.

Gout is characterized by the accumulation of MSU crystals at the site of inflammation.[97] Pain and inflammation caused by MSU crystals is attributed to the phagocytosis of MSU crystals by leucocytes which causes lysis and/or release of pro-inflammatory molecules.[127, 163, 168] Hydrogen bonding between lysosomal membranes and MSU crystals after phagocytosis has been

suggested as a mechanism for lysosome rupture which causes the release of leucocyte cell contents resulting in pain and inflammation.[197] Pretreatment of MSU crystals with proteins has been shown to block lysis and lysosomal enzyme release in neutrophils.[102] The MSU binders identified through phage-display biopanning help elucidate interactions involved in *in vivo* MSU crystal-protein binding and may aid in the development of alternative protein therapeutics that prevent MSU crystal phagocytosis and growth by coating MSU crystals with adsorbed proteins.

Appendix C: Supplemental Information

C.1: Supplemental information for Chapter 4

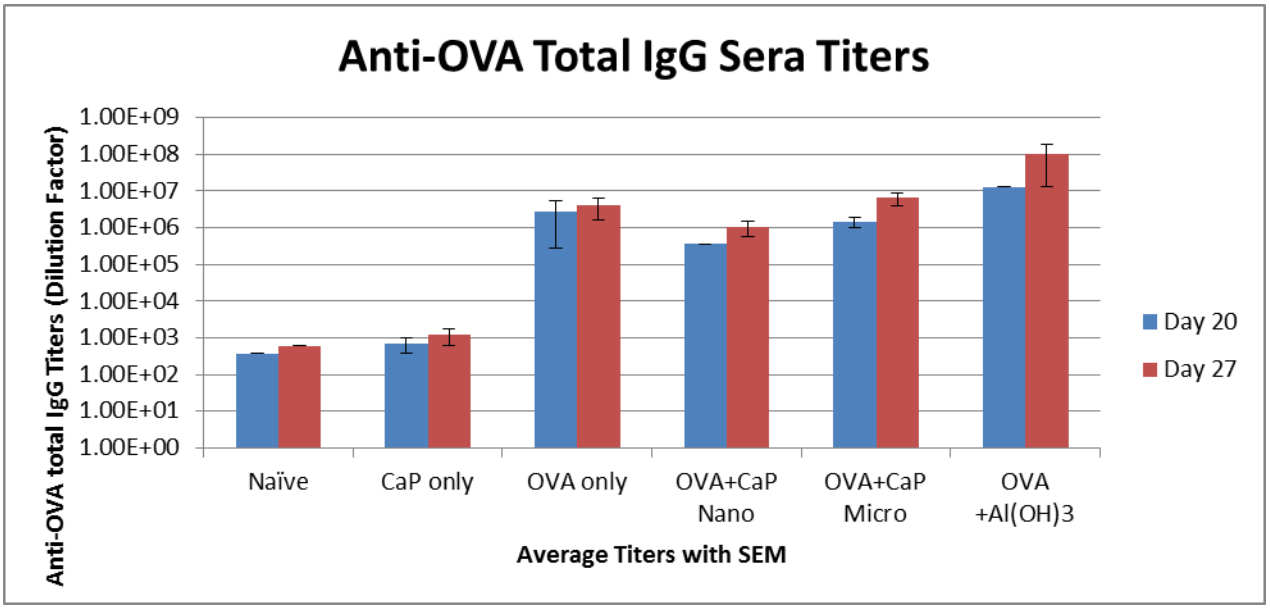

Fig. C.1.1: Anti-OVA total IgG titers at day 20 and 27

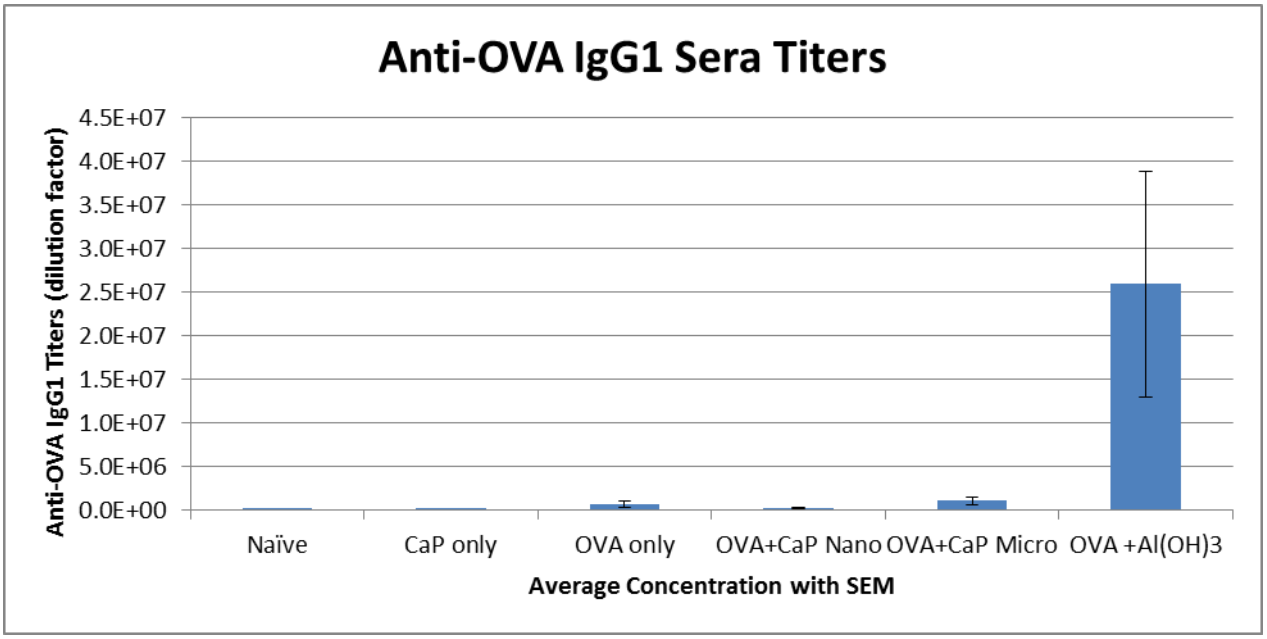

Fig. C.1.2: Anti-OVA total IgG1 titers

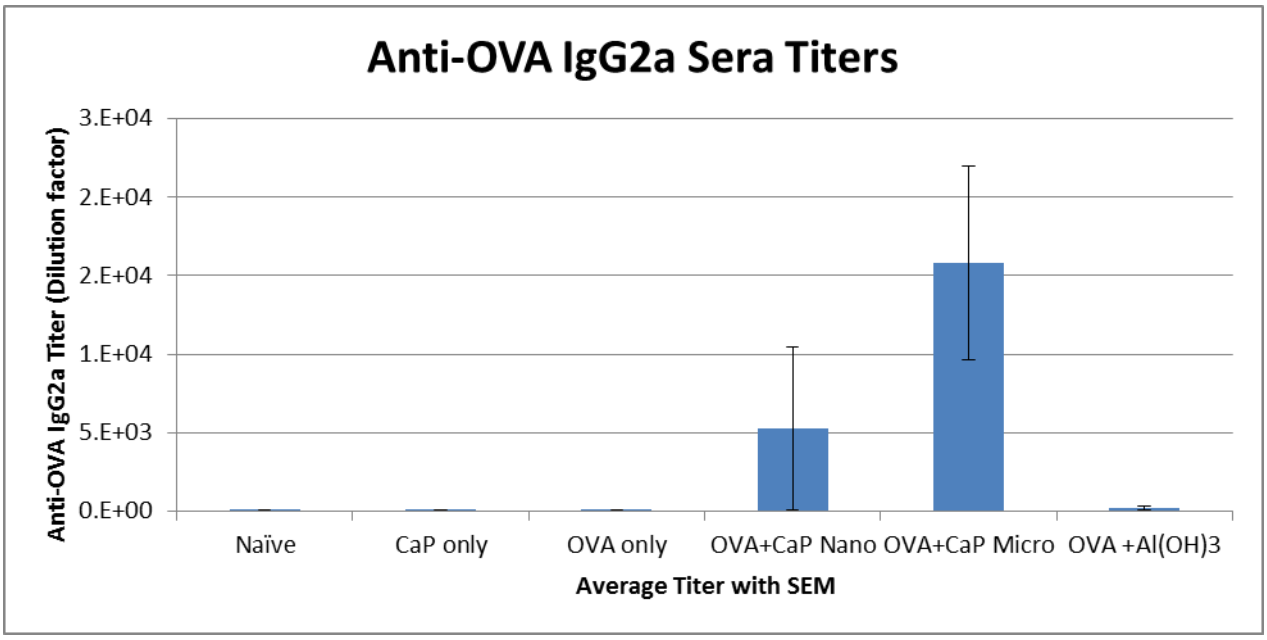

Fig. C.1.3: Anti-OVA total IgG2a titers

C.2: Supplemental information for Chapter 5

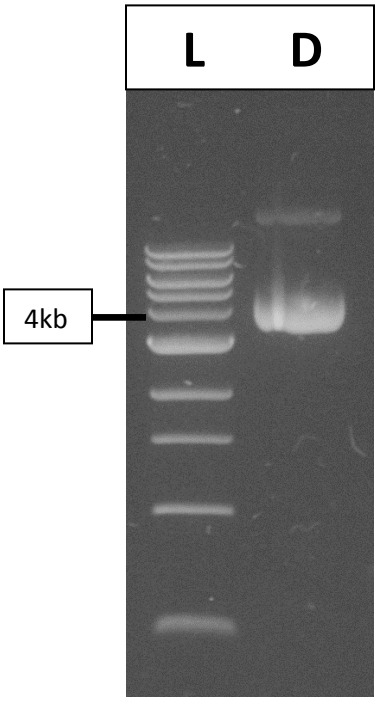

Fig. C.2.1: pVAX-OVA plasmid size, Lanes, L: DNA ladder, NEB N3232S, D: pVAX-OVA (expected size 4.1 kb)

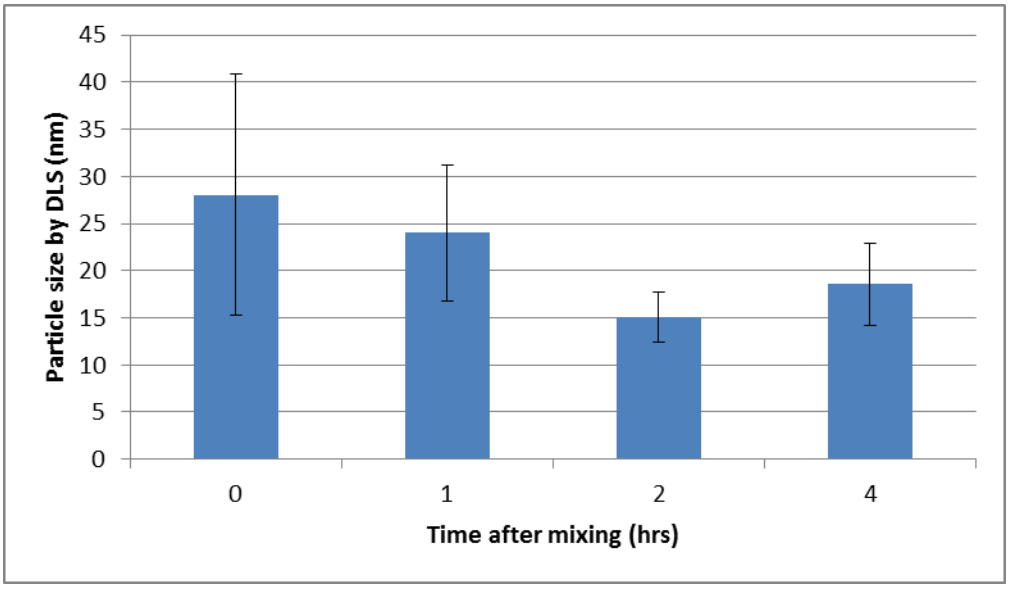

Fig. C.2.2: Particle size by DLS of CaP, cPN38, and pVAX-OVA particles used for *in vivo* immunizations.

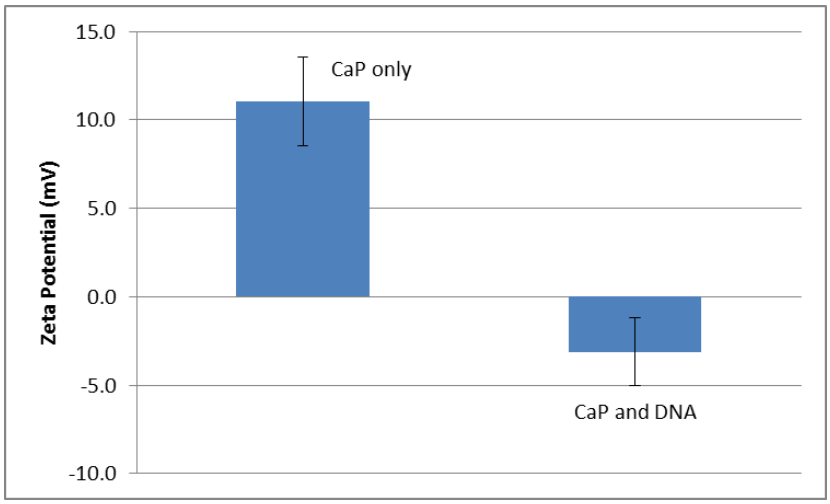

Fig. C.2.3: Zeta potential of CaP, cPN38, and pVAX-OVA particles used for *in vivo* immunizations.

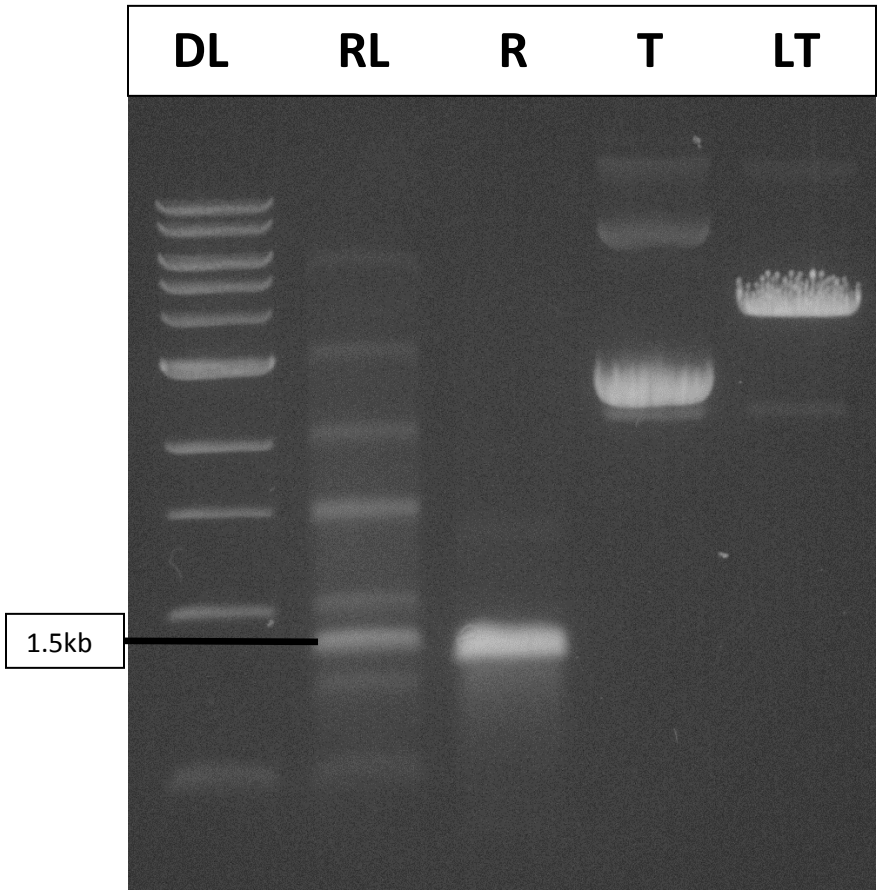

Fig. C.2.4: OVA mRNA size and template plasmid. Lanes, DL: DNA ladder, NEB N3232S, RL: RNA ladder, Invitrogen 15623-200, R: OVA mRNA product (expected size 1.3kb), T: pGEM4z-OVA-A64 template, LT: SpeI linearized pGEM4z-OVA-A64.

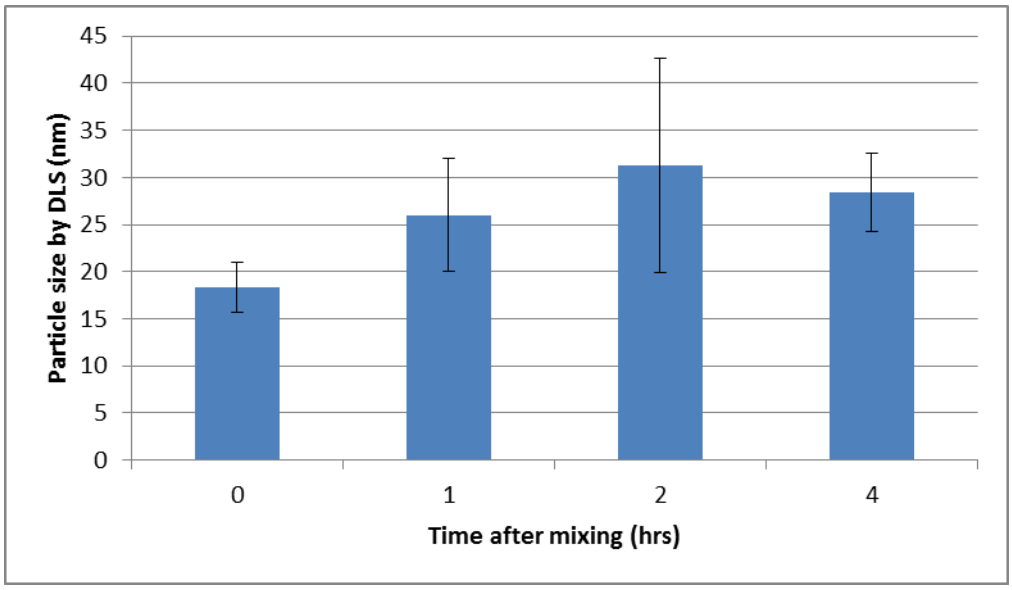

Fig. C.2.5: Particle size by DLS of CaP, cPN38, and OVA mRNA particles used for *in vivo* immunizations.

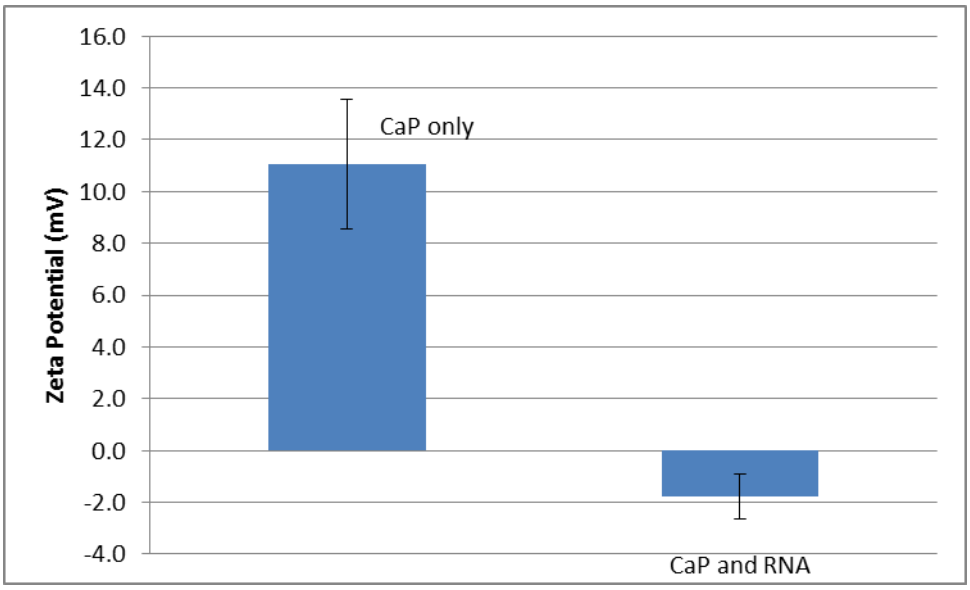

Fig. C.2.6: Zeta potential of CaP, cPN38, and OVA mRNA particles used for *in vivo* immunizations.

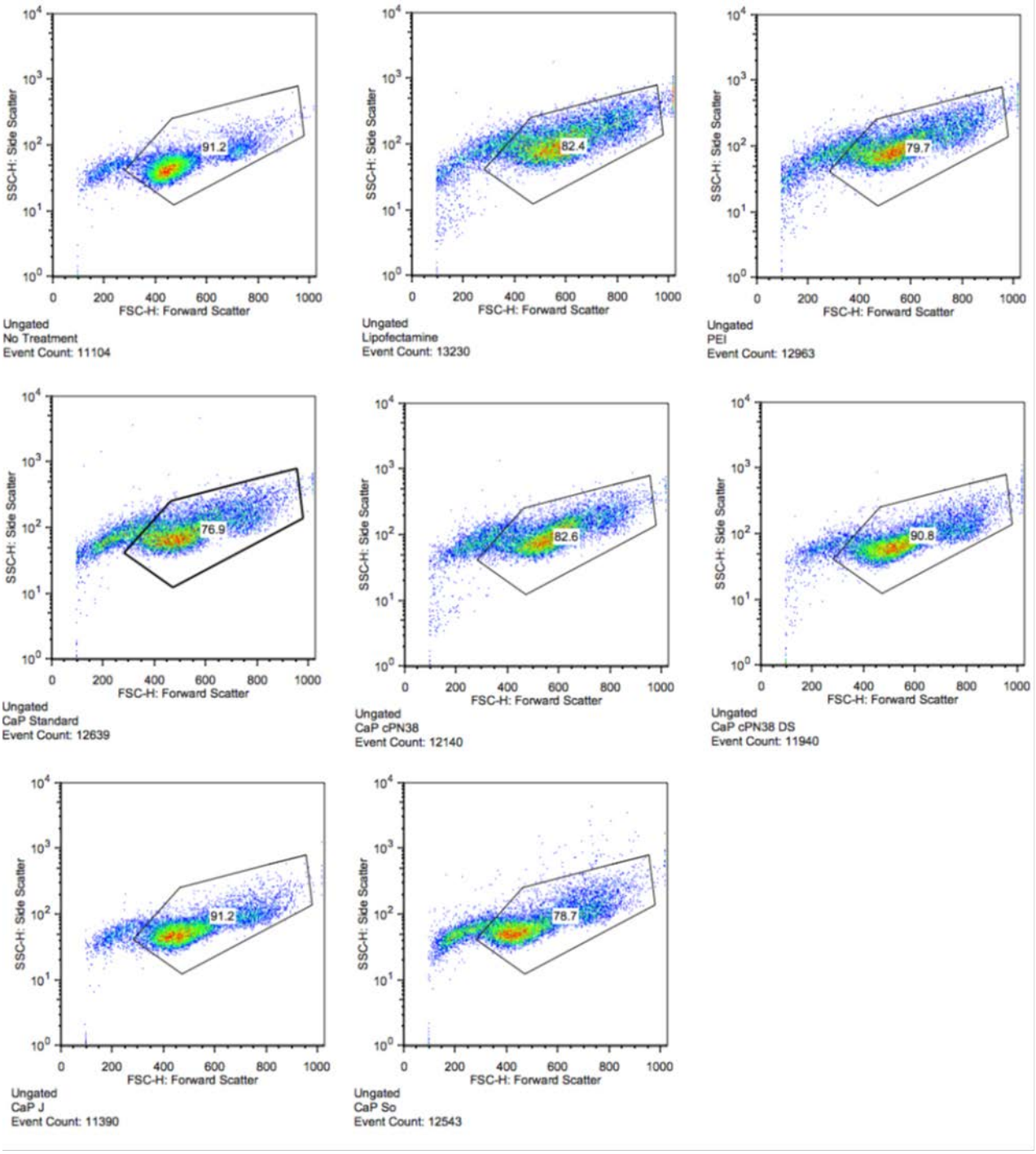

Fig. C.2.7: Example gating for RAW 264.7 cell transfections. Cell population gated from the FSC-H and SSC-H channels.

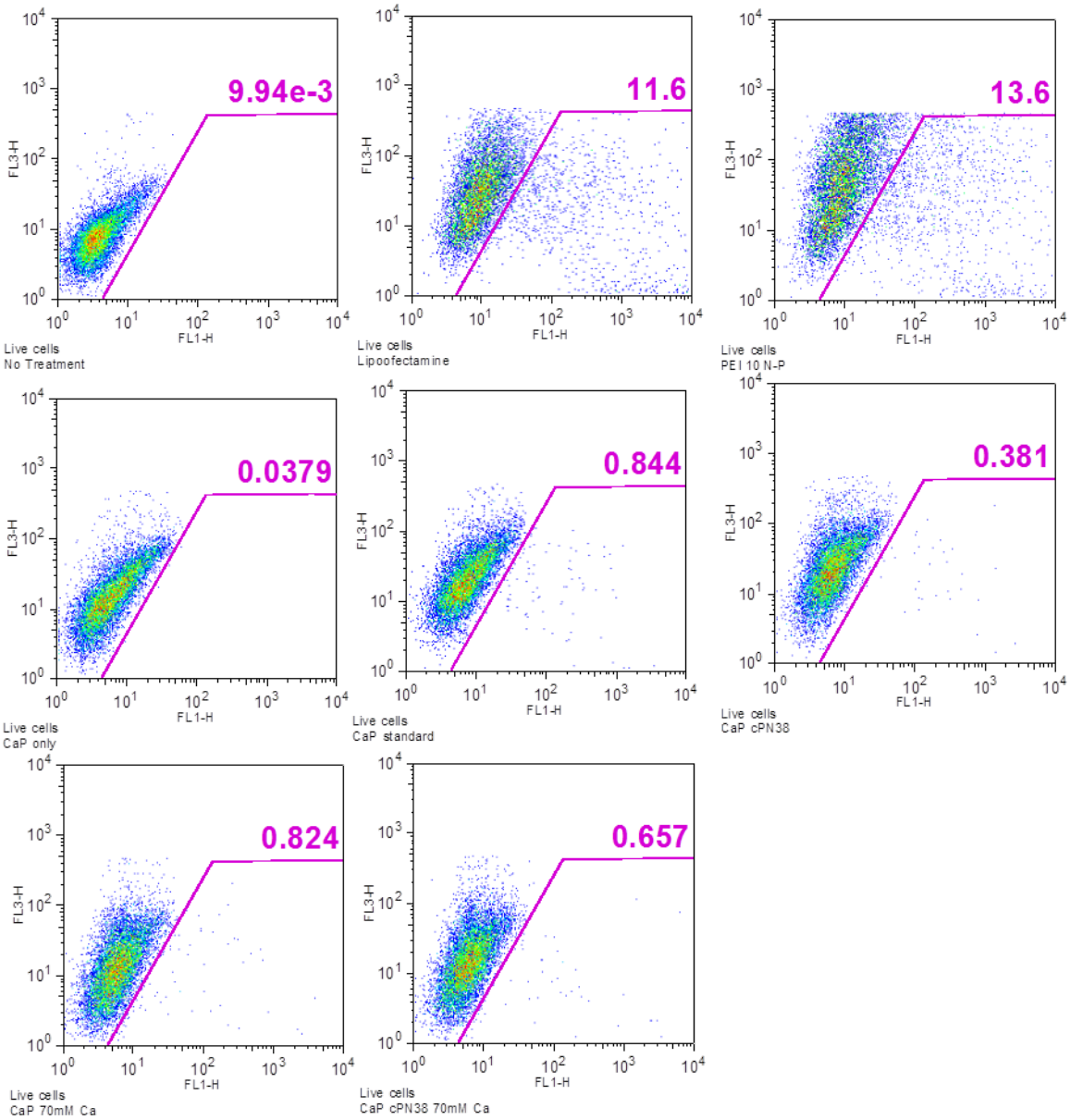

Fig. C.2.8: Example gating for transfection efficiency in RAW 264.7 cells. GFP+ cells detected in FL1-H channel and PI+ (dead cells) gated out in the FL3-H channel. Asymmetrical gates were drawn for GFP+ cells to remove false positives from autofluorescence. Transfection efficiency reported as GFP+ cells from the PI- population.

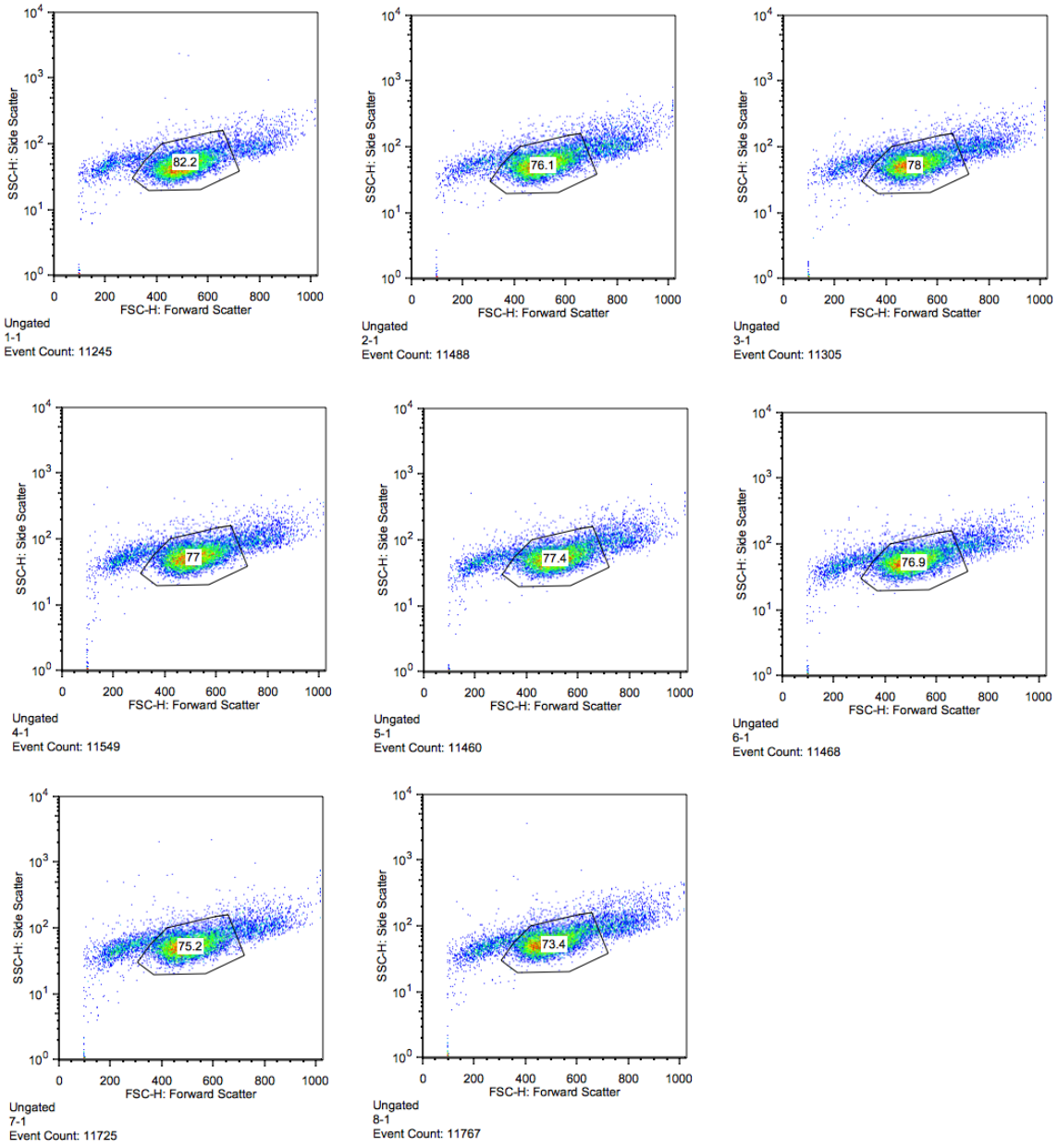

Fig. C.2.9: Gating of cell populations for RAW 264.7 cell DNA-Cy3 uptake. Cell population gated on FSC-H vs SSC-H channels. 1-1: No Treatment, 2-1: CaP Micro, 3-1: CaP Nano, 4-1: CaP Nano Mannosylated, 5-1: No Treatment, Trypan Blue (TB), 6-1: CaP Micro, TB, 7-1: CaP Nano, TB, 8-1: CaP Nano Mannosylated, TB. Cell population gated on FSC-H vs SSC-H channels.

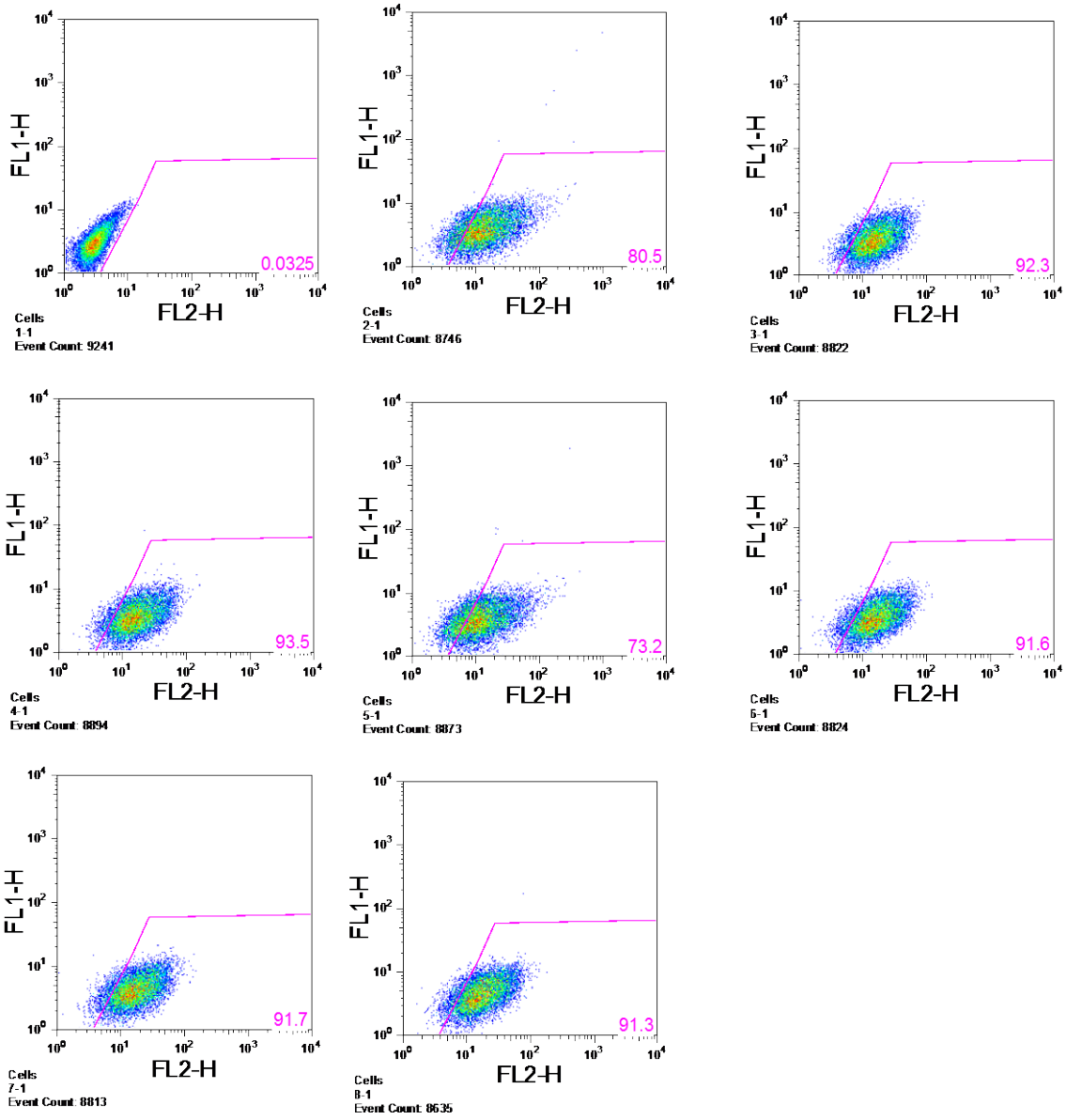

Fig. C.2.10: Gating of Cy3+ RAW 264.7 cells. Cy3+ cells gated on FL2-H channel. Asymmetrical gate drawn to exclude false positives from autofluorescence. 1-1: No Treatment, 2-1: CaP Micro, 3-1: CaP Nano, 4-1: CaP Nano Mannosylated, 5-1: No Treatment, Trypan Blue (TB), 6-1: CaP Micro, TB, 7-1: CaP Nano, TB, 8-1: CaP Nano Mannosylated, TB.

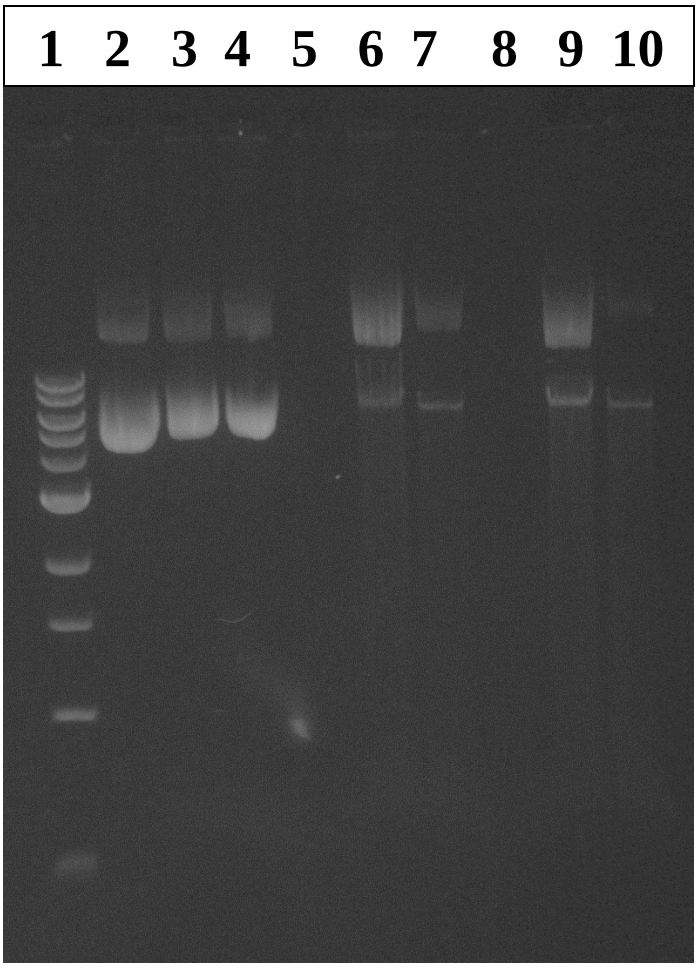

Fig. C.2.11: Protection of gWiz-GFP from DNAse. 1 uL of DNAse (2U/µL) (Ambion AM2238) added to 20uL of naked gWiz-GFP (0.05mg/mL), CaP standard (1xHBS, 125mM $CaCl_2$, and 0.05mg/mL gWiz-GFP), CaP nanoparticles (1xHBS, 60mM $CaCl_2$, 50µM cPN38, and 0.05mg/mL gWiz-GFP) and incubated at 37°C before loading onto a 1% agarose gel (1hr at 100V). Lanes: (1) DNA ladder, NEB N3232S, (2) naked DNA, (3) CaP standard, (4) CaP nanoparticles, (5) Naked DNA digested for 1 hr, (6) CaP standard digested for 1 hr, (7) CaP nanoparticles digested for 1 hr, (8) Naked DNA digested for 30min, (9) CaP standard digested for 30min, (10) CaP nanoparticles digest for 30 min.

Appendix D: Citations

[1] Aggerbeck H, Fenger C, Heron I. BOOSTER VACCINATION AGAINST DIPHTHERIA AND TETANUS IN MAN - COMPARISON OF CALCIUM-PHOSPHATE AND ALUMINUM HYDROXIDE AS ADJUVANTS .2. Vaccine. 1995;13.
[2] Aggerbeck H, Heron I. ADJUVANTICITY OF ALUMINUM HYDROXIDE AND CALCIUM-PHOSPHATE IN DIPHTHERIA-TETANUS VACCINES .1. Vaccine. 1995;13:1360-5.
[3] Aggerbeck H, Wantzin J, Heron I. Booster vaccination against diphtheria and tetanus in man. Comparison of three different vaccine formulations .3. Vaccine. 1996;14:1265-72.
[4] Agrawal AK, Gupta CM. Tuftsin-bearing liposomes in treatment of macrophage-based infections. Advanced Drug Delivery Reviews. 2000;41:135-46.
[5] Al-Qasas NS, Rohani S. Synthesis of pure hydroxyapatite and the effect of synthesis conditions on its yield, crystallinity, morphology and mean particle size. Separation Science and Technology. 2005;40.
[6] Altschul SF, Madden TL, Schaffer AA, Zhang JH, Zhang Z, Miller W, et al. Gapped BLAST and PSI-BLAST: a new generation of protein database search programs. Nucleic Acids Research. 1997;25:3389-402.
[7] Altschul SF, Wootton JC, Gertz EM, Agarwala R, Morgulis A, Schaffer AA, et al. Protein database searches using compositionally adjusted substitution matrices. Febs Journal. 2005;272:5101-9.
[8] Balass M, Kalef E, Fuchs S, Katchalski-Katzir E. A cyclic peptide with high affinity to alpha-bungarotoxin protects mice from the lethal effect of the toxin. Toxicon. 2001;39:1045-51.
[9] Baneyx F, Schwartz DT. Selection and analysis of solid-binding peptides. Current Opinion in Biotechnology. 2007;18:312-7.
[10] Basarkar A, Singh J. Nanoparticulate systems for polynucleotide delivery. International Journal of Nanomedicine. 2007;2:353-60.
[11] Batard P, Jordan M, Wurm F. Transfer of high copy number plasmid into mammalian cells by calcium phosphate transfection. Gene. 2001;270.
[12] Baxby D. Edward Jenner's inquiry; a bicentenary analysis. Vaccine. 1999;17:301-7.
[13] Berridge MJ, Lipp P, Bootman MD. The versatility and universality of calcium signalling. Nature Reviews Molecular Cell Biology. 2000;1:11-21.
[14] Bisht S, Bhakta G, Mitra S, Maitra A. pDNA loaded calcium phosphate nanoparticles: highly efficient non-viral vector for gene delivery. International Journal of Pharmaceutics. 2005;288.
[15] Bomford R. COMPARATIVE SELECTIVITY OF ADJUVANTS FOR HUMORAL AND CELL-MEDIATED-IMMUNITY .1. EFFECT ON THE ANTIBODY-RESPONSE TO BOVINE SERUM-ALBUMIN AND SHEEP RED-BLOOD-CELLS OF FREUNDS INCOMPLETE AND COMPLETE ADJUVANTS, ALHYDROGEL, CORYNEBACTERIUM-PARVUM, BORDETELLA-PERTUSSIS, MURAMYL DIPEPTIDE AND SAPONIN. Clinical and Experimental Immunology. 1980;39:426-34.
[16] Bomford R, Stapleton M, Winsor S, McKnight A, Andronova T. THE CONTROL OF THE ANTIBODY ISOTYPE RESPONSE TO RECOMBINANT HUMAN-IMMUNODEFICIENCY-VIRUS GP120 ANTIGEN BY ADJUVANTS. Aids Research and Human Retroviruses. 1992;8:1765-71.

[17] Bonfils E, Mendes C, Roche AC, Monsigny M, Midoux P. UPTAKE BY MACROPHAGES OF A BIOTINYLATED OLIGO-ALPHA-DEOXYTHYMIDYLATE BY USING MANNOSYLATED STREPTAVIDIN. Bioconjugate Chemistry. 1992;3.
[18] Bose S, Saha SK. Synthesis and characterization of hydroxyapatite nanopowders by emulsion technique. Chemistry of Materials. 2003;15.
[19] Boyer GS, Lanier AP, Templin DW. PREVALENCE RATES OF SPONDYLOARTHROPATHIES, RHEUMATOID-ARTHRITIS, AND OTHER RHEUMATIC DISORDERS IN AN ALASKAN INUPIAT ESKIMO POPULATION. Journal of Rheumatology. 1988;15:678-83.
[20] Boyle JS, Silva A, Brady JL, Lew AM. DNA immunization: Induction of higher avidity antibody and effect of route on T cell cytotoxicity. Proceedings of the National Academy of Sciences of the United States of America. 1997;94:14626-31.
[21] Bry L, Brigl M, Brenner MB. CD4(+)-T-cell effector functions and costimulatory requirements essential for surviving mucosal infection with Citrobacter rodentium. Infection and Immunity. 2006;74:673-81.
[22] Buck C. Smallpox inoculation - should we credit Chinese medicine? Complementary Therapies in Medicine. 2003;11.
[23] Cai Y, Liu Y, Yan W, Hu Q, Tao J, Zhang M, et al. Role of hydroxyapatite nanoparticle size in bone cell proliferation. Journal of Materials Chemistry. 2007;17.
[24] Cai Y, Yao J. Effect of proteins on the synthesis and assembly of calcium phosphate nanomaterials. Nanoscale. 2010;2:1842-8.
[25] Chen HB, Su XD, Neoh KG, Choe WS. Context-Dependent Adsorption Behavior of Cyclic and Linear Peptides on Metal Oxide Surfaces. Langmuir. 2009;25:1588-93.
[26] Cheng C, Convertine AJ, Stayton PS, Bryers JD. Multifunctional triblock copolymers for intracellular messenger RNA delivery. Biomaterials. 2012;33.
[27] Chiu D, Zhou W, Kitayaporn S, Schwartz DT, Murali-Krishna K, Kavanagh TJ, et al. Biomineralization and Size Control of Stable Calcium Phosphate Core-Protein Shell Nanoparticles: Potential for Vaccine Applications. Bioconjugate Chemistry. 2012;23.
[28] Choe WS, Sastry MSR, Thai CK, Dai H, Schwartz DT, Baneyx F. Conformational control of inorganic adhesion in a designer protein engineered for cuprous oxide binding. Langmuir. 2007;23:11347-50.
[29] Chung WJ, Kwon KY, Song J, Lee SW. Evolutionary screening of collagen-like peptides that nucleate hydroxyapatite crystals. Langmuir.27:7620-8.
[30] Comoy EE, Capron A, Thyphronitis G. In vivo induction of type 1 and 2 immune responses against protein antigens. International Immunology. 1997;9:523-31.
[31] Coulfield MJ, Shi L, Wang S, Wang B, Tobery TW, Mach H, et al. Effect of alternative aluminum adjuvants on the absorption and immunogenicity of HPV16 L1 VLPs in mice. Human Vaccines. 2007;3:139-45.
[32] Coutelier JP, Vanderlogt JTM, Heessen FWA, Warnier G, Vansnick J. IGG2A RESTRICTION OF MURINE ANTIBODIES ELICITED BY VIRAL-INFECTIONS. Journal of Experimental Medicine. 1987;165:64-9.
[33] Cruz LJ, Tacken PJ, Fokkink R, Joosten B, Stuart MC, Albericio F, et al. Targeted PLGA nano- but not microparticles specifically deliver antigen to human dendritic cells via DC-SIGN in vitro. Journal of Controlled Release.144:118-26.

[34] Cvjetanovic B, Uemura K. The Present Status of Field and Laboratory Studies of Typhoid and Paratyphoid Vaccines with Special Reference to Studies Sponsored by World Health Organization. Bull World Health Organ. 1965;32:29-36.
[35] Dai HX, Choe WS, Thai CK, Sarikaya M, Traxler BA, Baneyx F, et al. Nonequilibrium synthesis and assembly of hybrid inorganic-protein nanostructures using an engineered DNA binding protein. Journal of the American Chemical Society. 2005;127.
[36] Darveau RP, Chilton PM. Naturally occurring low biological reactivity lipopolysaccharides as vaccine adjuvants. Expert Review of Vaccines. 2013;12:707-9.
[37] Davenport FM, Hennessy AV, Askin FB. LACK OF ADJUVANT EFFECT OF ALPO4 ON PURIFIED INFLUENZA VIRUS HEMAGGLUTININS IN MAN. Journal of Immunology. 1968;100:1139-&.
[38] Dickason RR, Edwards RA, Bryan J, Huston DP. VERSATILE ESCHERICHIA-COLI THIOREDOXIN SPECIFIC MONOCLONAL-ANTIBODIES AFFORD CONVENIENT ANALYSIS AND PURIFICATION OF PROKARYOTE EXPRESSED SOLUBLE FUSION PROTEIN. Journal of Immunological Methods. 1995;185:237-44.
[39] Dickerson MB, Sandhage KH, Naik RR. Protein- and Peptide-Directed Syntheses of Inorganic Materials. Chemical Reviews. 2008;108:4935-78.
[40] Diebold SS, Kursa P, Wagner E, Cotten M, Zenke M. Mannose polyethylenimine conjugates for targeted DNA delivery into dendritic cells. Journal of Biological Chemistry. 1999;274.
[41] Dokka S, Toledo D, Shi XL, Ye JP, Rojanasakul Y. High-efficiency gene transfection of macrophages by lipoplexes. International Journal of Pharmaceutics. 2000;206.
[42] Donnelly JJ, Ulmer JB, Shiver JW, Liu MA. DNA vaccines. Annual Review of Immunology. 1997;15:617-48.
[43] Duan B, Wang M, Zhou WY, Cheung WL. Synthesis of Ca-P nanoparticles and fabrication of Ca-P/PHBV nanocomposite microspheres for bone tissue engineering applications. Applied Surface Science. 2008;255.
[44] Ducy P, Desbois C, Boyce B, Pinero G, Story B, Dunstan C, et al. Increased bone formation in osteocalcin-deficient mice. Nature. 1996;382.
[45] Dupuis M, McDonald DM, Ott G. Distribution of adjuvant MF59 and antigen gD2 after intramuscular injection in mice. Vaccine. 1999;18:434-9.
[46] Durnelie N, Benhayoune H, Richard D, Laurent-Maquin D, Balossier G. In vitro precipitation of electrodeposited calcium-deficient hydroxyapatite coatings on Ti6Al4V substrate. Materials Characterization. 2008;59:129-33.
[47] Escher G, Hoang A, Georges S, Tchoua U, El-Osta A, Krozowski Z, et al. Demethylation using the epigenetic modifier, 5-azacytidine, increases the efficiency of transient transfection of macrophages. Journal of Lipid Research. 2005;46.
[48] Espuelas S, Thumann C, Heurtault B, Schuber F, Frisch B. Influence of Ligand Valency on the Targeting of Immature Human Dendritic Cells by Mannosylated Liposomes. Bioconjugate Chemistry. 2008;19.
[49] Ferraz MP, Monteiro FJ, Manuel CM. Hydroxyapatite nanoparticles: A review of preparation methodologies. J Appl Biomater Biomech. 2004;2:74-80.
[50] Fifis T, Gamvrellis A, Crimeen-Irwin B, Pietersz GA, Li J, Mottram PL, et al. Size-dependent immunogenicity: Therapeutic and protective properties of nano-vaccines against tumors. Journal of Immunology. 2004;173.

[51] Foged C, Brodin B, Frokjaer S, Sundblad A. Particle size and surface charge affect particle uptake by human dendritic cells in an in vitro model. International Journal of Pharmaceutics. 2005;298:315-22.
[52] Ganesan K, Kovtun A, Neumann S, Heumann R, Epple M. Calcium phosphate nanoparticles: colloidally stabilized and made fluorescent by a phosphate-functionalized porphyrin. Journal of Materials Chemistry. 2008;18.
[53] Geerligs HJ, Weijer WJ, Welling GW, Wellingwester S. THE INFLUENCE OF DIFFERENT ADJUVANTS ON THE IMMUNE-RESPONSE TO A SYNTHETIC PEPTIDE COMPRISING AMINO-ACID RESIDUES 9-21 OF HERPES-SIMPLEX VIRUS TYPE-1 GLYCOPROTEIN-D. Journal of Immunological Methods. 1989;124:95-102.
[54] George A, Veis A. Phosphorylated Proteins and Control over Apatite Nucleation, Crystal Growth, and Inhibition. Chemical Reviews. 2008;108.
[55] Giannini SL, Hanon E, Moris P, Van Mechelen M, Morel S, Dessy F, et al. Enhanced humoral and memory B cellular immunity using HPV16/18 L1 VLP vaccine formulated with the MPL/aluminium salt combination (AS04) compared to aluminium salt only. Vaccine. 2006;24:5937-49.
[56] Giger EV, Puigmarti-Luis J, Schlatter R, Castagner B, Dittrich PS, Leroux J-C. Gene delivery with bisphosphonate-stabilized calcium phosphate nanoparticles. Journal of Controlled Release. 2011;150.
[57] Glenny A, Pope C, Waddington H, Wallace U. The antigenic value of toxoid precipitated by potassium alum. Journal of Pathology and Bacteriology; 1926.
[58] Godbey WT, Wu KK, Mikos AG. Poly(ethylenimine) and its role in gene delivery. Journal of Controlled Release. 1999;60:149-60.
[59] Goldsmith MA, Weiss A. EARLY SIGNAL TRANSDUCTION BY THE ANTIGEN RECEPTOR WITHOUT COMMITMENT TO T-CELL ACTIVATION. Science. 1988;240:1029-31.
[60] Goto N, Kato H, Maeyama J, Eto K, Yoshihara S. STUDIES ON THE TOXICITIES OF ALUMINUM HYDROXIDE AND CALCIUM-PHOSPHATE AS IMMUNOLOGICAL ADJUVANTS FOR VACCINES. Vaccine. 1993;11.
[61] Goto N, Kato H, Maeyama J, Shibano M, Saito T, Yamaguchi J, et al. Local tissue irritating effects and adjuvant activities of calcium phosphate and aluminium hydroxide with different physical properties. Vaccine. 1997;15:1364-71.
[62] Graham FL, van der Eb AJ. A new technique for the assay of infectivity of human adenovirus 5 DNA. Virology. 1973;52:456-67.
[63] Grosh CD, Schwartz DT, Baneyx F. Protein-Based Control of Silver Growth Habit Using Electrochemical Deposition. Crystal Growth & Design. 2009;9.
[64] Gungormus M, Fong H, Kim IW, Evans JS, Tamerler C, Sarikaya M. Regulation of in vitro calcium phosphate mineralization by combinatorially selected hydroxyapatite-binding peptides. Biomacromolecules. 2008;9:966-73.
[65] Gupta RK. Aluminum compounds as vaccine adjuvants. Advanced Drug Delivery Reviews. 1998;32.
[66] Gupta RK, Chang AC, Griffin P, Rivera R, Siber GR. In vivo distribution of radioactivity in mice after injection of biodegradable polymer microspheres containing C-14-labeled tetanus toxoid. Vaccine. 1996;14:1412-6.

[67] Gupta RK, Relyveld EH, Lindblad EB, Bizzini B, Benefraim S, Gupta CK. ADJUVANTS - A BALANCE BETWEEN TOXICITY AND ADJUVANTICITY. Vaccine. 1993;11:293-306.
[68] Gupta RK, Rost BE, Relyveld E, Siber GR. Adjuvant properties of aluminum and calcium compounds. Pharm Biotechnol. 1995;6:229-48.
[69] Gupta RK, Siber GR. COMPARISON OF ADJUVANT ACTIVITIES OF ALUMINUM PHOSPHATE, CALCIUM-PHOSPHATE AND STEARYL TYROSINE FOR TETANUS TOROID. Biologicals. 1994;22:53-63.
[70] Gupta RK, Siber GR. ADJUVANTS FOR HUMAN VACCINES - CURRENT STATUS, PROBLEMS AND FUTURE-PROSPECTS. Vaccine. 1995;13:1263-76.
[71] Gurunathan S, Klinman DM, Seder RA. DNA vaccines: Immunology, application, and optimization. Annual Review of Immunology. 2000;18:927-74.
[72] Hamaoka T, Katz DH, Bloch KJ, Benacerr.B. HAPTEN-SPECIFIC IGE ANTIBODY-RESPONSES IN MICE .1. SECONDARY IGE RESPONSES IN IRRADIATED RECIPIENTS OF SYNGENEIC PRIMED SPLEEN-CELLS. Journal of Experimental Medicine. 1973;138:306-11.
[73] Hansen B, Sokolovska A, HogenEsch H, Hem SL. Relationship between the strength of antigen adsorption to an aluminum-containing adjuvant and the immune response. Vaccine. 2007;25:6618-24.
[74] Harvey DJ, Wing DR, Kuster B, Wilson IBH. Composition of N-linked carbohydrates from ovalbumin and Co-purified glycoproteins. Journal of the American Society for Mass Spectrometry. 2000;11:564-71.
[75] Hawley AE, Davis SS, Illum L. TARGETING OF COLLOIDS TO LYMPH-NODES - INFLUENCE OF LYMPHATIC PHYSIOLOGY AND COLLOIDAL CHARACTERISTICS. Advanced Drug Delivery Reviews. 1995;17.
[76] He Q, Mitchell AR, Johnson SL, Wagner-Bartak C, Morcol T, Bell SJD. Calcium phosphate nanoparticle adjuvant. Clinical and Diagnostic Laboratory Immunology. 2000;7:899-903.
[77] He Q, Mitchell A, Morcol T, Bell SJD. Calcium phosphate nanoparticles induce mucosal immunity and protection against herpes simplex virus type 2. Clinical and Diagnostic Laboratory Immunology. 2002;9:1021-4.
[78] Heer AK, Shamshiev A, Donda A, Uematsu S, Akira S, Kopf M, et al. TLR signaling fine-tunes anti-influenza B cell responses without regulating effector T cell responses. Journal of Immunology. 2007;178:2182-91.
[79] Heimlich JM, Regnier FE, White JL, Hem SL. The in vitro displacement of adsorbed model antigens from aluminium-containing adjuvants by interstitial proteins. Vaccine. 1999;17:2873-81.
[80] Higgs R, Higgins SC, Ross PJ, Mills KHG. Immunity to the respiratory pathogen Bordetella pertussis. Mucosal Immunology. 2012;5:485-500.
[81] Hnilova M, Oren EE, Seker UOS, Wilson BR, Collino S, Evans JS, et al. Effect of Molecular Conformations on the Adsorption Behavior of Gold-Binding Peptides. Langmuir. 2008;24:12440-5.
[82] Hoang QQ, Sicheri F, Howard AJ, Yang DSC. Bone recognition mechanism of porcine osteocalcin from crystal structure. Nature. 2003;425.
[83] HogenEsch H. Mechanisms of stimulation of the immune response by aluminum adjuvants. Vaccine. 2002;20.
[84] Holmgren A. THIOREDOXIN. Annual Review of Biochemistry. 1985;54:237-71.

[85] Holmgren A, Sjoberg BM. IMMUNOCHEMISTRY OF THIOREDOXIN .1. PREPARATION AND CROSS-REACTIVITY OF ANTIBODIES AGAINST THIOREDOXIN FROM ESCHERICHIA-COLI AND BACTERIOPHAGE T-4. Journal of Biological Chemistry. 1972;247:4160-&.
[86] Hunter GK, O'Young J, Grohe B, Karttunen M, Goldberg HA. The Flexible Polyelectrolyte Hypothesis of Protein-Biomineral Interaction. Langmuir. 2010;26:18639-46.
[87] Huntington JA, Stein PE. Structure and properties of ovalbumin. Journal of Chromatography B. 2001;756:189-98.
[88] Imboden JB, Stobo JD. TRANSMEMBRANE SIGNALING BY THE T-CELL ANTIGEN RECEPTOR - PERTURBATION OF THE T3-ANTIGEN RECEPTOR COMPLEX GENERATES INOSITOL PHOSPHATES AND RELEASES CALCIUM-IONS FROM INTRACELLULAR STORES. Journal of Experimental Medicine. 1985;161:446-56.
[89] Ishii N, Fukushima J, Kaneko T, Okada E, Tani K, Tanaka SI, et al. Cationic liposomes are a strong adjuvant for a DNA vaccine of human immunodeficiency virus type 1. Aids Research and Human Retroviruses. 1997;13:1421-8.
[90] Jiang DP, Premachandra GS, Johnston C, Hem SL. Structure and adsorption properties of commercial calcium phosphate adjuvant. Vaccine. 2004;23.
[91] Johnson AG, Gaines S, Landy M. STUDIES ON THE O ANTIGEN OF SALMONELLA TYPHOSA .5. ENHANCEMENT OF ANTIBODY RESPONSE TO PROTEIN ANTIGENS BY THE PURIFIED LIPOPOLYSACCHARIDE. Journal of Experimental Medicine. 1956;103:225-46.
[92] Jordan M, Schallhorn A, Wurm FM. Transfecting mammalian cells: Optimization of critical parameters affecting calcium-phosphate precipitate formation. Nucleic Acids Research. 1996;24.
[93] Joyappa DH, Kumar CA, Banumathi N, Reddy GR, Suryanarayana VVS. Calcium phosphate nanoparticle prepared with foot and mouth disease virus P1-3CD gene construct protects mice and guinea pigs against the challenge virus. Veterinary Microbiology. 2009;139.
[94] Kakizawa Y, Miyata K, Furukawa S, Kataoka K. Size-controlled formation of a calcium phosphate-based organic-inorganic hybrid vector for gene delivery using poly(ethylene glycol)-block-poly(aspartic acid). Advanced Materials. 2004;16.
[95] Kalita SJ, Bhardwaj A, Bhatt HA. Nanocrystalline calcium phosphate ceramics in biomedical engineering. Materials Science & Engineering C-Biomimetic and Supramolecular Systems. 2007;27.
[96] Kenney JS, Hughes BW, Masada MP, Allison AC. INFLUENCE OF ADJUVANTS ON THE QUANTITY, AFFINITY, ISOTYPE AND EPITOPE SPECIFICITY OF MURINE ANTIBODIES. Journal of Immunological Methods. 1989;121:157-66.
[97] Kim KY, Schumacher HR, Hunsche E, Wertheimer AI, Kong SX. A literature review of the epidemiology and treatment of acute gout. Clinical Therapeutics. 2003;25:1593-617.
[98] Kleinschneegans AS, Kuntz L, Fonteneau P, Loor F. AN INDIRECT ASYMMETRICAL SANDWICH ELISA USING ANTI-ALLOTYPE ANTIBODIES FOR THE SPECIFIC AND QUANTITATIVE MEASUREMENT OF MOUSE IGG2A OF IGH-1B ALLOTYPE. Journal of Immunological Methods. 1989;125:207-13.
[99] Knuschke T, Sokolova V, Rotan O, Wadwa M, Tenbusch M, Hansen W, et al. Immunization with Biodegradable Nanoparticles Efficiently Induces Cellular Immunity and Protects against Influenza Virus Infection. Journal of Immunology. 2013;190:6221-9.

[100] Koff WC, Russell ND, Walport M, Feinberg MB, Shiver JW, Karim SA, et al. Accelerating the development of a safe and effective HIV vaccine: HIV vaccine case study for the Decade of Vaccines. Vaccine. 2013;31:B204-B8.
[101] Kool M, Soullie T, van Nimwegen M, Willart MAM, Muskens F, Jung S, et al. Alum adjuvant boosts adaptive immunity by inducing uric acid and activating inflammatory dendritic cells. Journal of Experimental Medicine. 2008;205:869-82.
[102] Kozin F, Ginsberg MH, Skosey JL. POLYMORPHONUCLEAR LEUKOCYTE RESPONSES TO MONOSODIUM URATE CRYSTALS - MODIFICATION BY ADSORBED SERUM-PROTEINS. Journal of Rheumatology. 1979;6:519-26.
[103] Krieg AM. CpG motifs in bacterial DNA and their immune effects. Annual Review of Immunology. 2002;20:709-60.
[104] Kutzler MA, Weiner DB. DNA vaccines: ready for prime time? Nature Reviews Genetics. 2008;9:776-88.
[105] Lavallie ER, Diblasio EA, Kovacic S, Grant KL, Schendel PF, McCoy JM. A THIOREDOXIN GENE FUSION EXPRESSION SYSTEM THAT CIRCUMVENTS INCLUSION BODY FORMATION IN THE ESCHERICHIA-COLI CYTOPLASM. Bio-Technology. 1993;11:187-93.
[106] Lee D, Upadhye K, Kumta PN. Nano-sized calcium phosphate (CaP) carriers for non-viral gene delivery. Materials Science and Engineering B-Advanced Functional Solid-State Materials. 2012;177.
[107] Lew AM, Anders RF, Edwards SJ, Langford CJ. COMPARISON OF ANTIBODY AVIDITY AND TITER ELICITED BY PEPTIDE AS A PROTEIN CONJUGATE OR AS EXPRESSED IN VACCINIA. Immunology. 1988;65:311-4.
[108] Li J, Chen Y-C, Tseng Y-C, Mozumdar S, Huang L. Biodegradable calcium phosphate nanoparticle with lipid coating for systemic siRNA delivery. Journal of Controlled Release. 2010;142:416-21.
[109] Li-Chan E, Nakai S. BIOCHEMICAL BASIS FOR THE PROPERTIES OF EGG WHITE. Critical Reviews in Poultry Biology. 1989;2:21-58.
[110] Liljeqvist S, Stahl S. Production of recombinant subunit vaccines: protein immunogens, live delivery systems and nucleic acid vaccines. Journal of Biotechnology. 1999;73:1-33.
[111] Limbrey S, Brickley M, Marques C, Swinson D. Identification of urate crystals in gouty individuals. Journal of Archaeological Science. 2011;38:2497-501.
[112] Lindblad EB. Aluminium adjuvants - in retrospect and prospect. Vaccine. 2004;22.
[113] Lindblad EB, Elhay MJ, Silva R, Appelberg R, Andersen P. Adjuvant modulation of immune responses to tuberculosis subunit vaccines. Infection and Immunity. 1997;65:623-9.
[114] Liu J, Farmer JD, Lane WS, Friedman J, Weissman I, Schreiber SL. CALCINEURIN IS A COMMON TARGET OF CYCLOPHILIN-CYCLOSPORINE-A AND FKBP-FK506 COMPLEXES. Cell. 1991;66:807-15.
[115] Liu MA. DNA vaccines: an historical perspective and view to the future. Immunological Reviews. 2011;239:62-84.
[116] Liu T, Tang A, Zhang GY, Chen YX, Zhang JY, Peng SS, et al. Calcium phosphate nanoparticles as a novel nonviral vector for efficient trasfection of DNA in cancer gene therapy. Cancer Biotherapy and Radiopharmaceuticals. 2005;20:141-9.
[117] Liu Y, Wang T, He F, Liu Q, Zhang D, Xiang S, et al. An efficient calcium phosphate nanoparticle-based nonviral vector for gene delivery. International Journal of Nanomedicine. 2011;6.

[118] Loyter A, Scangos GA, Ruddle FH. MECHANISMS OF DNA UPTAKE BY MAMMALIAN-CELLS - FATE OF EXOGENOUSLY ADDED DNA MONITORED BY THE USE OF FLUORESCENT DYES. Proceedings of the National Academy of Sciences of the United States of America-Biological Sciences. 1982;79.
[119] Lu ZJ, Murray KS, Vancleave V, Lavallie ER, Stahl ML, McCoy JM. EXPRESSION OF THIOREDOXIN RANDOM PEPTIDE LIBRARIES ON THE ESCHERICHIA-COLI CELL-SURFACE AS FUNCTIONAL FUSIONS TO FLAGELLIN - A SYSTEM DESIGNED FOR EXPLORING PROTEIN-PROTEIN INTERACTIONS. Bio-Technology. 1995;13:366-72.
[120] Luo D, Saltzman WM. Synthetic DNA delivery systems. Nature Biotechnology. 2000;18:33-7.
[121] Malyala P, O'Hagan DT, Singh M. Enhancing the therapeutic efficacy of CpG oligonucleotides using biodegradable microparticles. Advanced Drug Delivery Reviews. 2009;61:218-25.
[122] Mandel NS, Mandel GS. MONOSODIUM URATE MONOHYDRATE, GOUT CULPRIT. Journal of the American Chemical Society. 1976;98:2319-23.
[123] Mannhalter JW, Neychev HO, Zlabinger GJ, Ahmad R, Eibl MM. MODULATION OF THE HUMAN IMMUNE-RESPONSE BY THE NON-TOXIC AND NON-PYROGENIC ADJUVANT ALUMINUM HYDROXIDE - EFFECT ON ANTIGEN UPTAKE AND ANTIGEN PRESENTATION. Clinical and Experimental Immunology. 1985;61:143-51.
[124] Manolova V, Flace A, Bauer M, Schwarz K, Saudan P, Bachmann MF. Nanoparticles target distinct dendritic cell populations according to their size. European Journal of Immunology. 2008;38:1404-13.
[125] Marciani DJ. Vaccine adjuvants: role and mechanisms of action in vaccine immunogenicity. Drug Discovery Today. 2003;8:934-43.
[126] Martin RM, Brady JL, Lew AM. The need for IgG2c specific antiserum when isotyping antibodies from C57BL/6 and NOD mice. Journal of Immunological Methods. 1998;212:187-92.
[127] Martinon F, Petrilli V, Mayor A, Tardivel A, Tschopp J. Gout-associated uric acid crystals activate the NALP3 inflammasome. Nature. 2006;440:237-41.
[128] Martins MA, Santos C, Almeida MM, Costa MEV. Hydroxyapatite micro- and nanoparticles: Nucleation and growth mechanisms in the presence of citrate species. Journal of Colloid and Interface Science. 2008;318:210-6.
[129] Matsushima N, Hikichi K. AGE-CHANGES IN THE CRYSTALLINITY OF BONE-MINERAL AND IN THE DISORDER OF ITS CRYSTAL. Biochimica Et Biophysica Acta. 1989;992:155-9.
[130] McCluskie MJ, Millan CLB, Gramzinski RA, Robinson HL, Santoro JC, Fuller JT, et al. Route and method of delivery of DNA vaccine influence immune responses in mice and non-human primates. Molecular Medicine. 1999;5:287-300.
[131] McLennan DN, Porter CJH, Charman SA. Subcutaneous drug delivery and the role of the lymphatics. Drug Discovery Today: Technologies. 2005;2:89-96.
[132] Mills CD, Kincaid K, Alt JM, Heilman MJ, Hill AM. M-1/M-2 macrophages and the Th1/Th2 paradigm. Journal of Immunology. 2000;164:6166-73.
[133] Mine Y, Yang M. Epitope characterization of ovalbumin in BALB/c mice using different entry routes. Biochimica Et Biophysica Acta-Proteins and Proteomics. 2007;1774:200-12.
[134] Minigo G, Scholzen A, Tang CK, Hanley JC, Kalkanidis M, Pietersz GA, et al. Poly-L-lysine-coated nanoparticles: A potent delivery system to enhance DNA vaccine efficacy. Vaccine. 2007;25:1316-27.

[135] Mitraki A, King J. PROTEIN FOLDING INTERMEDIATES AND INCLUSION BODY FORMATION. Bio-Technology. 1989;7:690-7.
[136] Monsigny M, Petit C, Roche AC. COLORIMETRIC DETERMINATION OF NEUTRAL SUGARS BY A RESORCINOL SULFURIC-ACID MICROMETHOD. Analytical Biochemistry. 1988;175.
[137] Morgado MG, Cam P, Grisliebe C, Cazenave PA, Jouvinmarche E. FURTHER EVIDENCE THAT BALB/C AND C57BL/6-GAMMA-2A GENES ORIGINATE FROM 2 DISTINCT ISOTYPES. Embo Journal. 1989;8:3245-51.
[138] Morgan TT, Muddana HS, Altinoglu EI, Rouse SM, Tabakovic A, Tabouillot T, et al. Encapsulation of Organic Molecules in Calcium Phosphate Nanocomposite Particles for Intracellular Imaging and Drug Delivery. Nano Letters. 2008;8.
[139] Morokata T, Ishikawa J, Yamada T. Antigen dose defines T helper 1 and T helper 2 responses in the lungs of C57BL/6 and BALB/c mice independently of splenic responses. Immunology Letters. 2000;72:119-26.
[140] Najjar VA, Nishioka K. TUFTSIN - A NATURAL PHAGOCYTOSIS STIMULATING PEPTIDE. Nature. 1970;228:672-&.
[141] Nembrini C, Stano A, Dane KY, Ballester M, van der Vlies AJ, Marsland BJ, et al. Nanoparticle conjugation of antigen enhances cytotoxic T-cell responses in pulmonary vaccination. Proceedings of the National Academy of Sciences of the United States of America. 2011;108.
[142] Niedel JE, Kuhn LJ, Vandenbark GR. PHORBOL DIESTER RECEPTOR CO-PURIFIES WITH PROTEIN KINASE-C. Proceedings of the National Academy of Sciences of the United States of America-Biological Sciences. 1983;80:36-40.
[143] Okajima T, Tanabe T, Yasuda T. NONUREA SODIUM DODECYL-SULFATE POLYACRYLAMIDE-GEL ELECTROPHORESIS WITH HIGH-MOLARITY BUFFERS FOR THE SEPARATION OF PROTEINS AND PEPTIDES. Analytical Biochemistry. 1993;211:293-300.
[144] Olton D, Li J, Wilson ME, Rogers T, Close J, Huang L, et al. Nanostructured calcium phosphates (NanoCaPs) for non-viral gene delivery: Influence of the synthesis parameters on transfection efficiency. Biomaterials. 2007;28.
[145] Ortizbravo E, Schumacher HR. COMPONENTS GENERATED LOCALLY AS WELL AS SERUM ALTER THE PHLOGISTIC EFFECT OF MONOSODIUM URATE CRYSTALS IN-VIVO. Journal of Rheumatology. 1993;20:1162-6.
[146] Oussoren C, Zuidema J, Crommelin DJA, Storm G. Lymphatic uptake and biodistribution of liposomes after subcutaneous injection .2. Influence of liposomal size, lipid composition and lipid dose. Biochimica Et Biophysica Acta-Biomembranes. 1997;1328.
[147] Palmer LC, Newcomb CJ, Kaltz SR, Spoerke ED, Stupp SI. Biomimetic Systems for Hydroxyapatite Mineralization Inspired By Bone and Enamel. Chemical Reviews. 2008;108.
[148] Pedraza CE, Bassett DC, McKee MD, Nelea V, Gbureck U, Barralet JE. The importance of particle size and DNA condensation salt for calcium phosphate nanoparticle transfection. Biomaterials. 2008;29.
[149] Petrushina I, Tran M, Sadzikava N, Ghochikyan A, Vasilevko V, Agadjanyan MG, et al. Importance of IgG2c isotype in the immune response to beta-amyloid in amyloid precursor protein/transgenic mice. Neuroscience Letters. 2003;338:5-8.

[150] Probst J, Weide B, Scheel B, Pichler BJ, Hoerr I, Rammensee HG, et al. Spontaneous cellular uptake of exogenous messenger RNA in vivo is nucleic acid-specific, saturable and ion dependent. Gene Therapy. 2007;14:1175-80.
[151] Rabadjieva D, Gergulova R, Titorenkova R, Tepavitcharova S, Dyulgerova E, Balarew C, et al. Biomimetic transformations of amorphous calcium phosphate: kinetic and thermodynamic studies. Journal of Materials Science-Materials in Medicine. 2010;21:2501-9.
[152] Reddy N, Ong GL, Behr TM, Sharkey RM, Goldenberg DM, Mattes MJ. Rapid blood clearance of mouse IgG2a and human IgG1 in many nude and nu/+ mouse strains is due to low IgG2a serum concentrations. Cancer Immunology Immunotherapy. 1998;46:25-33.
[153] Reddy ST, Rehor A, Schmoekel HG, Hubbell JA, Swartz MA. In vivo targeting of dendritic cells in lymph nodes with poly(propylene sulfide) nanoparticles. Journal of Controlled Release. 2006;112:26-34.
[154] Reddy ST, Swartz MA, Hubbell JA. Targeting dendritic cells with biomaterials: developing the next generation of vaccines. Trends in Immunology. 2006;27:573-9.
[155] Reddy ST, van der Vlies AJ, Simeoni E, Angeli V, Randolph GJ, O'Neill CP, et al. Exploiting lymphatic transport and complement activation in nanoparticle vaccines. Nature Biotechnology. 2007;25.
[156] Reed SG, Bertholet S, Coler RN, Friede M. New horizons in adjuvants for vaccine development. Trends in Immunology. 2009;30:23-32.
[157] Relyveld EH. Preparation and use of calcium phosphate adsorbed vaccines. Dev Biol Stand. 1986;65:131-6.
[158] Relyveld E, Chermann JC. HUMORAL RESPONSE IN RABBITS IMMUNIZED WITH CALCIUM-PHOSPHATE ADJUVANTED HIV-1 GP160 ANTIGEN. Biomedicine & Pharmacotherapy. 1994;48:79-83.
[159] Rimaniol A-C, Gras G, Clayette P. In vitro interactions between macrophages and aluminum-containing adjuvants. Vaccine. 2007;25:6784-92.
[160] Rodriguez-Lorenzo LM, Vallet-Regi M. Controlled crystallization of calcium phosphate apatites. Chemistry of Materials. 2000;12.
[161] Roy I, Mitra S, Maitra A, Mozumdar S. Calcium phosphate nanoparticles as novel non-viral vectors for targeted gene delivery. International Journal of Pharmaceutics. 2003;250:25-33.
[162] Ruponen M, Honkakoski P, Ronkko S, Pelkonen J, Tammi M, Urtti A. Extracellular and intracellular barriers in non-viral gene delivery. Journal of Controlled Release. 2003;93:213-7.
[163] Ryckman C, Gilbert C, de Medicis R, Lussier A, Vandal K, Tessier PA. Monosodium urate monohydrate crystals induce the release of the proinflammatory protein S100A8/A9 from neutrophils. Journal of Leukocyte Biology. 2004;76:433-40.
[164] Sakata KM, Tashiro K, Hirashima M, Hayashi H. SELECTIVE REGULATION OF CHEMOTACTIC LYMPHOKINE PRODUCTION .1. SELECTIVE POTENTIATION OF EOSINOPHIL CHEMOTACTIC LYMPHOKINE PRODUCTION IN ALUM HYDROXY GEL- AND BORDETELLA-PERTUSSIS VACCINE-TREATED GUINEA-PIGS. Journal of Immunology. 1985;135:3463-7.
[165] Sarikaya M, Tamerler C, Jen AKY, Schulten K, Baneyx F. Molecular biomimetics: nanotechnology through biology. Nature Materials. 2003;2.
[166] Sarikaya M, Tamerler C, Schwartz DT, Baneyx FO. Materials assembly and formation using engineered polypeptides. Annual Review of Materials Research. 2004;34.
[167] Schein CH. PRODUCTION OF SOLUBLE RECOMBINANT PROTEINS IN BACTERIA. Bio-Technology. 1989;7:1141-7.

[168] Schiltz C, Liote F, Prudhommeaux F, Meunier A, Champy R, Callebert J, et al. Monosodium urate monohydrate crystal-induced inflammation in vivo - Quantitative histomorphometric analysis of cellular events. Arthritis and Rheumatism. 2002;46:1643-50.
[169] Schroder K, Hertzog PJ, Ravasi T, Hume DA. Interferon-gamma: an overview of signals, mechanisms and functions. Journal of Leukocyte Biology. 2004;75:163-89.
[170] Schulte S, Sukhova GK, Libby P. Genetically programmed biases in Th1 and Th2 immune responses modulate atherogenesis. American Journal of Pathology. 2008;172:1500-8.
[171] Schwartz L, Brown GV, Genton B, Moorthy VS. A review of malaria vaccine clinical projects based on the WHO rainbow table. Malaria Journal. 2012;11.
[172] Segvich SJ, Smith HC, Kohn DH. The adsorption of preferential binding peptides to apatite-based materials. Biomaterials. 2009;30:1287-98.
[173] Seker UOS, Wilson B, Dincer S, Kim IW, Oren EE, Evans JS, et al. Adsorption behavior of linear and cyclic genetically engineered platinum binding peptides. Langmuir. 2007;23:7895-900.
[174] Siemion IZ, Kluczyk A. Tuftsin: On the 30-year anniversary of Victor Najjar's discovery. Peptides. 1999;20:645-74.
[175] Singh M, Ugozzoli M, Kazzaz J, Chesko J, Seonawan E, Mannucci D, et al. A preliminary evaluation of alternative adjuvants to alum using a range of established and new generation vaccine antigens. Vaccine. 2006;24:1680-6.
[176] Sokolova VV, Radtke I, Heumann R, Epple M. Effective transfection of cells with multi-shell calcium phosphate-DNA nanoparticles. Biomaterials. 2006;27.
[177] Sokolova V, Knuschke T, Kovtun A, Buer J, Epple M, Westendorf AM. The use of calcium phosphate nanoparticles encapsulating Toll-like receptor ligands and the antigen hemagglutinin to induce dendritic cell maturation and T cell activation. Biomaterials. 2010;31:5627-33.
[178] Stahl PD, Ezekowitz RAB. The mannose receptor is a pattern recognition receptor involved in host defense. Current Opinion in Immunology. 1998;10.
[179] Stevens L. EGG-WHITE PROTEINS. Comparative Biochemistry and Physiology B-Biochemistry & Molecular Biology. 1991;100:1-9.
[180] Takeda K, Kaisho T, Akira S. Toll-like receptors. Annual Review of Immunology. 2003;21:335-76.
[181] Tang W-X, Chen X-P, Zhao Y-Y, Wang J-H, Wang W, Chen Z-W. Preparation and identification of monoclonal antibodies against recombinant human thioredoxins. Hybridoma. 2007;26:338-41.
[182] Thai CK, Dai HX, Sastry MSR, Sarikaya M, Schwartz DT, Baneyx F. Identification and characterization of Cu2O- and ZnO-binding polypeptides by Escherichia coli cell surface display: Toward an understanding of metal oxide binding. Biotechnology and Bioengineering. 2004;87:129-37.
[183] Thompson CD, Frazier-Jessen MR, Rawat R, Nordan RP, Brown RT. Evaluation of methods for transient transfection of a murine macrophage cell line, RAW 264.7. Biotechniques. 1999;27.
[184] Titball RW. Vaccines against intracellular bacterial pathogens. Drug Discovery Today. 2008;13:596-600.
[185] Topham DJ, Castrucci MR, Wingo FS, Belz GT, Doherty PC. The role of antigen in the localization of naive, acutely activated, and memory CD8(+) T cells to the lung during influenza pneumonia. Journal of Immunology. 2001;167.

[186] Ulanova M, Tarkowski A, Hahn-Zoric M, Hanson LA. The common vaccine adjuvant aluminum hydroxide up-regulates accessory properties of human monocytes via an interleukin-4-dependent mechanism. Infection and Immunity. 2001;69:1151-9.
[187] Ulmer JB, Mason PW, Geall A, Mandl CW. RNA-based vaccines. Vaccine. 2012;30:4414-8.
[188] Un K, Kawakami S, Suzuki R, Maruyama K, Yamashita F, Hashida M. Development of an ultrasound-responsive and mannose-modified gene carrier for DNA vaccine therapy. Biomaterials. 2010;31.
[189] Uskokovic V, Uskokovic DP. Nanosized hydroxyapatite and other calcium phosphates: Chemistry of formation and application as drug and gene delivery agents. Journal of Biomedical Materials Research Part B-Applied Biomaterials. 2011;96B:152-91.
[190] Walls RS. EOSINOPHIL RESPONSE TO ALUM ADJUVANTS - INVOLVEMENT OF T-CELLS IN NON-ANTIGEN-DEPENDENT MECHANISMS. Proceedings of the Society for Experimental Biology and Medicine. 1977;156:431-5.
[191] Wang H-B, Weller PF. Pivotal Advance: Eosinophils mediate early alum adjuvant-elicited B cell priming and IgM production. Journal of Leukocyte Biology. 2008;83:817-21.
[192] Wardowska A, Dzierzbicka K, Trzonkowski P, Mysliwski A. Immunomodulatory properties of new conjugates of muramyl dipeptide and nor-muramyl dipeptide with retro-tuftsin (Arg-Pro-Lys-Thr-OMe). International Immunopharmacology. 2006;6:1560-8.
[193] Weeratna RD, McCluskie MJ, Xu Y, Davis HL. CpG DNA induces stronger immune responses with less toxicity than other adjuvants. Vaccine. 2000;18:1755-62.
[194] Weichsel A, Gasdaska JR, Powis G, Montfort WR. Crystal structures of reduced, oxidized, and mutated human thioredoxins: Evidence for a regulatory homodimer. Structure. 1996;4.
[195] Weiger MC, Park JJ, Roy MD, Stafford CM, Karim A, Becker ML. Quantification of the binding affinity of a specific hydroxyapatite binding peptide. Biomaterials. 2010;31:2955-63.
[196] Weissburg RP, Berman PW, Cleland JL, Eastman D, Farina F, Frie S, et al. CHARACTERIZATION OF THE MN GP120 HIV-1 VACCINE - ANTIGEN-BINDING TO ALUM. Pharmaceutical Research. 1995;12:1439-46.
[197] Weissman.G, Rita GA. MOLECULAR BASIS OF GOUTY INFLAMMATION - INTERACTION OF MONOSODIUM URATE CRYSTALS WITH LYSOSOMES AND LIPOSOMES. Nature-New Biology. 1972;240:167-&.
[198] Welzel T, Meyer-Zaika W, Epple M. Continuous preparation of functionalised calcium phosphate nanoparticles with adjustable crystallinity. Chemical Communications. 2004:1204-5.
[199] Wilson JT, Keller S, Manganiello MJ, Cheng C, Lee C-C, Opara C, et al. pH-Responsive Nanoparticle Vaccines for Dual-Delivery of Antigens and Immunostimulatory Oligonucleotides. Acs Nano. 2013;7:3912-25.
[200] Wopenka B, Pasteris JD. A mineralogical perspective on the apatite in bone. Materials Science & Engineering C-Biomimetic and Supramolecular Systems. 2005;25:131-43.
[201] Yang M, Mine Y. Novel T-cell epitopes of ovalbumin in BALB/c mouse: Potential for peptide-immunotherapy. Biochemical and Biophysical Research Communications. 2009;378:203-8.
[202] Yasukawa T, Kaneiishii C, Maekawa T, Fujimoto J, Yamamoto T, Ishii S. INCREASE OF SOLUBILITY OF FOREIGN PROTEINS IN ESCHERICHIA-COLI BY COPRODUCTION OF THE BACTERIAL THIOREDOXIN. Journal of Biological Chemistry. 1995;270.

[203] Zhang C, Yang J, Quan Z, Yang P, Li C, Hou Z, et al. Hydroxyapatite Nano- and Microcrystals with Multiform Morphologies: Controllable Synthesis and Luminescence Properties. Crystal Growth & Design. 2009;9:2725-33.
[204] Zhang S, Cubas R, Li M, Chen C, Yao Q. Virus-like particle vaccine activates conventional B2 cells and promotes B cell differentiation to IgG2a producing plasma cells. Molecular Immunology. 2009;46:1988-2001.
[205] Zhang W, Tang YC, Zhang J, Liu JN. Characterization of an anti-thioredoxin monoclonal antibody. Biotechnology Letters. 2006;28:183-8.
[206] Zhang Z, Goldschmidt T, Salter H. Possible allelic structure of IgG2a and IgG2c in mice. Molecular Immunology. 2012;50:169-71.
[207] Zhao J, Liu Y, Sun WB, Zhang H. Amorphous calcium phosphate and its application in dentistry. Chemistry Central Journal. 2011;5.
[208] Zhou W, Baneyx F. Aqueous, Protein-Driven Synthesis of Transition Metal-Doped ZnS Immuno-Quantum Dots. Acs Nano. 2011;5.
[209] Zhou W, Schwartz DT, Baneyx F. Single-Pot Biofabrication of Zinc Sulfide Immuno-Quantum Dots. Journal of the American Chemical Society. 2010;132.